Development of a Tsunami Forecast Model for Monterey, CA

Yong Wei

Table of Contents

Abstract 12

1. Background and Objectives 12

2. Forecast Methodology 13

3.Model development 14

3.1 Study area and NOS tide station 15

3.2 Digital Elevation Model (DEM) of Monterey, California 16

3.3 Model Setup 17

4. Results and Discussions 19

4.1 Model Validation 19

4.2 Model stability tests using synthetic tsunami events 21

5. Summary and Conclusions 23

7. References 24

Figures: 27

Tables: 91

Appendix A. 97

Appendix B. Propagation database: Pacific Ocean Unit Sources 98

Appendix C. SIFT testing results 99

C1. Purpose 99

C2. Testing procedure 100

List of Figures:

Figure 1 Location of Monterey, California. 27

Figure 2 Average population density of Monterey County in 2007. 28

Figure 3. Probabilities of Mw 6.7 or stronger earthquakes occurring on faults in the San Francisco Bay Region during 2001-2031, where the probability of occurrence on each fault in indicated in ovals, and colors indicate the corresponding probabilities of each fault segment. Credit: Working Group on California Earthquake Probabilities (2003) ... 29

Figure 4 Aerial photo overlooking Monterey Harbor. 30

Figure 5 Bathymetry and topography of the outermost A grid for the reference model at Monterey, CA. 31

Figure 6 Bathymetry and topography of the outermost A grid for the optimized forecast model at Monterey, CA. 32

Figure 7 Bathymetry and topography of the intermediate B grid for the reference model at Monterey, CA. 33

Figure 8 Bathymetry and topography of the intermediate B grid for the optimized forecast model at Monterey, CA. 34

Figure 9 Bathymetry and topography of the innermost C grid for the reference model at Monterey, CA. 35

Figure 10 Bathymetry and topography of the innermost C grid for the optimized forecast model at Monterey, CA. 35

Figure 11 Location map of historical events. 36

Figure 12 Model validation at Monterey for 28 March 1964 Alaska tsunami. (a) Computed and observed time series at Monterey tide station; (b) Computed maximum wave amplitude in grid C of the reference model; (c) Computed maximum current speed in grid C of the reference model; (d) Computed maximum wave amplitude in grid C of forecast model; (e) Computed current speed in grid C of forecast model. The black rectangular in (b) and (c) indicates the computational domain of forecast model grid C in (d) and (e). 37

Figure 13 Model validation at Monterey for 4 October 1994 Kuril Islands tsunami. (a) Computed and observed time series at the Monterey tide station; (b) Computed maximum wave amplitude in C grid of the reference model; (c) Computed maximum current speed in C grid of the reference model; (d) Computed maximum wave amplitude in C grid of forecast model; (e) Computed current speed in C grid of forecast model. The black rectangular in (b) and (c) indicates the computational domain of forecast model C grid in (d) and (e). 38

Figure 14 Model validation at Monterey for 4 October 1994 Kuril Islands tsunami. (a) Computed and observed time series at the Monterey tide station; (b) Computed maximum wave amplitude in C grid of the reference model; (c) Computed maximum current speed in C grid of the reference model; (d) Computed maximum wave amplitude in C grid of forecast model; (e) Computed current speed in C grid of forecast model. The black

rectangular in (b) and (c) indicates the computational domain of forecast model C grid in (d) and (e)..... 39

Figure 15 Model validation at Monterey for 23 June 2001 Peru tsunami. (a) Computed and observed time series at the Monterey tide station; (b) Computed maximum wave amplitude in C grid of the reference model; (c) Computed maximum current speed in C grid of the reference model; (d) Computed maximum wave amplitude in C grid of forecast model; (e) Computed current speed in C grid of forecast model. The black rectangular in (b) and (c) indicates the computational domain of forecast model C grid in (d) and (e)..... 40

Figure 16 Model validation at Monterey for 3 May 2006 Tonga tsunami. (a) Computed and observed time series at the Monterey tide station; (b) Computed maximum wave amplitude in C grid of the reference model; (c) Computed maximum current speed in C grid of the reference model; (d) Computed maximum wave amplitude in C grid of forecast model; (e) Computed current speed in C grid of forecast model. The black rectangular in (b) and (c) indicates the computational domain of forecast model C grid in (d) and (e)..... 41

Figure 17 Model validation at Monterey for 11 November 2006 Kuril Islands tsunami. (a) Computed and observed time series at the Monterey tide station; (b) Computed maximum wave amplitude in C grid of the reference model; (c) Computed maximum current speed in C grid of the reference model; (d) Computed maximum wave amplitude in C grid of forecast model; (e) Computed current speed in C grid of forecast model. The black rectangular in (b) and (c) indicates the computational domain of forecast model C grid in (d) and (e)..... 42

Figure 18 Model validation at Monterey for 13 January 2007 Kuril Islands tsunami. (a) Computed and observed time series at the Monterey tide station; (b) Computed maximum wave amplitude in C grid of the reference model; (c) Computed maximum current speed in C grid of the reference model; (d) Computed maximum wave amplitude in C grid of forecast model; (e) Computed current speed in C grid of forecast model. The black rectangular in (b) and (c) indicates the computational domain of forecast model C grid in (d) and (e)..... 43

Figure 19 Model validation at Monterey for 15 August 2007 Peru tsunami. (a) Computed and observed time series at the Monterey tide station; (b) Computed maximum wave amplitude in C grid of the reference model; (c) Computed maximum current speed in C grid of the reference model; (d) Computed maximum wave amplitude in C grid of forecast model; (e) Computed current speed in C grid of forecast model. The black rectangular in (b) and (c) indicates the computational domain of forecast model C grid in (d) and (e)..... 44

Figure 20 Model validation at Monterey for 29 September 2009 Samoa tsunami. (a) Computed and observed time series at the Monterey tide station; (b) Computed maximum wave amplitude in C grid of the reference model; (c) Computed maximum current speed in C grid of the reference model; (d) Computed maximum wave amplitude in C grid of forecast model; (e) Computed current speed in C grid of forecast model. The black rectangular in (b) and (c) indicates the computational domain of forecast model C grid in (d) and (e)..... 45

Figure 21 Model validation at Monterey for 27 February 2010 Chile tsunami. (a) Computed and observed time series at the Monterey tide station; (b) Computed maximum wave amplitude in C grid of the reference model; (c) Computed maximum current speed in C grid of the reference model; (d) Computed maximum wave amplitude in C grid of forecast model; (e) Computed current speed in C grid of forecast model. The black rectangular in (b) and (c) indicates the computational domain of forecast model C grid in (d) and (e)..... 46

Figure 22 Model validation at Monterey for 11 March 2011 Japan tsunami. (a) Computed and observed time series at the Monterey tide station; (b) Computed maximum wave amplitude in C grid of the reference model; (c) Computed maximum current speed in C grid of the reference model; (d) Computed maximum wave amplitude in C grid of forecast model; (e) Computed current speed in C grid of forecast model. The black rectangular in (b) and (c) indicates the computational domain of forecast model C grid in (d) and (e)..... 47

Figure 23 Model results at Monterey for 1 April 1946 Alaska tsunami. (a) Computed and observed time series at the Monterey tide station; (b) Computed maximum wave amplitude in C grid of the reference model; (c) Computed maximum current speed in C grid of the reference model; (d) Computed maximum wave amplitude in C grid of forecast model; (e) Computed current speed in C grid of forecast model. The black rectangular in (b) and (c) indicates the computational domain of forecast model C grid in (d) and (e)..... 48

Figure 24 Model stability testing results at Monterey for synthetic mega tsunami scenario ACSZ 1-10. (a) Computed time series at the Monterey warning point; (b) Computed maximum wave amplitude in A grid of the forecast model; (c) Computed maximum current speed in B grid of the forecast model; (d) Computed maximum wave amplitude in C grid of the forecast model; (e) Computed current speed in C grid of the forecast model. 49

Figure 25 Model stability testing results at Monterey for synthetic mega tsunami scenario ACSZ 11-20. (a) Computed time series at the Monterey warning point; (b) Computed maximum wave amplitude in A grid of the forecast model; (c) Computed maximum current speed in B grid of the forecast model; (d) Computed maximum wave amplitude in C grid of the forecast model; (e) Computed current speed in C grid of the forecast model. 50

Figure 26 Model stability testing results at Monterey for synthetic mega tsunami scenario ACSZ 21-30. (a) Computed time series at the Monterey warning point; (b) Computed maximum wave amplitude in A grid of the forecast model; (c) Computed maximum current speed in B grid of the forecast model; (d) Computed maximum wave amplitude in C grid of the forecast model; (e) Computed current speed in C grid of the forecast model. 51

Figure 27 Model stability testing results at Monterey for synthetic mega tsunami scenario ACSZ 31-40. (a) Computed time series at the Monterey warning point; (b) Computed maximum wave amplitude in A grid of the forecast model; (c) Computed maximum current speed in B grid of the forecast model; (d) Computed maximum wave amplitude in

C grid of the forecast model; (e) Computed current speed in C grid of the forecast model. 52

Figure 28 Model stability testing results at Monterey for synthetic mega tsunami scenario ACSZ 41-50. (a) Computed time series at the Monterey warning point; (b) Computed maximum wave amplitude in A grid of the forecast model; (c) Computed maximum current speed in B grid of the forecast model; (d) Computed maximum wave amplitude in C grid of the forecast model; (e) Computed current speed in C grid of the forecast model. 53

Figure 29 Model stability testing results at Monterey for synthetic mega tsunami scenario ACSZ 46-55. (a) Computed time series at the Monterey warning point; (b) Computed maximum wave amplitude in A grid of the forecast model; (c) Computed maximum current speed in B grid of the forecast model; (d) Computed maximum wave amplitude in C grid of the forecast model; (e) Computed current speed in C grid of the forecast model. 54

Figure 30 Model stability testing results at Monterey for synthetic mega tsunami scenario ACSZ 56-65. (a) Computed time series at the Monterey warning point; (b) Computed maximum wave amplitude in A grid of the forecast model; (c) Computed maximum current speed in B grid of the forecast model; (d) Computed maximum wave amplitude in C grid of the forecast model; (e) Computed current speed in C grid of the forecast model. 55

Figure 31 Model stability testing results at Monterey for synthetic mega tsunami scenario CSSZ 1-10. (a) Computed time series at the Monterey warning point; (b) Computed maximum wave amplitude in A grid of the forecast model; (c) Computed maximum current speed in B grid of the forecast model; (d) Computed maximum wave amplitude in C grid of the forecast model; (e) Computed current speed in C grid of the forecast model. 56

Figure 32 Model stability testing results at Monterey for synthetic mega tsunami scenario CSSZ 11-20. (a) Computed time series at the Monterey warning point; (b) Computed maximum wave amplitude in A grid of the forecast model; (c) Computed maximum current speed in B grid of the forecast model; (d) Computed maximum wave amplitude in C grid of the forecast model; (e) Computed current speed in C grid of the forecast model. 57

Figure 33 Model stability testing results at Monterey for synthetic mega tsunami scenario CSSZ 21-30. (a) Computed time series at the Monterey warning point; (b) Computed maximum wave amplitude in A grid of the forecast model; (c) Computed maximum current speed in B grid of the forecast model; (d) Computed maximum wave amplitude in C grid of the forecast model; (e) Computed current speed in C grid of the forecast model. 58

Figure 34 Model stability testing results at Monterey for synthetic mega tsunami scenario CSSZ 31-40. (a) Computed time series at the Monterey warning point; (b) Computed maximum wave amplitude in A grid of the forecast model; (c) Computed maximum current speed in B grid of the forecast model; (d) Computed maximum wave amplitude in

C grid of the forecast model; (e) Computed current speed in C grid of the forecast model. 59

Figure 35 Model stability testing results at Monterey for synthetic mega tsunami scenario CSSZ 41-50. (a) Computed time series at the Monterey warning point; (b) Computed maximum wave amplitude in A grid of the forecast model; (c) Computed maximum current speed in B grid of the forecast model; (d) Computed maximum wave amplitude in C grid of the forecast model; (e) Computed current speed in C grid of the forecast model. 60

Figure 36 Model stability testing results at Monterey for synthetic mega tsunami scenario CSSZ 51-60. (a) Computed time series at the Monterey warning point; (b) Computed maximum wave amplitude in A grid of the forecast model; (c) Computed maximum current speed in B grid of the forecast model; (d) Computed maximum wave amplitude in C grid of the forecast model; (e) Computed current speed in C grid of the forecast model. 61

Figure 37 Model stability testing results at Monterey for synthetic mega tsunami scenario CSSZ 61-70. (a) Computed time series at the Monterey warning point; (b) Computed maximum wave amplitude in A grid of the forecast model; (c) Computed maximum current speed in B grid of the forecast model; (d) Computed maximum wave amplitude in C grid of the forecast model; (e) Computed current speed in C grid of the forecast model. 62

Figure 38 Model stability testing results at Monterey for synthetic mega tsunami scenario CSSZ 71-80. (a) Computed time series at the Monterey warning point; (b) Computed maximum wave amplitude in A grid of the forecast model; (c) Computed maximum current speed in B grid of the forecast model; (d) Computed maximum wave amplitude in C grid of the forecast model; (e) Computed current speed in C grid of the forecast model. 63

Figure 39 Model stability testing results at Monterey for synthetic mega tsunami scenario CSSZ 81-90. (a) Computed time series at the Monterey warning point; (b) Computed maximum wave amplitude in A grid of the forecast model; (c) Computed maximum current speed in B grid of the forecast model; (d) Computed maximum wave amplitude in C grid of the forecast model; (e) Computed current speed in C grid of the forecast model. 64

Figure 40 Model stability testing results at Monterey for synthetic mega tsunami scenario NTSZ 1-10. (a) Computed time series at the Monterey warning point; (b) Computed maximum wave amplitude in A grid of the forecast model; (c) Computed maximum current speed in B grid of the forecast model; (d) Computed maximum wave amplitude in C grid of the forecast model; (e) Computed current speed in C grid of the forecast model. 65

Figure 41 Model stability testing results at Monterey for synthetic mega tsunami scenario NTSZ 11-20. (a) Computed time series at the Monterey warning point; (b) Computed maximum wave amplitude in A grid of the forecast model; (c) Computed maximum current speed in B grid of the forecast model; (d) Computed maximum wave amplitude in

C grid of the forecast model; (e) Computed current speed in C grid of the forecast model. 66

Figure 42 Model stability testing results at Monterey for synthetic mega tsunami scenario NTSZ 21-30. (a) Computed time series at the Monterey warning point; (b) Computed maximum wave amplitude in A grid of the forecast model; (c) Computed maximum current speed in B grid of the forecast model; (d) Computed maximum wave amplitude in C grid of the forecast model; (e) Computed current speed in C grid of the forecast model. 67

Figure 43 (a) Computed time series at the Monterey warning point; (b) Computed maximum wave amplitude in A grid of the forecast model; (c) Computed maximum current speed in B grid of the forecast model; (d) Computed maximum wave amplitude in C grid of the forecast model; (e) Computed current speed in C grid of the forecast model. 68

Figure 44 (a) Computed time series at the Monterey warning point; (b) Computed maximum wave amplitude in A grid of the forecast model; (c) Computed maximum current speed in B grid of the forecast model; (d) Computed maximum wave amplitude in C grid of the forecast model; (e) Computed current speed in C grid of the forecast model. 69

Figure 45 Model stability testing results at Monterey for synthetic mega tsunami scenario NVSZ 11-20. (a) Computed time series at the Monterey warning point; (b) Computed maximum wave amplitude in A grid of the forecast model; (c) Computed maximum current speed in B grid of the forecast model; (d) Computed maximum wave amplitude in C grid of the forecast model; (e) Computed current speed in C grid of the forecast model. 70

Figure 46 Model stability testing results at Monterey for synthetic mega tsunami scenario NVSZ 21-30. (a) Computed time series at the Monterey warning point; (b) Computed maximum wave amplitude in A grid of the forecast model; (c) Computed maximum current speed in B grid of the forecast model; (d) Computed maximum wave amplitude in C grid of the forecast model; (e) Computed current speed in C grid of the forecast model. 71

Figure 47 Model stability testing results at Monterey for synthetic mega tsunami scenario NVSZ 28-37. (a) Computed time series at the Monterey warning point; (b) Computed maximum wave amplitude in A grid of the forecast model; (c) Computed maximum current speed in B grid of the forecast model; (d) Computed maximum wave amplitude in C grid of the forecast model; (e) Computed current speed in C grid of the forecast model. 72

Figure 48 Model stability testing results at Monterey for synthetic mega tsunami scenario MOSZ 1-10. (a) Computed time series at the Monterey warning point; (b) Computed maximum wave amplitude in A grid of the forecast model; (c) Computed maximum current speed in B grid of the forecast model; (d) Computed maximum wave amplitude in C grid of the forecast model; (e) Computed current speed in C grid of the forecast model. 73

Figure 49 Model stability testing results at Monterey for synthetic mega tsunami scenario MOSZ 8-17. (a) Computed time series at the Monterey warning point; (b) Computed maximum wave amplitude in A grid of the forecast model; (c) Computed maximum current speed in B grid of the forecast model; (d) Computed maximum wave amplitude in C grid of the forecast model; (e) Computed current speed in C grid of the forecast model. 74

Figure 50 Model stability testing results at Monterey for synthetic mega tsunami scenario NGSZ 1-10. (a) Computed time series at the Monterey warning point; (b) Computed maximum wave amplitude in A grid of the forecast model; (c) Computed maximum current speed in B grid of the forecast model; (d) Computed maximum wave amplitude in C grid of the forecast model; (e) Computed current speed in C grid of the forecast model. 75

Figure 51 Model stability testing results at Monterey for synthetic mega tsunami scenario NGSZ 6-15. (a) Computed time series at the Monterey warning point; (b) Computed maximum wave amplitude in A grid of the forecast model; (c) Computed maximum current speed in B grid of the forecast model; (d) Computed maximum wave amplitude in C grid of the forecast model; (e) Computed current speed in C grid of the forecast model. 76

Figure 52 Model stability testing results at Monterey for synthetic mega tsunami scenario EPSZ 1-10. (a) Computed time series at the Monterey warning point; (b) Computed maximum wave amplitude in A grid of the forecast model; (c) Computed maximum current speed in B grid of the forecast model; (d) Computed maximum wave amplitude in C grid of the forecast model; (e) Computed current speed in C grid of the forecast model. 77

Figure 53 Model stability testing results at Monterey for synthetic mega tsunami scenario EPSZ 9-18. (a) Computed time series at the Monterey warning point; (b) Computed maximum wave amplitude in A grid of the forecast model; (c) Computed maximum current speed in B grid of the forecast model; (d) Computed maximum wave amplitude in C grid of the forecast model; (e) Computed current speed in C grid of the forecast model. 78

Figure 54 Model stability testing results at Monterey for synthetic mega tsunami scenario RNSZ 1-10. (a) Computed time series at the Monterey warning point; (b) Computed maximum wave amplitude in A grid of the forecast model; (c) Computed maximum current speed in B grid of the forecast model; (d) Computed maximum wave amplitude in C grid of the forecast model; (e) Computed current speed in C grid of the forecast model. 79

Figure 55 Model stability testing results at Monterey for synthetic mega tsunami scenario RNSZ 13-22. (a) Computed time series at the Monterey warning point; (b) Computed maximum wave amplitude in A grid of the forecast model; (c) Computed maximum current speed in B grid of the forecast model; (d) Computed maximum wave amplitude in C grid of the forecast model; (e) Computed current speed in C grid of the forecast model. 80

Figure 56 Model stability testing results at Monterey for synthetic mega tsunami scenario KISZ 1-10. (a) Computed time series at the Monterey warning point; (b) Computed maximum wave amplitude in A grid of the forecast model; (c) Computed maximum current speed in B grid of the forecast model; (d) Computed maximum wave amplitude in C grid of the forecast model; (e) Computed current speed in C grid of the forecast model. 81

Figure 57 Model stability testing results at Monterey for synthetic mega tsunami scenario KISZ 11-20. (a) Computed time series at the Monterey warning point; (b) Computed maximum wave amplitude in A grid of the forecast model; (c) Computed maximum current speed in B grid of the forecast model; (d) Computed maximum wave amplitude in C grid of the forecast model; (e) Computed current speed in C grid of the forecast model. 82

Figure 58 Model stability testing results at Monterey for synthetic mega tsunami scenario KISZ 21-30. (a) Computed time series at the Monterey warning point; (b) Computed maximum wave amplitude in A grid of the forecast model; (c) Computed maximum current speed in B grid of the forecast model; (d) Computed maximum wave amplitude in C grid of the forecast model; (e) Computed current speed in C grid of the forecast model. 83

Figure 59 Model stability testing results at Monterey for synthetic mega tsunami scenario KISZ 31-40. (a) Computed time series at the Monterey warning point; (b) Computed maximum wave amplitude in A grid of the forecast model; (c) Computed maximum current speed in B grid of the forecast model; (d) Computed maximum wave amplitude in C grid of the forecast model; (e) Computed current speed in C grid of the forecast model. 84

Figure 60 Model stability testing results at Monterey for synthetic mega tsunami scenario KISZ 42-51. (a) Computed time series at the Monterey warning point; (b) Computed maximum wave amplitude in A grid of the forecast model; (c) Computed maximum current speed in B grid of the forecast model; (d) Computed maximum wave amplitude in C grid of the forecast model; (e) Computed current speed in C grid of the forecast model. 85

Figure 61 Model stability testing results at Monterey for synthetic mega tsunami scenario KISZ 52-61. (a) Computed time series at the Monterey warning point; (b) Computed maximum wave amplitude in A grid of the forecast model; (c) Computed maximum current speed in B grid of the forecast model; (d) Computed maximum wave amplitude in C grid of the forecast model; (e) Computed current speed in C grid of the forecast model. 86

Figure 62 Model stability testing results at Monterey for synthetic mega tsunami scenario KISZ 56-65. (a) Computed time series at the Monterey warning point; (b) Computed maximum wave amplitude in A grid of the forecast model; (c) Computed maximum current speed in B grid of the forecast model; (d) Computed maximum wave amplitude in C grid of the forecast model; (e) Computed current speed in C grid of the forecast model. 87

Figure 63 Model stability testing results at Monterey for synthetic mega tsunami scenario KISZ 66-75. (a) Computed time series at the Monterey warning point; (b) Computed maximum wave amplitude in A grid of the forecast model; (c) Computed maximum current speed in B grid of the forecast model; (d) Computed maximum wave amplitude in C grid of the forecast model; (e) Computed current speed in C grid of the forecast model. 88

Figure 64 Model stability testing results at Monterey for synthetic tsunami scenario NTSZ b22. (a) Computed time series at the Monterey warning point; (b) Computed maximum wave amplitude in A grid of the forecast model; (c) Computed maximum current speed in B grid of the forecast model; (d) Computed maximum wave amplitude in C grid of the forecast model; (e) Computed current speed in C grid of the forecast model. 89

Figure 65 Model stability testing results at Monterey for synthetic micro tsunami scenario EPSZ b15. (a) Computed time series at the Monterey warning point; (b) Computed maximum wave amplitude in A grid of the forecast model; (c) Computed maximum current speed in B grid of the forecast model; (d) Computed maximum wave amplitude in C grid of the forecast model; (e) Computed current speed in C grid of the forecast model. 90

List of Tables:

Table 1. Historical tsunami events that have affected Monterey California..... 92

Table 2. Model setup and input parameters of Monterey forecast model and reference model..... 93

Table 3 Historical events used for model validation for Monterey, California, where ASCZ represents the Aleutian-Alaska-Cascadia subduction zone, KISZ the Kamchatka-Kuril-Japan-Izu-Mariana-Yap subduction zone, CSSZ the Central South America subduction zone, and NTSZ the New Zealand-Kermadec-Tonga subduction zone..... 94

Table 4 Tsunami source of 51 synthetic scenarios used for stability testing, where ACSZ = Alaska-Aleutian-Canada source zone, CSSZ = Central and South America source zone; NTSZ = New Zealand-Kermadec-Tonga source zone; NVSZ = New Britain-Solomons-Vanuatu source zone; MOSZ = Manus OCB source zone; NGSZ = North New Guinea source zone; EPSZ = East Philippines source zone; RNSZ = Ryukyu-Kyushu-Nankai source zone; KISZ = Kamchatka-Kuril-Japan trench source zone..... 96

Abstract

As part of NOAA's tsunami forecast system, this study addresses the development, validation, and stability tests of the tsunami forecast model for Monterey, California. Based on the Method of Splitting Tsunami (MOST), the tsunami forecast model is constructed at a spatial resolution of 1 arc sec (~ 30 m) in the finest grid to accomplish a 4-hour simulation of wave inundation onto dry land within 10 minutes of CPU time. A referenced inundation model is developed in parallel using grids of higher resolution up to 1/3 arc sec (~ 8.3 m) to provide a modeling reference for the forecast model. The model validations using historical tsunami events show good agreement between the model computation and observations, and provide quantitative estimation of the inundation, tsunami runup and computed maximum values for these events. The stability of the forecast model is evaluated based on 42 hypothetical scenarios generated in all subduction zones of the Pacific Rim at magnitudes ranging from M_w 7.5 to M_w 9.3. A micro tsunami test provides further model stability test under no-wave condition. Model computation shows that a M_w 9.3 event from central Alaska-Aleutian Subduction Zone may potentially generate tsunami runup as high as 7.3 m at the coastline of the City of Monterey, where the common land level is about 8 m.

1. Background and Objectives

The National Oceanic and Atmospheric Administration (NOAA) Center for Tsunami, Research (NCTR) at the NOAA Pacific Marine Environmental Laboratory (PMEL) has developed a tsunami forecasting capability for operational use by NOAA's two Tsunami Warning Centers located in Hawaii and Alaska (Titov *et al.*, 2005). The system is designed to efficiently provide basin-wide warning of approaching tsunami waves accurately and quickly. The system, termed Short-term Inundation Forecast of Tsunamis, combines real-time tsunami event data with numerical models to produce estimates of tsunami wave arrival times and amplitudes at a coastal community of interest. This system integrates several key components: deep-ocean observations of tsunamis in real time, a basin-wide pre-computed propagation database of water level and flow velocities based on potential seismic unit sources, an inversion algorithm to refine the tsunami source based on deep-ocean observations during an event, and high-resolution tsunami forecast models.

Monterey is a coastal community located in northern California, 115 miles south of San Francisco and 350 miles north of Los Angeles (Figure 1), with a population of 30,641 in the City of Monterey and 408,238 in Monterey County as of July 2008. Figure 2 shows the coast of Monterey Bay has highest population density in the county, about

325-1832 people per square mile. Most of the residents are living in a low-lying area prone to tsunami inundation with elevation less than 8 m. Monterey Harbor is part of the Monterey Bay National Marine Sanctuary and is an attraction for both residents and visitors, providing access to many recreational and commercial opportunities. The entire coastal area of Monterey County is susceptible to tsunamis, especially the low-lying areas and riverine valleys to the north. In the past 100 years, Monterey County has experienced 8 tsunamis and was impacted significantly by the 1960 Chile tsunami. In response to natural hazards, the county of Monterey developed a Multi-Jurisdictional Hazard Mitigation Plan in 2007 that is to be updated every five years (http://www.co.monterey.ca.us/oes/hazard-mitigation.asp). For tsunami, this plan included a tsunami hazard map implementing the USC tsunami inundation limit (Barberopoulou et al., 2009), as well as the "potential tsunami hazard elevations". The latter is to accommodate the typical tsunami runup, 6.4 to 15 m (21 to 50 feet), from large tsunamis in the Pacific Ocean over the last 80 years in Monterey County. The objective of the present study is to develop an operational forecast model for Monterey, California, for the purpose of minimizing false alarms that disrupt port activities and to provide the region with accurate and timely information necessary to make decisions in the event of tsunami generation,

2. Forecast Methodology

A high-resolution inundation model was used as the basis for development of a tsunami forecast model to operationally provide an estimate of wave arrival time, wave height, and inundation at Monterey, California following tsunami generation. All tsunami forecast models are run in real time while a tsunami is propagating across the open ocean. The Monterey model was designed and tested to perform under stringent time constraints given that time is generally the single limiting factor in saving lives and property. The goal of this work is to maximize the length of time that the community of Monterey has to react to a tsunami threat by providing accurate information quickly to emergency managers and other officials responsible for the community and infrastructure.

The general tsunami forecast model, based on the Method of Splitting Tsunami (MOST), is used in the tsunami inundation and forecasting system to provide real-time tsunami forecasts at selected coastal communities. The model runs in minutes while employing high-resolution grids constructed by the National Geophysical Data Center. The Method of Splitting Tsunami (MOST) is a suite of numerical simulation codes capable of simulating three processes of tsunami evolution: earthquake, transoceanic propagation, and inundation of dry land. The MOST model has been extensively tested

against a number of laboratory experiments and benchmarks (Synolakis *et al.*, 2008) and was successfully used for simulations of many historical tsunami events. The main objective of a forecast model is to provide an accurate, yet rapid, estimate of wave arrival time, wave height, and inundation in the minutes following a tsunami event. Titov and González (1997) describe the technical aspects of forecast model development, stability, testing, and robustness, and Tang *et al*. (2009) provides detailed description of forecast methodology.

A basin-wide database of pre-computed water elevations and flow velocities for unit sources covering worldwide subduction zones has been generated to expedite forecasts (Gica *et al.*, 2008). As the tsunami wave propagates across the ocean and successively reaches tsunameter observation sites, recorded sea level is ingested into the tsunami forecast application in near real-time and incorporated into an inversion algorithm to produce an improved estimate of the tsunami source. A linear combination of the pre-computed database is then performed based on this tsunami source, now reflecting the transfer of energy to the fluid body, to produce synthetic boundary conditions of water elevation and flow velocities to initiate the forecast model computation.

Accurate forecasting of the tsunami impact on a coastal community largely relies on accuracies of bathymetry and topography in numerical computation. The high spatial and temporal grid resolution necessary for modeling accuracy poses a challenge in the run-time requirement for real-time forecasts. Each tsunami forecast model consists of three telescoped grids with increasing spatial resolution in the finest grid, and temporal resolution for simulation of wave inundation onto dry land. The forecast model utilizes the most recent bathymetry and topography available to reproduce the correct wave dynamics during the inundation computation. Forecast models, including the Monterey model, are constructed for at-risk populous coastal communities in the Pacific and Atlantic Oceans. Previous and present development of forecast models in the Pacific have validated the accuracy and efficiency of each forecast model currently implemented in the real-time tsunami forecast system (Bernard et al., 2014; Titov *et al*., 2005; Titov, 2009; Tang *et al*., 2008 & 2012; Wei *et al*., 2008, 2013 & 2015).

3.Model development

A tsunami forecast model using MOST usually consists of three nested grids, , referred to as A, B, and C-grids, that employ increasing spatial resolutions. Tsunami wave dynamics offshore are predicted using a low-resolution A grid, while the wave dynamics in shallow, near-shore area is computed in C grid, where the model results are compared with observations at tide gauges for historical tsunamis. The goal is to achieve

a 4 to 10 hour simulation of tsunami propagation and flooding within 10 min of wall-clock time. NOAA's National Geophysical Data Center (NGDC) provides Digital Elevation Models (DEMs), mostly at a grid resolution of 1/3 arc sec (~ 10 m), for a coastal community at risk. The NGDC's DEMs are integrated from a variety of data sources to use unified vertical datum, Mean High Water (MHW), and horizontal datum, World Geodetic System 1984 (WGS84, http://ngdc.noaa.gov/mgg/inundation/tsunami/inundation.html).

3.1 Study area and NOS tide station

The City of Monterey is situated on the Monterey Bay National Marine Sanctuary, a federally protected ocean area extending 450 km along the coast, where the San Andreas fault system traverses in a northwest-southeast direction and controls much of the overall geologic character of the region. This series of sub-parallel faults forms the boundary between the Pacific and North American tectonic plates, the former of which is sliding northwest several centimeters per year relative to the latter. In the vicinity of the sanctuary, the San Andreas fault system is basically composed of four fault zones: the San Gregorio fault that extends from Monterey to Half Moon Bay and is predominantly offshore; the Monterey – Tularcitos fault zone that extends over a wide area from Monterey to Santa Cruz within Monterey Bay; The San Simeon fault; and the infamous San Andreas fault that is almost entirely onshore in this region. An earthquake probability study by the USGS) determined that there is a 62 percent chance of a magnitude 6.7 or greater earthquake occurring on one of the faults in the greater San Francisco Bay Area between 2003 and 2032 (Working Group on California Earthquake Probabilities, 2003). In this time period, there is a 10 percent chance of a magnitude 6.7 or greater earthquake on the San Gregorio fault and a 21 percent chance of a similar earthquake on the San Andreas fault (Figure 3),

Monterey is subject to both distant and local tsunami threats. Table 1 shows historical tsunamis that have affected Monterey Bay with associated observations of tsunami heights of these events. The 1964 Alaska tsunami affected the entire California coastline. The tsunami waves were particularly high from Crescent City to Monterey with heights on the open coast ranging from 2.1 – 6.4 m. The recorded wave amplitude at Monterey Bay tide gauge, located on the south side on the Monterey Bay, is about 1 m, but reached as high as 3.4 m on the north side of Monterey Bay at Santa Cruz Harbor. The 1946 Unimak tsunami barely produced any noticeable waves at Monterey Harbor but reached over 3 m at Santa Cruz. Other recorded tsunami waves before 2010 are mostly smaller than 0.2 m in amplitude, causing no damage to the coastline. The last major tsunamis

hitting Monterey Bay were the 2010 Chile and 2011 Tohoku, causing maximum wave amplitudes of 0.28 m and 0.7 m at the tide gauge, respectively.

The submarine canyon offshore of Monterey Bay has been identified as a region of mass movement features. Slumps, debris flows and other submarine landslides are concentrated along canyon walls and the lower continental slope, with many additional distinct and youthful slumps at the base of the headward walls of Monterey Canyon (Greene et al., 2002). Land mass movement features in the Monterey Bay region suggest that a potential for tsunami generation exists (Greene and Ward, 2003). A small landslide occurred at the head of Monterey Canyon during the 1989 Loma Prieta Mw 6.9 earthquake with a small tsunami about 0.5 m high reported to have entered the Moss Landing Harbor and a turbidity current reported to have traveled down the canyon axis (Greene and Hicks, 1990; Schwing et al., 1990; Garfield et al., 1994). Ward (2005) showed that a 0.1 km^3 of material failure in Monterey Canyon could induce more than 7 meters of runup over 25 km of the coast, posing severe tsunami threats to the City of Monterey.

The NOS tide station at Monterey Harbor is located at (121.889278W, 36.605056N) with a Mean Sea Level (MSL) water depth of about 2.5 m on wharf #2, north of the main boat harbor (Figure 4). The tide station was established in November of 1973, and the present installation occurred in September of 1988. The mean tidal range at Monterey Harbor is about 1 m, and the mean sea level is increasing at the rate of 1.34 +/- 1.35 mm per year. 11 of the 25 historical events listed in Table 1 are used to validate the present forecast model. The 11 tsunami events include the 26 March 1964 Alaska, 4 October 1994 Kuril, 10 June 1996 Andreanof, 23 June 2001 Peru, 3 May 2007 Tonga, 15 November 2006 Kuril, 13 January 2007 Kuril, 15 August 2007 Peru, 29 September 2009 Samoa, 27 February 2010 Chile, and 11 March 2011 Tohoku.

3.2 Digital Elevation Model (DEM) of Monterey, California

Accurate bathymetry and topography in offshore and coastal regions play a key role, both globally and locally, in tsunami generation, propagation and inundation. The global bathymetric and topographic datasets are available for public-domain research. Marks and Smith (2006) conducted an evaluation on 6 publicly available global bathymetry grids: DBDB2 (Digital Bathymetric Data Base by Naval Research Laboratory), ETOPO2 (Earth Topography by National Geophysical Data Center), GEBCO (General Bathymetric Charts of the Oceans by British Oceanographic Data Center), GINA (Geographic Information Network of Alaska), Smith and Sandwell (1997) and S2004. They concluded the original Smith and Sandwell grid might be the best source among

these global bathymetric grids. Subsequently, they developed a new 1-min global topography grid S2004 that combines the Smith and Sandwell grid below 1,000 m depth and equatorward of 72°, and GEBCO grids in shallow water and polar regions. NOAA Center for Tsunami Research (NCTR) developed a Pacific-Basin 30sec grid, derived primarily from the Smith and Sandwell grid and the SRTM30_PLUS grid, with amendments in areas where NCTR has better bathymetry. This comprehensive dataset covers the entire Pacific Ocean and part of the Arctic Ocean from E120° to W68°, and S80° to N80°.

While developing bathymetric and topographic grids for specific coastal communities, NCTR has been collaborating with NGDC on the Tsunami Inundation Gridding Project since 2005 to build high-resolution digital elevation models (DEMs) for more U.S. coastal regions, and satisfy the needs of tsunami forecast model development in the near future. Currently, the finished datasets, along with the associated documentation, are downloadable in ESRI ArcGIS ASCII grid format at http://www.ngdc.noaa.gov/dem/.

The Monterey DEM was delivered to PMEL by NGDC in January of 2008 at a grid resolution of 1/3 arc sec for areas between latitudes of 122.52°W - 121.52°W, and latitudes of 36.09°N - 37.11°N (Taylor et al., 2008). Data sources used by NGDC to derive the Monterey DEM include NOAA's National Ocean Service (NOS), Office of Coastal Survey (OCS) and Coastal Services Center (CSC), California State University Seafloor Mapping Laboratory, the U.S. Geological Survey (USGS), and the California Department of Fish and Game Marine Region GIS unit (CDFG). The horizontal and vertical datum of the dataset are the World Geodetic System 1984 (WGS 84) and the mean high water, respectively. The spatial resolution ranges from 1 m to 1 km for the bathymetric datasets, and 2.5 m to ~ 8.3 m (1/3 arc second) for the topographic datasets (Taylor et al., 2008).

Bathymetry and topography implemented in the Monterey forecast model are derived from NGDC's DEM described above, which is deemed as the best-available elevation model for Monterey at the time when it was developed. When new digital elevation models become available, forecast models may be updated and the new results will be posted at http://nctr.pmel.noaa.gov/forecast_reports/.

3.3 Model Setup

Figures 5 to 10 show the computational grids, derived from the aforementioned Monterey DEMs, of the reference inundation model and the optimized forecast model.

Figures 5 and 6 show the computational domain of outermost grid, A grid, covers most of coastlines of California. The A grid has a grid resolution of 36 arc seconds (~ 1,080 m) for the reference model (Figure 5), and a grid resolution of 2 arc minutes (~ 3,740 m) for the forecast model (Figure 6). Both A grids are bounded at a water depth greater than 4,000 m at their western boundaries. This way, the inundation models adopt most of the boundary conditions in the deep water from the pre-computed propagation database (Gica et al., 2008). For the same reason, the A grid is extended to 30°N to avoid settling the south boundary on the shallow continental shelf. The study area of Monterey is positioned in the middle of the A grid to minimize the influence of boundary forcing.

The intermediate grid, B grid, covers the entire Monterey Bay, and its western boundary is extended to water depths greater than 3,000 m. The B grid has a grid resolution of 3 arc seconds (~ 90 m) for the reference model (Figure 7), and a grid resolution of 18 arc minutes (~ 540 m) for the forecast model (Figure 8).. In comparison with the A grids, the B grids provide more details of wave dynamics transitioned from deep water to shallow shelf, where the nonlinearity of waves is amplified the most. It's worth noting that the submarine canyon offshore of Monterey Bay is included in both B grids.

The innermost grid, C grid, covers the south part of Monterey bay and the entire Monterey Harbor. Figures 9 and 10 indicate that the coast of Monterey Bay is featured with with a sloping beach with gradual decrease of water depth cross-shore. The contours of the water depth are nearly parallel to the shoreline, implying less complex directionality and nonlinearity of the tsunami wave dynamics. This bathymetric setting allows us to use a small C-grid coverage for the forecast model (Figure 10) in comparison with that for the reference model (Figure 9) since reducing computational time is a also major consideration in development of a forecast model.

Table 2 provides the details of model setup and input parameters for all grids of both models. It's worth noting that the main difference between the forecast model and the reference model lies in the grid resolution implemented in each grid. In comparison with the forecast model, the reference model employs denser grid spacing, and larger computational domains (Table 2). The main purpose of developing a reference model is to provide more accurate description of the bathymetry and topography, and thus more accurate modeling results that a corresponding forecast model can refer to. As indicated in Table 2, the reference model takes about 1,500 min of CPU time to finish a 4-hour simulation because of finer grid resolutions and larger computational domains. The forecast model needs only 10.4 min to accomplish the same 4-hour run, and is therefore

much more operationally efficient. This study also examines the model accuracy of the forecast measured in reference to the reference model.

4. Results and Discussions

4.1 Model Validation

The deep-ocean tsunameter array (also named as Deep-Ocean Assessment and Report of Tsunami (DART) in the United States) has been playing a critical role in tsunami detection and measurements. These real-time waveforms of tsunami are used to estimate tsunami sources while a tsunami is still in progress. As aforementioned, previous studies have shown successful applications of NOAA's tsunami forecast system to obtain the tsunami sources from real-time DART measurements, which is subsequently used to provide real-time propagation and coastal inundation forecast. Since 2003, these real-time inversions of tsunami sources have provided forecast accuracies up to 90% of the tsunami waveforms at distant coastlines. In this study, both the forecast model and the reference model for Monterey will be validated using 11 historical events. These events include the 4 October 1994 Kuril, the 10 June 1996 Andreanof, the 23 June 2011 Peru, the 3 May 2006 Tonga, the 15 November 2006 Kuril, the 13 January 2007 Kuril, the 1 April 2007 Solomon, the 15 August 2007 Peru, the 29 September 2009, the 27 February 2010 Chile, and the 11 March 2011 Japan. Except for the 11 events, the great 1964 Alaska tsunami also produced notable wave amplitude up to 1 m. The distinct tsunami waves registered by Monterey tide station during the 1964 event are valuable to validate the Monterey forecast model due to its high signal-to-noise ratio compared to other events. This study also computed the destructive tsunamis of 1 April 1946 Unimak, to demonstrate the wave dynamics at the coast of Monterey. Figure 11 provides an overview of the earthquake epicenters of these historical events. Table 3 provides details of tsunami source configuration for all historical events used for model validation in this study. All tsunami sources are inverted from tsunami waveforms recorded at deep-ocean DARTs, or at tide gauges for events occurred long before DARTs (such as the 1 April 1946 Unimak and 27 March 1964 Alaska). The last column in Table 3 shows the source combination of each event on the basis of tsunami propagation database. It's worth noting that some of these source combinations were obtained in real time, some were obtained using an older propagation database (Gica et al., 2008), and the others were obtained in hindcast studies.

Figures 12 to 23 show good agreement between model results and observations for most of the events with sizable signal-to-noise ratio in the observations. The model time series of the 27 March 1964 Alaska tsunami computed by the forecast model is excellent in comparison with the observations up to hours after tsunami arrival, except for some

phase shifts and slightly larger wave amplitude due to the uncertainty of the tsunami source. The time series of the reference model shows larger amplitude with a maximum of 2.3 m in comparison that obtained forecast model and observations. Figure 11 (b) and (d) show that the computed tsunami amplitudes in the reference model are about 40% larger than those in the forecast model along the coastline of Monterey. According to historical accounts at Monterey during the 27 March 1964 Alaska tsunami, there was no noticeable damage along the coastline of Monterey. It gives more credits to the forecast model that shows no inundation at Monterey (Figure 12a), while the reference model shows major flooding in the low-lying areas to the east of Monterey Harbor (Figure 12d). It should be noted here that the model discrepancy between the reference model and forecast model is small for all other historical events validated in this study, meaning it is an event-dependent, instead of a systematic, modeling issue. This issue is currently under investigation and will be addressed in a future update of this report.

Real-time DART measurements were used to derive valid tsunami sources during the events of 3 May 2006 Tonga, 15 November 2006 Kuril Islands, 13 January 2007 Kuril Islands, 15 August 2007 Peru, the 29 September 2009, the 27 February 2010 Chile, and the 11 March 2011 Japan. The computed time series at the Monterey tide station for these events show good agreement with the first several hours of measurements for the 2006 Tonga, 2007 Kuril, 2007 Peru, 2010 Chile and 2011 Tohuku (Figures 16a, 18a, 19a, 21a and 22a). Misfits between model results and measurements for some events are either due to low signal-to-noise ratio of the tsunami waveforms (Figures 14a,15a, 20a), or because the tide gauge was not functioning properly during the event, such as the 15 November 2006 tsunami (Figure 17a). It's worth mentioning that the comparison between model and observation is excellent for the 4 October 1994 Kuril tsunami, even though this tsunami source was not inverted from DART measurements.

When comparing modeling results , we can see minor discrepancies in the first 4 to 5 waves between the reference model and forecast model. However, small offsets in both amplitude and phase appear in the late waves, which are expected between models using different spatial and temporal resolutions. The comparison between model and observation for the 2010 Chile (Figure 21) and 2011 Japan (Figure 22) events are excellent, in particular the reference model seems to reproduce the resonance patter well inside Monterey Bay. In comparison with the forecast model, the reference model employs a grid resolution of three times higher to adequately describe the local bathymetric and topographic features, and thus able to enhance the modeling capability in capture of the late waves. The reference model provides model reference for the computational accuracy of its optimized version, the tsunami forecast model. Despite the

differences in the late waves (i.e. six hours after the first tsunami arrival), one can see that the main characteristics of the tsunami waves, such as the maximum wave amplitude and the wave period, are accurately computed in the forecast model. In comparison with a reference model, the major advantage of a forecast model is its computational efficiency, about 150 times less time consuming (Table 2), while still able to achieve similar model accuracy.

The maximum computed current speed at Monterey is generally small offshore. In spite of the flow speed at the headland northwest of Monterey Harbor, the computed results show larger current speed at the entrance of Monterey Harbor as well as inside the boat harbor, indicating potential harbor damages due to strong current. Strong current was responsible for significant damage in the Crescent City boat harbor during the 15 November 2006 Kuril Islands tsunami (Kelly et al., 2006; Uslu et al., 2007). For the 1964 Alaska tsunami, the computed wave current speed by forecast model is about 0.8 – 1.0 m/s (1.6 – 2.0 knots) near the entrance of Monterey harbor and inside the boat harbor (Figure 12e), whereas the current speed induced by the 1946 Unimak tsunami is about half of that (Figure 23e).

4.2 Model stability tests using synthetic tsunami events

Model stability of the forecast model is evaluated using 42 synthetic events, 40 large source scenarios of M_w 9.3, 1 small source scenario of M_w 7.5, and one "no-wave" scenario of Mw 4.8, generated in the source zones around the Pacific Rim (Table 4). Each M_w 9.3 scenario consists of a combination of 20 unit sources covering a rupture area of 1000 km by 100 km with a uniform 28.4 m slip on each unit source A M_w 9.3 scenario imitates an equivalent or greater event of the 2004 Indian tsunami, which caused severe devastation along the coastline of Indian Ocean and accounted for hundreds of thousands of deaths. Our modeling experiences have shown that the singularities in the bathymetry and topography may cause model instabilities not only when the waves are large, but also when they are small enough to be taken over by accumulated numerical errors induced by those singularities. For such a reason, the present study also evaluates model stabilities due to a small synthetic tsunami scenario of M_w 7.5, which applies one-meter slip on one unit source (a source area of 100 km × 50 km). Another key test is the "no wave" scenario, 0.0001 m slip on one unit source in the present study, to examine the model stability under extremely small (close to null) wave forcing along the model boundaries. A successful no-wave test expects only wave activities in the same order of the boundary forcing without unreasonable amplification.

Figures 24 to 63 show the computational results of maximum computed wave amplitude and current speed for all synthetic scenarios. Each figure shows the computed time series at a warning point that best represents the location of the tide station, the results of maximum wave amplitude in all A, B, C grids, and the maximum current speed in the C grid. We note that no model instabilities were observed in all of these model runs, with or without tsunami inundation occurring. The M_w 9.3 scenario ACSZ 31-40 from central Aleutian-Alaska Subduction Zone produces the most severe tsunami strike along the Monterey coastline, while a M_w 9.3 event generated in the northern region of South America, such as CSSZ 41-50, has almost no impact at Monterey. Among all the M_w 9.3 scenarios, the computed maximum wave amplitude at the warning point ranges from 0.19 m in scenario CSSZ 41-50 to 5.2 m in scenario ACSZ 31-40. Similarly, the computed maximum wave trough at the warning point ranges from -0.23 m in CSSZ 41-50 to -7.6 m in scenario ACSZ 31-40. The computed maximum tsunami runup height reaches 7.3 m above mean high water (~ 7.8 m above mean sea level) in Monterey for scenario ACSZ 31-40. Considering most of the Monterey area has a land elevation of 8 m, a potential M_w 9.3 mega tsunami from central Aleutian-Alaska Subduction Zone may be catastrophic for this area. The fault area of ACSZ 31-40 is similar to the rupture area of the earthquake (M_w 9.2) that triggered the destructive 1964 Alaska tsunami, which however did not cause much damage in Monterey. The Mw 9.3 tsunami scenarios also reveal another two noticeable phenomena: (1) The B grid, covering the entire Monterey Bay, clearly shows that the tsunamis from all directions in the Pacific will tend to induce larger waves at north end of the Monterey Bay, where the City of Santa Cruz is located at, than at its south end where situates the City of Monterey. This has been confirmed by the historical destructive tsunamis of 1946 and 1964. The resonance modes of Monterey Bay triggered by tsunamis may be responsible for these effects (Tolkova and Power, 2011). (2) The modeling results show that the tsunamis from NTSZ, NVSZ, MOSZ and KISZ can induce large late waves that arrive 8 to 12 hours after the first arrival, and even 20 hours later if from CSSZ. Most of these late waves are possibly due to the reflected waves by the ocean ridges or islands in the Pacific.

The small synthetic scenarios generated negligible waves less than 1 cm at the warning point, and show no modeling instabilities (Figures 64 and 65). With little boundary forcing, the no-wave scenario produces negligible ripples at the order of 10^{-5} cm throughout the entire computational domain, meaning the present forecast model is robust to produce results without numerical amplification.

5. Summary and Conclusions

This study develops a tsunami forecast model for the community of Monterey, California. The developed model will be implemented into NOAA's tsunami forecast system to provide real-time modeling forecast of the water elevation, current speed, runup, and inundation for the coastal community at Monterey and its vicinity. This study discusses details of each individual component of the tsunami forecast model, including the bathymetry and topography, the basic model setup and model parameters. The forecast model employs grids as fine as 30 m and can accomplish 4-hour simulation after tsunami arrival in 10 minutes of CPU time. Using grids as fine as 8 m, a reference inundation model is also developed to provide model reference for the forecast model.

Model validations are carried out for both the Monterey forecast model and the reference model using 13 historical tsunami events to compare modeling results and the observations at the tide station. The computed time series are comparable with historical records at the Monterey tide gauge, especially those of sizable signal-to-noise ratio. Model validation using historical tsunamis shows these events did not cause serious inundation along the coastline of Monterey. This study tests the model stability of the forecast model using a total of 42 synthetic source scenarios from major subduction zones in the Pacific, including 40 Mw 9.3 scenarios, one Mw 7.5 scenario, and a Mw 4.8 scenario. These tests ensure the stability of the developed forecast model under the strike up to wave amplitude of 7.3 m along the coastlines of Monterey.

All model validation and stability tests demonstrated that the developed tsunami forecast model and reference model for Monterey are accurate, robust and efficient. The forecast model of Monterey Bay is ready to be implemented in short-term real-time tsunami forecast. Both the forecast model and the reference model also have potential values for long-term tsunami inundation study.

6. Acknowledgments

The author thanks Dr. Edison Gica and Jean Newman for their work in developing the propagation database. The author would like to Dr. Hongqiang Zhou for his technical review of this report. The author would also like to especially acknowledge and thank Lindsey Wright and Sandra Bigley for their editorial review of this report. Collaborative contributions of the National Weather Service, the National Geophysical Data Center, and the National Data Buoy Center were invaluable. Funding for this publication and all work leading to development of a tsunami forecast model for Monterey, California was provided by the National Oceanic and Atmospheric Administration. This publication is also partially funded by the Joint Institute for the Study of the Atmosphere and Ocean

(JISAO) under NOAA Cooperative Agreement No. NA17RJ1232, JISAO Contribution No. ****. This is PMEL Contribution No. ****.

7. References

Barberopoulou, A., J.C. Borrero, B. Uslu, N. Kalligeris, J.D. Goltz, R.I. Wilson, and C.E. Synolakis (2009): New maps of California to improve tsunami preparedness. Eos Trans. AGU, 90(16), 137–144.

Bernard, E., Y. Wei, L. Tang, and V.V. Titov (2014): Impact of Near-Field, Deep-Ocean Tsunami Observations on Forecasting the 7 December 2012 Japanese Tsunami. Pure and Appl. Geophys., 171(12), doi: 10.1007/s00024-013-0720-8, 3483-3491.

Garfield, N., T. A. Rago, K. J. Schnebele, and C. A. Collins (1994), Evidence of a turbidity current in Monterey Submarine Canyon associated with the 1989 Loma Prieta earthquake, Cont. Shelf Res., 14, 673 – 686.

Gica, E., M. Spillane, V.V. Titov, C. Chamberlin, and J.C. Newman (2008): Development of the forecast propagation database for NOAA's Short-term Inundation Forecast for Tsunamis (SIFT). NOAA Tech. Memo. OAR PMEL-139, 89 pp.

Greene, H.G. and K.R. Hicks (1990). Ascension-Monterey canyon system: History and development. In: *Geology and Tectonics of the Central California Coastal Region, San Francisco to Monterey*, edited by R.E. Garrison, H.G. Greene, K.R. Hicks, G.E. Weber, and T.L. Wright. *American Association of Petroleum Geologists, Pacific Section, Volume and Guidebook*, **GB 67**: 229-250.

Greene, H.G., N.M. Maher and C.K. Paull (2002), Physiography of the Monterey Bay National Marine Sanctuary and implications about continental margin development, Marine Geology, 181, 55-82.

Greene, H.G. and S.N. Ward (2003), Mass movement features along the central California margin and their modeled consequences for tsunami generation, Submarine Mass Movements and Their Consequences, edited by Locat, L. and Mienert J., Kluwer Academic Publishers, Netherlands.

Kelly, A., L. Dengler, B. Uslu, A. Barberopoulou, S. Yim, and K.J. Bergen (2006), Recent tsunami highlights need for awareness of tsunami duration*, Eos Trans.* AGU, 87, 566-567.

Marks, K.M., and Smith, W.H.F. (2006): An evaluation of publicly available global bathymetry grids. Marine Geophysical Researches, 27, 19-34.

Schwing, F.B., Norton, J.G. and Pilskaln, C.H. (1990). Earthquake and bay: Response of Monterey Bay to the Loma Prieta Earthquake. *Eos, Transactions American Geophysical Union 71. doi: 10.1029/90EO00035. issn: 0096-3941.*

Smith, W. H. F. and D. T. Sandwell, 1997, Global Seafloor Topography from Satellite Altimetry and Ship Depth Soundings, Science 277: 1956-1962,

Synolakis, C.E., E.N. Bernard, V.V. Titov, U. Kanoglu and F.I. Gonzalez (2008), Validation and verification of tsunami numerical models, Pure and Applied Geophysics, 165(11-12), 2197-2228.

Tang, L.J., Chamberlin, C., Titov, V.V. (2008): A Stand-by Inundation Model of Kahului, Hawaii for NOAA Short-term Inundation Forecasting For Tsunamis (SIFT). NOAA Tech. Memo. OAR PMEL-XXX, 56p.

Tang, L., V.V. Titov, E. Bernard, Y. Wei, C. Chamberlin, J.C. Newman, H. Mofjeld, D. Arcas, M. Eble, C. Moore, B. Uslu, C. Pells, M.C. Spillane, L.M. Wright, and E. Gica (2012): Direct energy estimation of the 2011 Japan tsunami using deep-ocean pressure measurements. J. Geophys. Res., 117, C08008, doi: 10.1029/2011JC007635.

Tang, L., V.V. Titov, E. Bernard, Y. Wei, C. Chamberlin, J.C. Newman, H. Mofjeld, D. Arcas, M. Eble, C. Moore, B. Uslu, C. Pells, M.C. Spillane, L.M. Wright, and E. Gica (2012): Direct energy estimation of the 2011 Japan tsunami using deep-ocean pressure measurements. J. Geophys. Res., 117, C08008, doi: 10.1029/2011JC007635.

Tang, L., V.V. Titov, Y. Wei, H.O. Mofjeld, M. Spillane, D. Arcas, E.N. Bernard, C. Chamberlin, E. Gica and J. Newman (2008), Tsunami forecast analysis for the May 2006 Tonga tsunami, *Journal of Geophysical Research*, 113, C12015, doi: 10.1029/2008JC004922.

Taylor, L.A., B.W. Eakins, K.S. Carignan, R.R. Warnken, T. Sazonova, and D.C. Schoolcraft (2008), Digital elevation model for Monterey, California: procedures, data sources and analysis, prepared for the Pacific Marine Environmental Laboratory (PMEL) NOAA Center for Tsunami Research by the NOAA National Geophysical Data Center, 33p.

Titov, V.V. (2009), Tsunami forecasting, in *the Sea*, vol. 15, edited by E. Bernard, and A. Robinson, Chap. 12, pp. 367-396, Harvard Univ. Press, Cambridge, Mass.

Titov, V.V., Gonzalez, F.I., Bernard, E.N., Eble, M.C., Mofjeld, H.O., Newman, J.C. and Venturato, A.J. (2005). Real-time tsunami forecasting: challenges and solutions. Natural Hazards, 35(1), 41-58.

Titov, V.V., H.O. Mofjeld, F.I. Gonzalez and J.C. Newman (1999): Offshore forecasting of Alaska-Aleutian subduction zone tsunamis in Hawaii. NOAA Technical Memorandum. ERL PMEL-114, January 1999, 22 pp.

Tolkova, E., and W. Power (2011): Obtaining natural oscillatory modes of bays and harbors via Empirical Orthogonal Function analysis of tsunami wave fields. *Ocean Dynam.*, *61*(6), doi: 10.1007/s10236-011-0388-5, 731–751.

Uslu, B., J.C. Borrero, L.A. Dengler, and C.E. Synolakis (2007), Tsunami inundation at Crescent City, California generated by earthquake along the Cascadia Subduction Zone, *Geophy. Res. Lett.*, 34, L20601, doi:10.1029/2007GL030188.

Ward, S.N. and S. Simon (2005), Tsunami thoughts, Canadian Society of Exploration Geophysicists Recorder, 30(10), 38-44.

Wei, Y, E. N. Bernard, L. Tang, R. Weiss, V.V. Titov, C. Moore, M. Spillane, M. Hopkins and U. Kanoglu (2008): Real-time experimental forecast of the Peruvian tsunami of August 2007 for U.S. coastlines. *Geophys. Res. Lett*., *35*, L04609, doi: 10.1029/2007GL032250.

Wei, Y., C. Chamberlin, V. Titov, L. Tang, and E.N. Bernard (2013):_Modeling of the 2011 Japan tsunami - Lessons for near-field forecast. Pure Appl. Geophys., 170(6–8), doi: 10.1007/s00024-012-0519-z, 1309–1331.

Wei, Y., H. Fritz, V. Titov, B. Uslu, C. Chamberlin, and N. Kalligeris (2015): Source models and near-field impact of the April 1, 2007 solomon islands tsunami. Published online, Pure Appl. Geophys., doi: 10.1007/s00024-014-1013-6.

Working Group on California Earthquake Probabilities (2003), Earthquake Probabilities in the San Francisco Bay Region: 2002 -2031, U.S. Geological Survey Open File Report 03-214, 235p.

Figures:

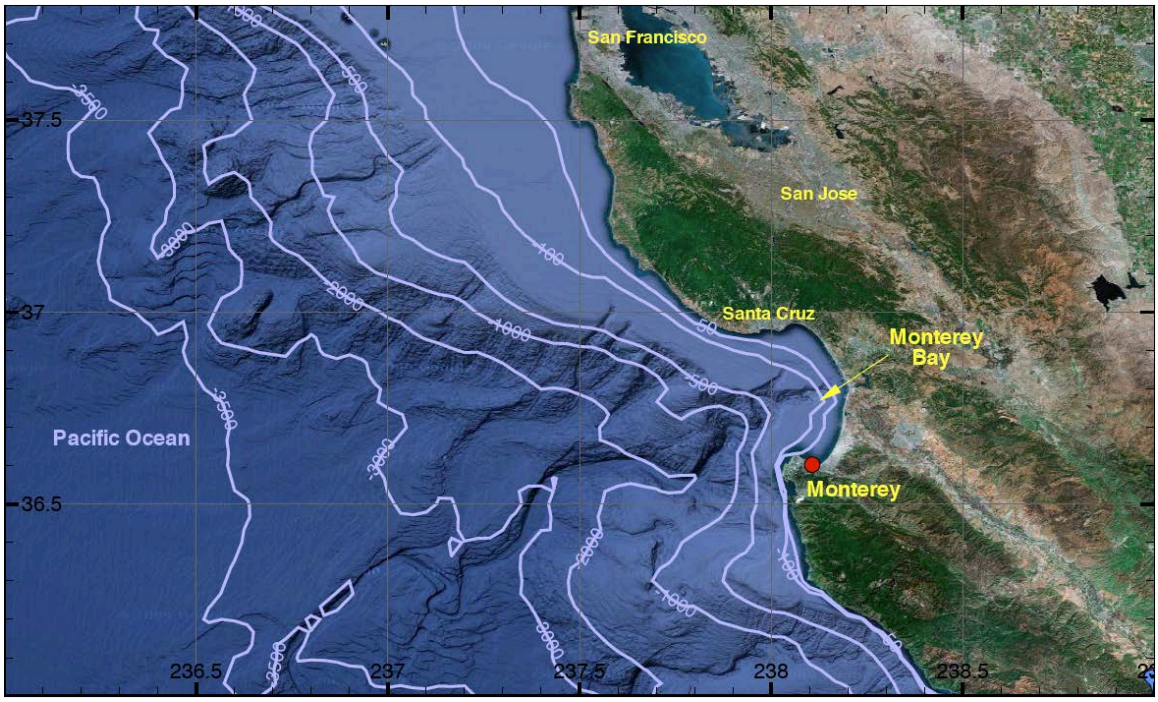

Figure 1 Location of Monterey, California.

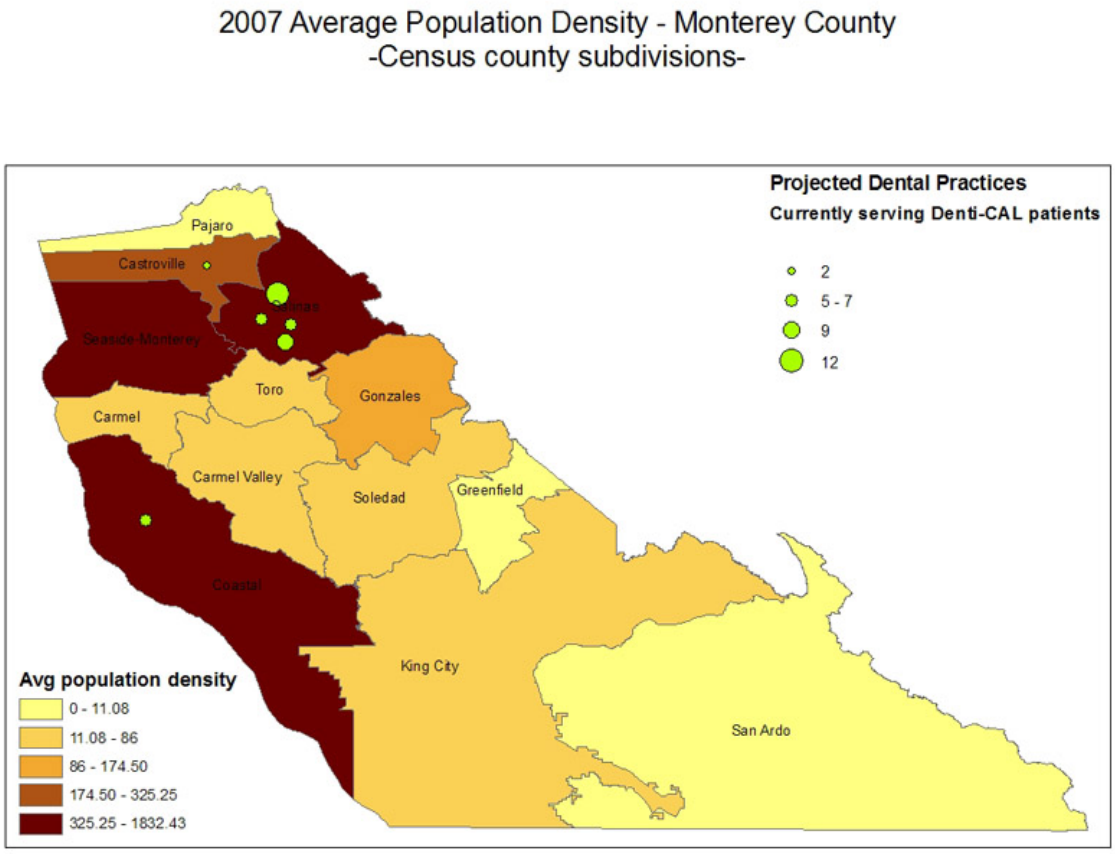

Figure 2 Average population density of Monterey County in 2007.

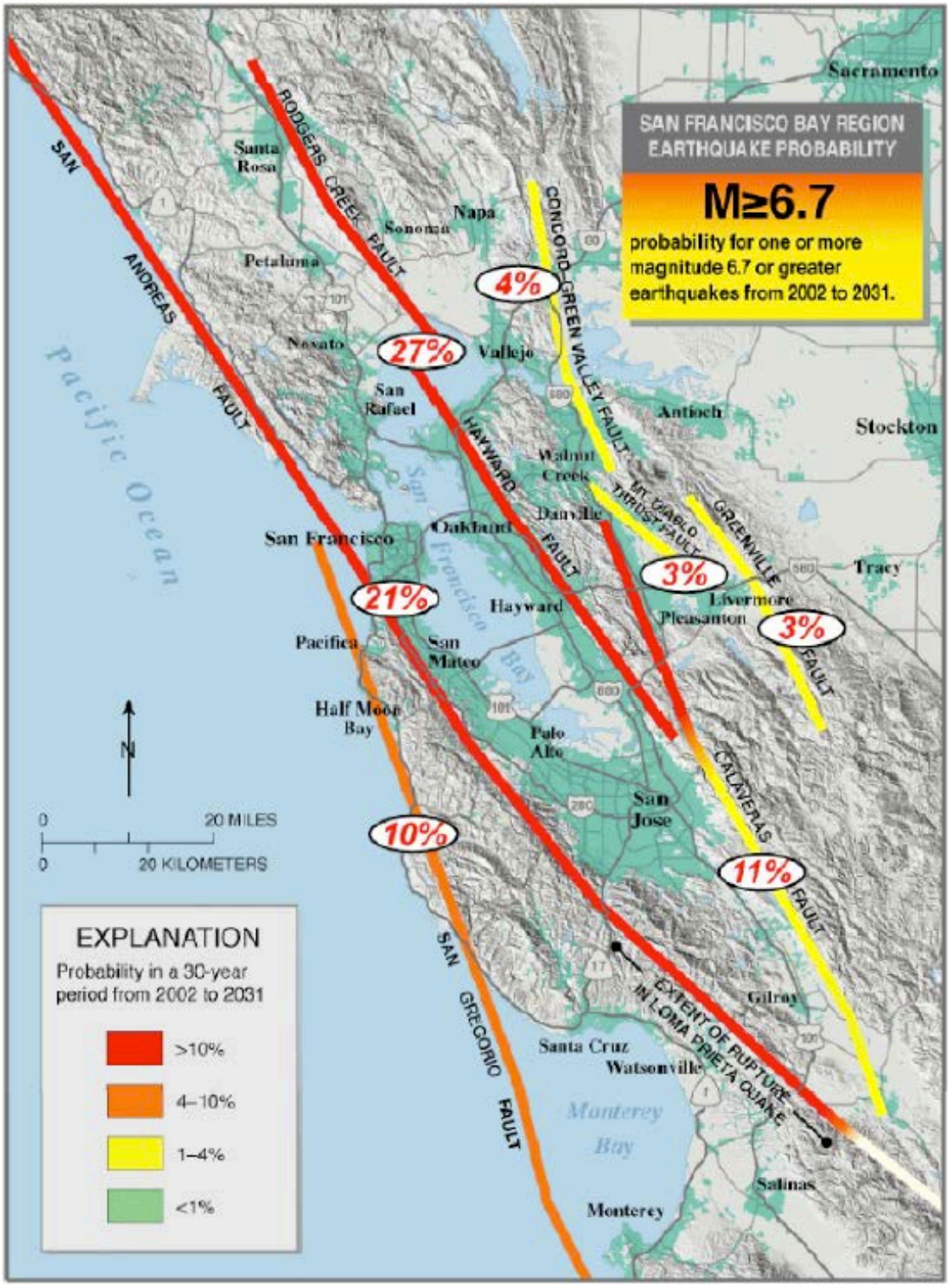

Figure 3. Probabilities of Mw 6.7 or stronger earthquakes occurring on faults in the San Francisco Bay Region during 2001-2031, where the probability of occurrence on each fault in indicated in ovals, and colors indicate the corresponding probabilities of each fault segment. Credit: Working Group on California Earthquake Probabilities (2003)

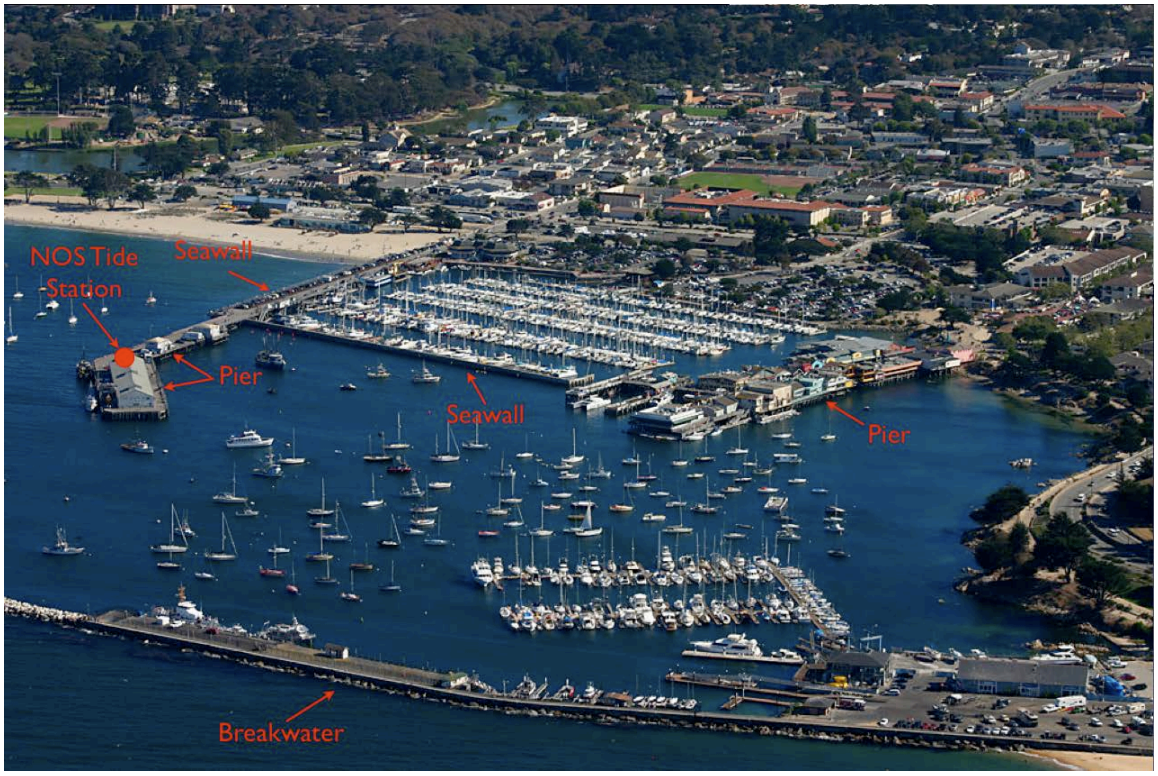

Figure 4 Aerial photo overlooking Monterey Harbor.

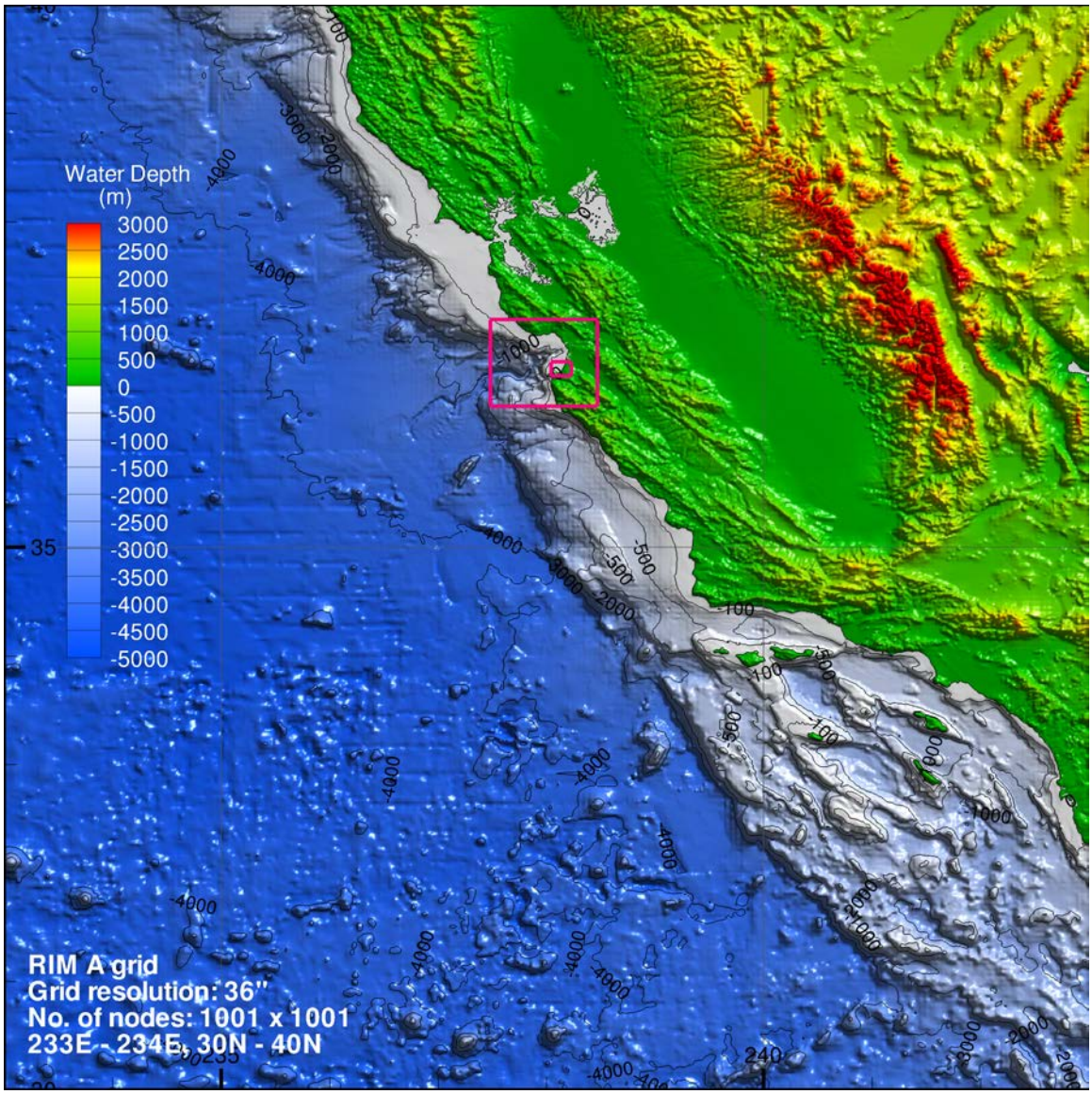

Figure 5 Bathymetry and topography of the outermost A grid for the reference model at Monterey, CA.

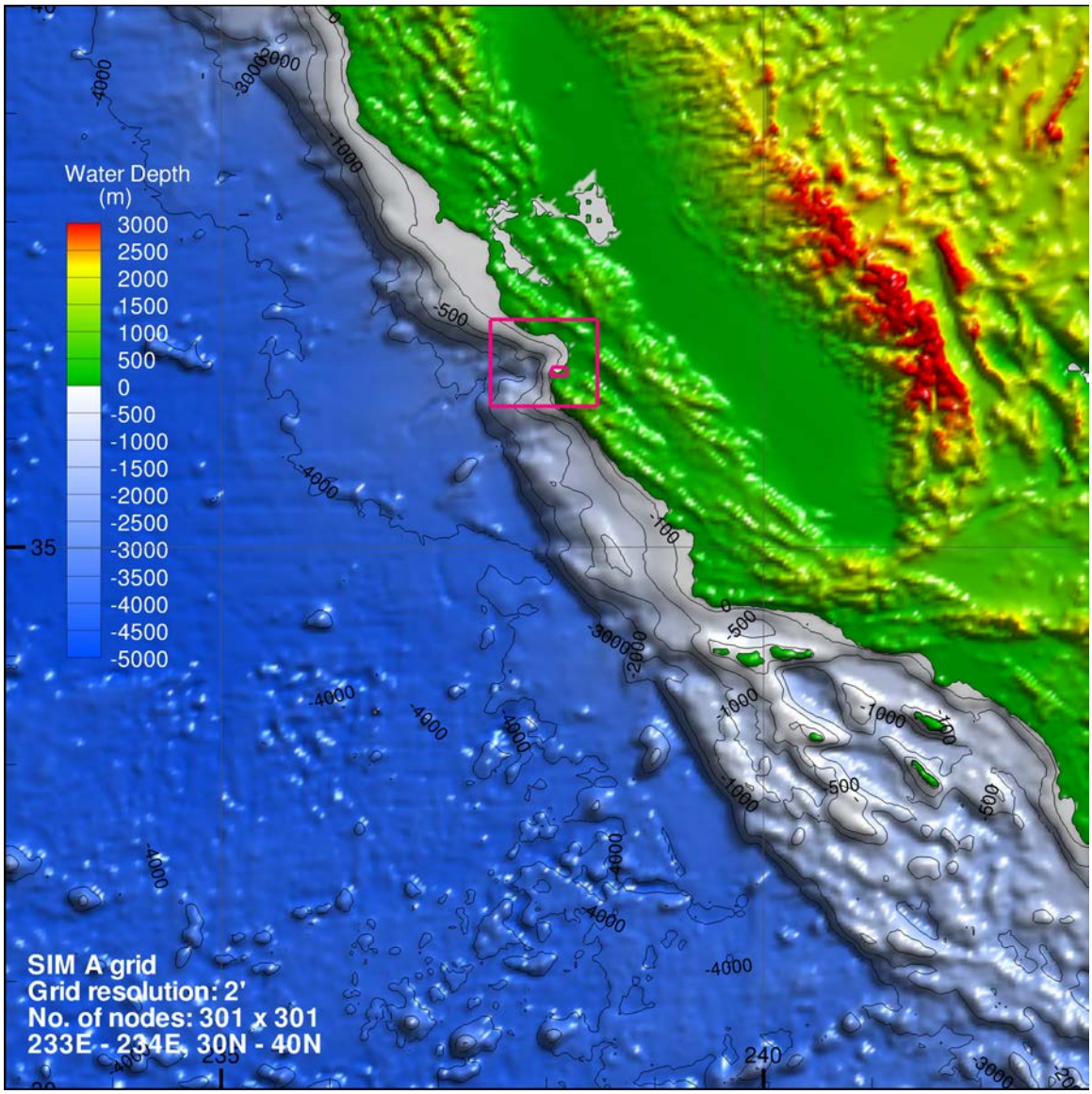

Figure 6 Bathymetry and topography of the outermost A grid for the optimized forecast model at Monterey, CA.

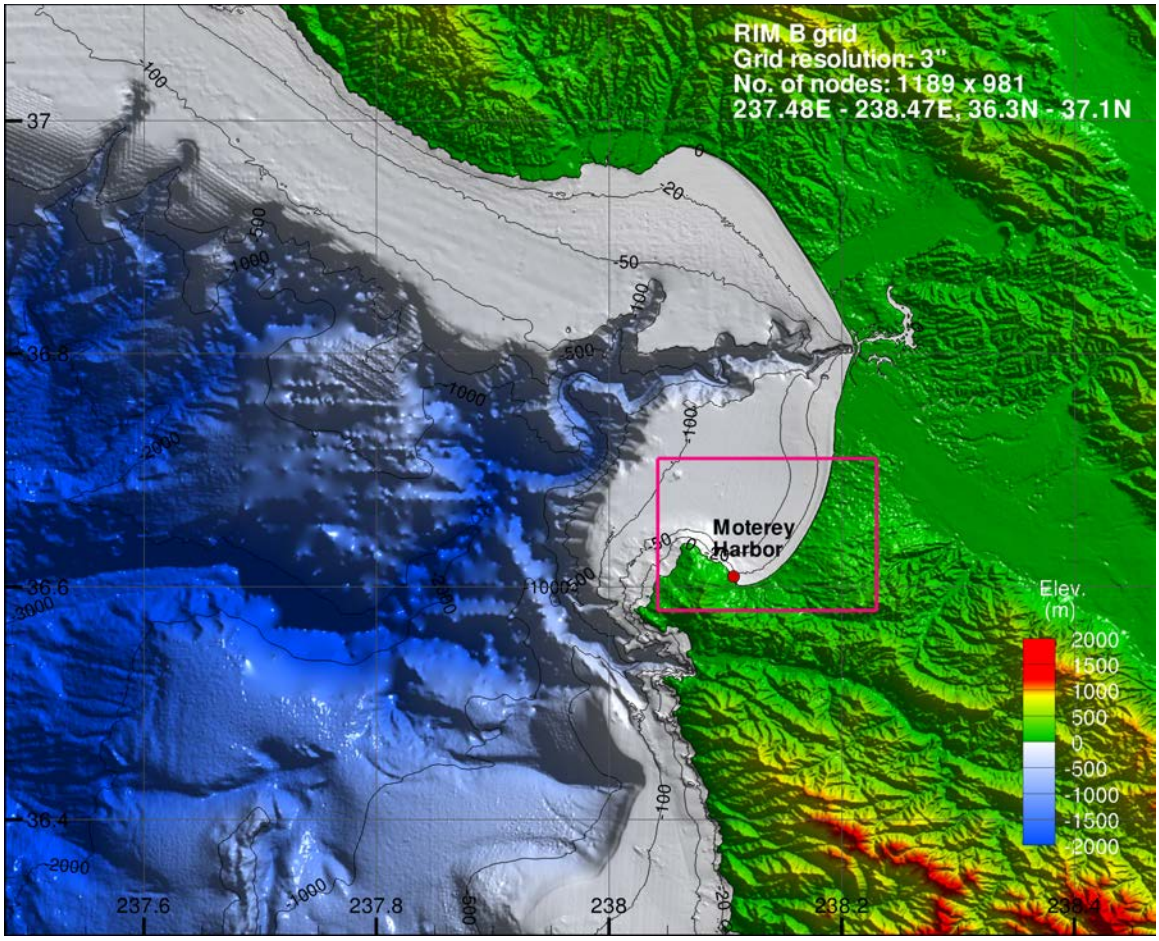

Figure 7 Bathymetry and topography of the intermediate B grid for the reference model at Monterey, CA.

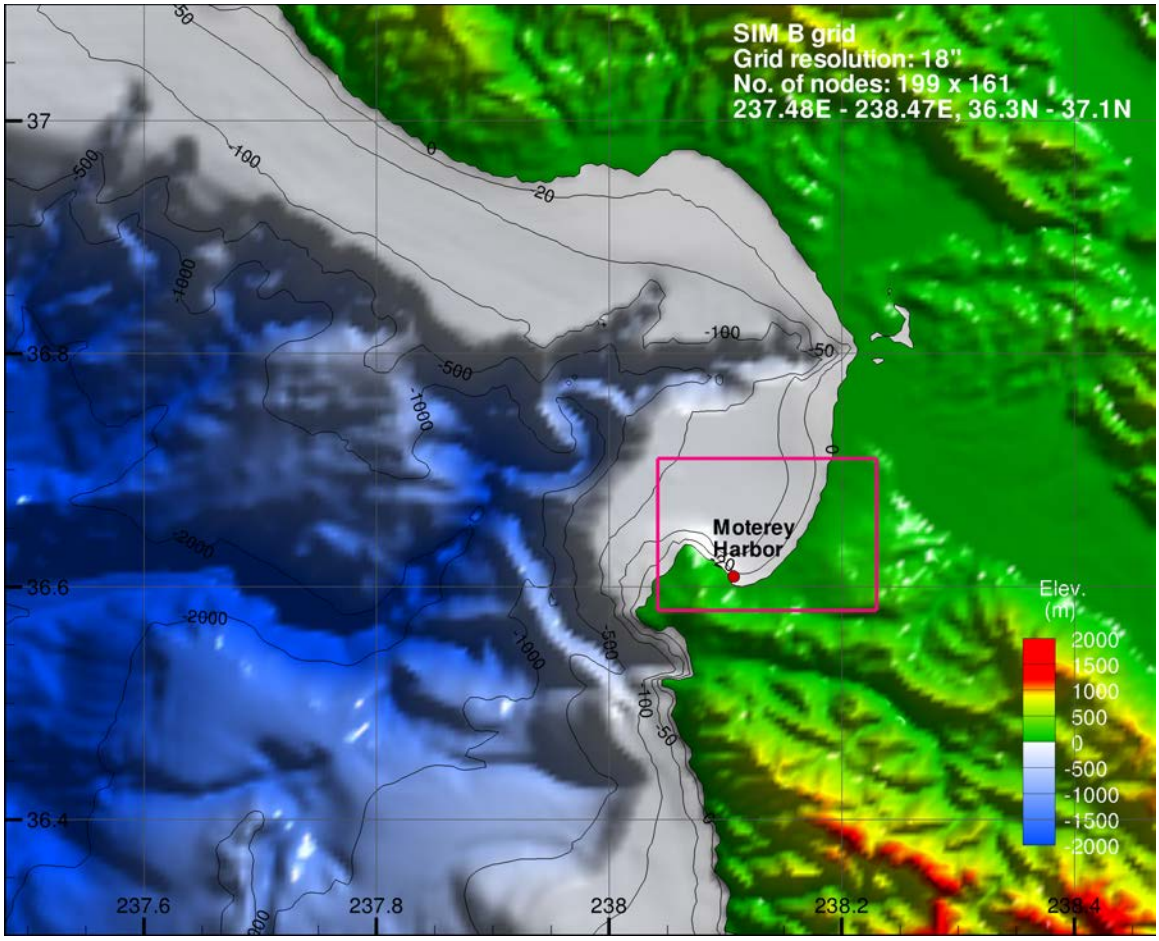

Figure 8 Bathymetry and topography of the intermediate B grid for the optimized forecast model at Monterey, CA.

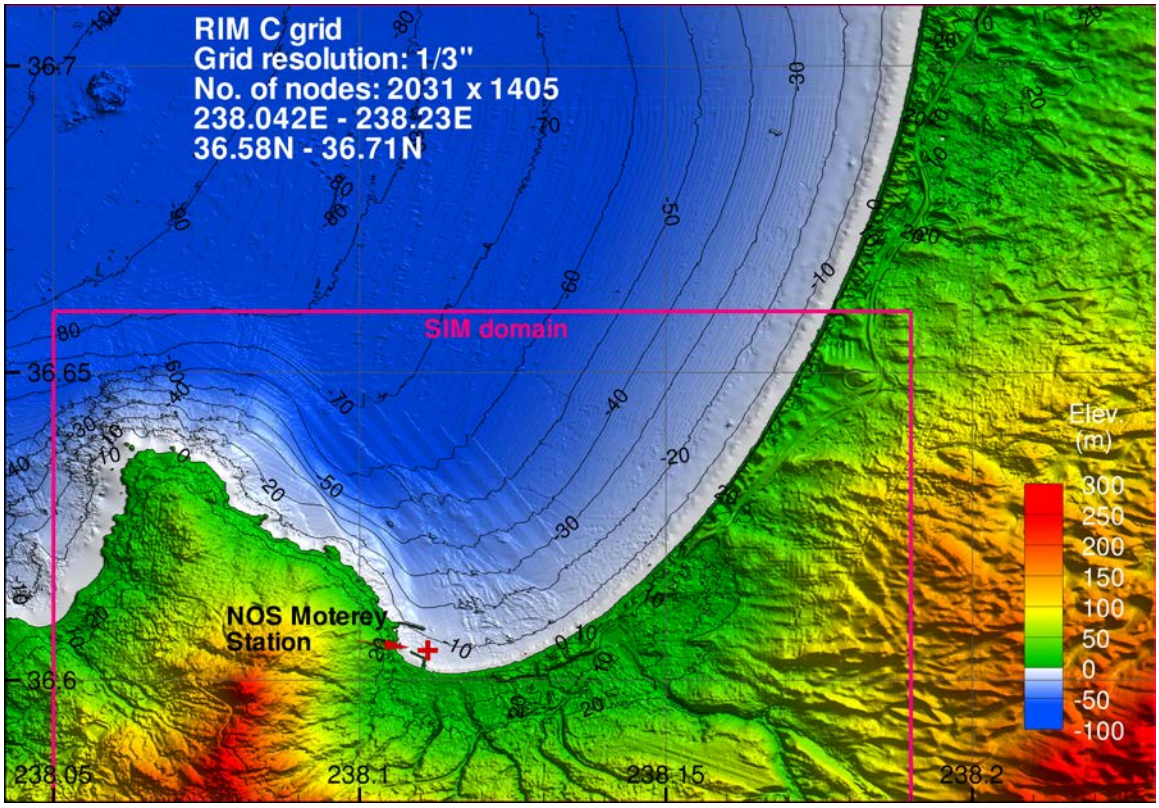

Figure 9 Bathymetry and topography of the innermost C grid for the reference model at Monterey, CA.

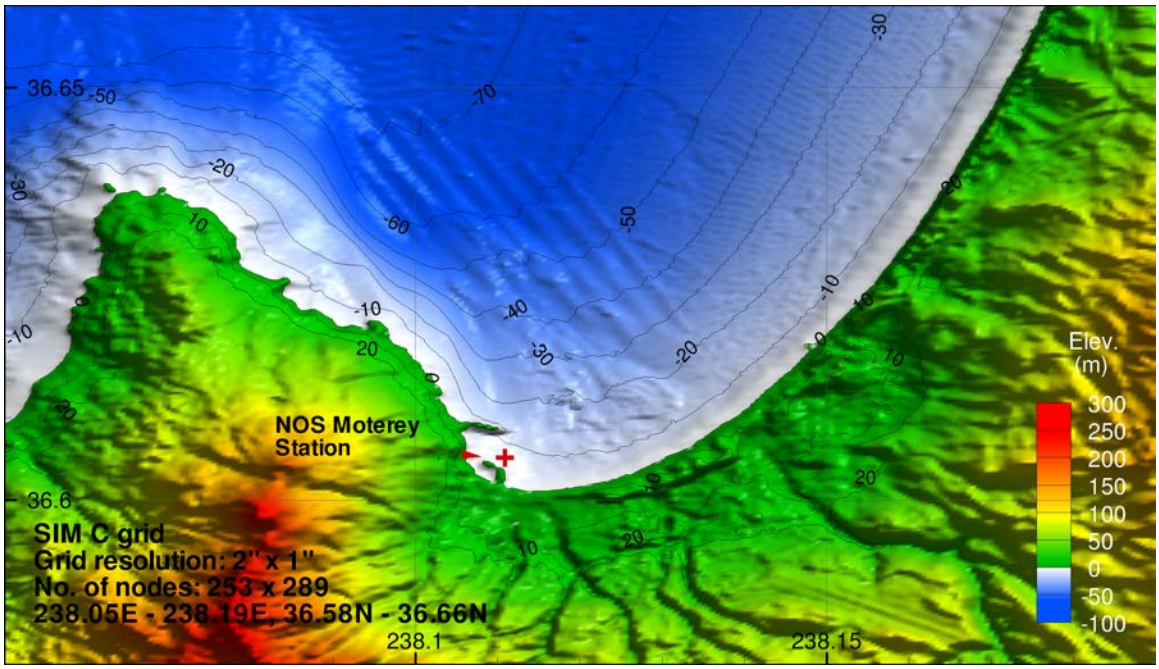

Figure 10 Bathymetry and topography of the innermost C grid for the optimized forecast model at Monterey, CA.

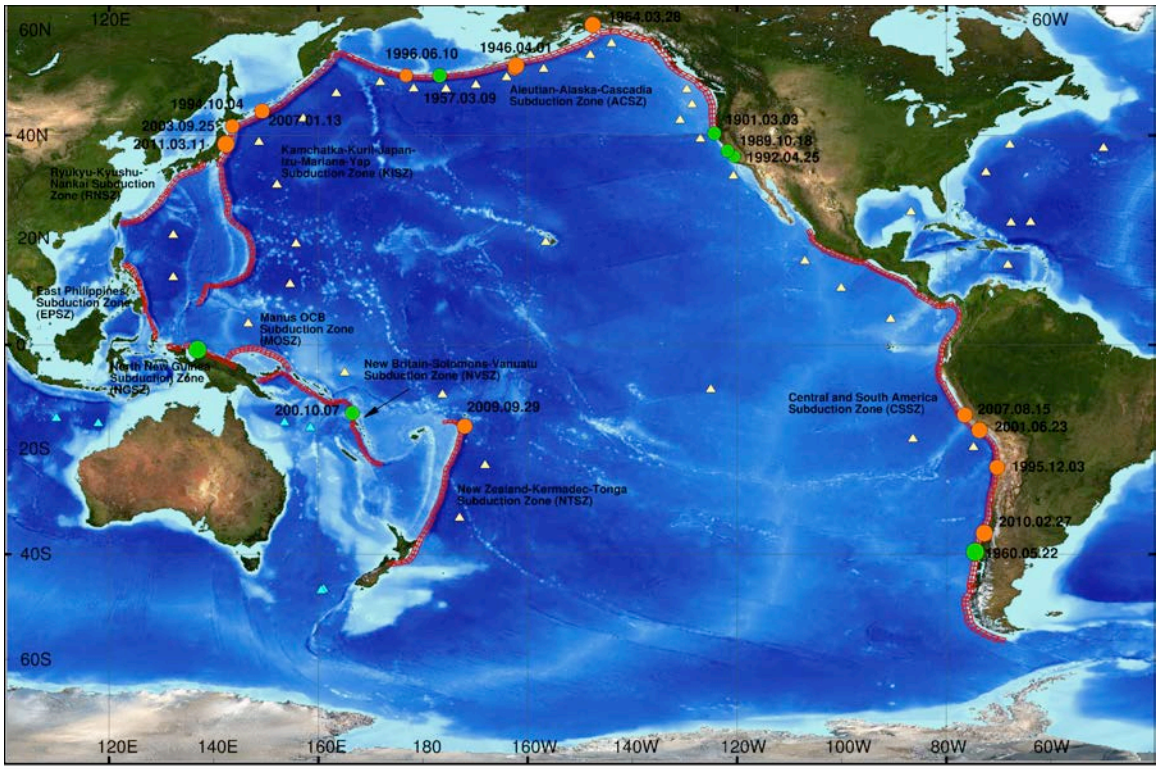

Figure 11 Location map of historical events.

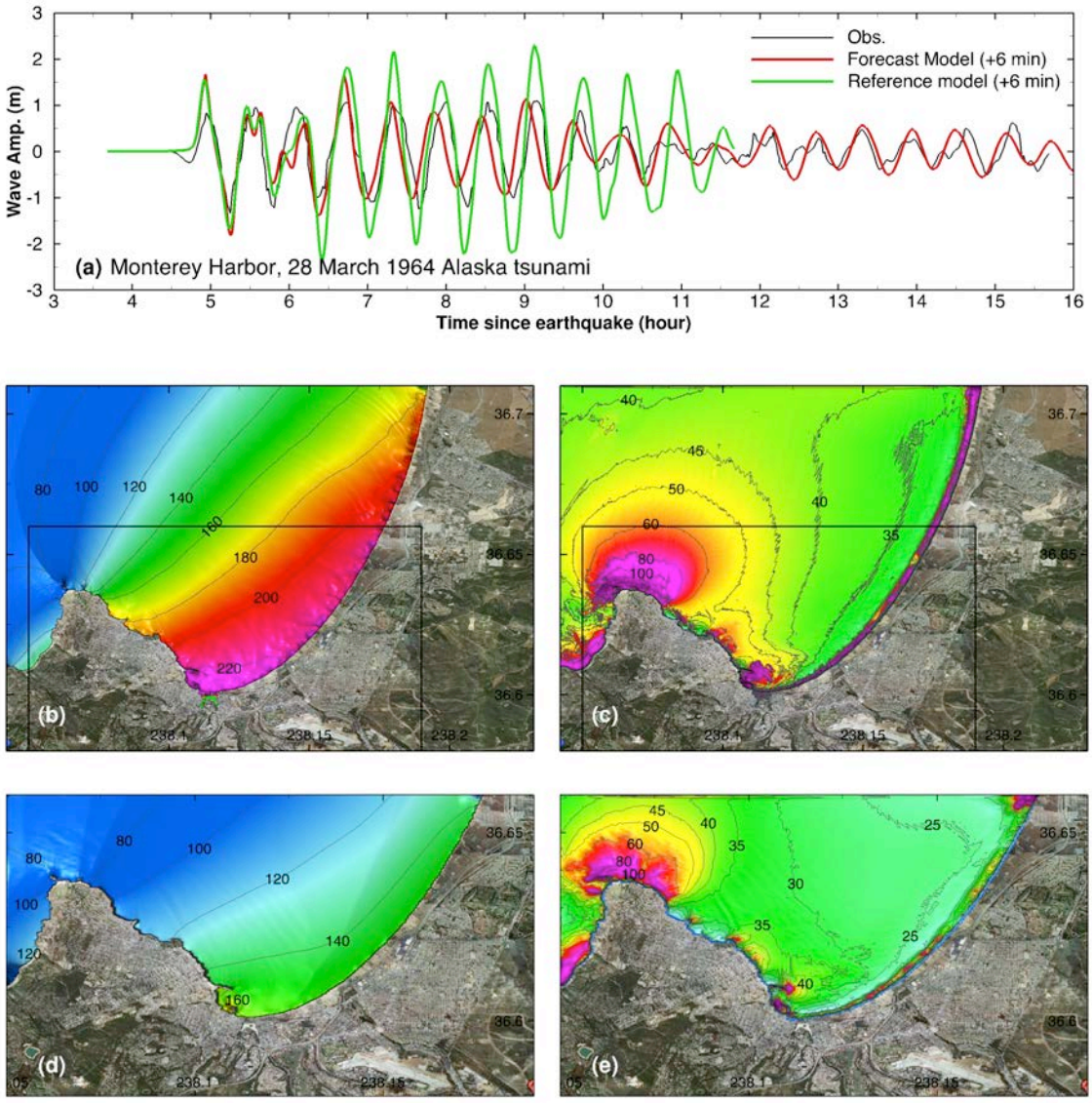

Figure 12 Model validation at Monterey for 28 March 1964 Alaska tsunami. (a) Computed and observed time series at Monterey tide station; (b) Computed maximum wave amplitude in grid C of the reference model; (c) Computed maximum current speed in grid C of the reference model; (d) Computed maximum wave amplitude in grid C of forecast model; (e) Computed current speed in grid C of forecast model. The black rectangular in (b) and (c) indicates the computational domain of forecast model grid C in (d) and (e).

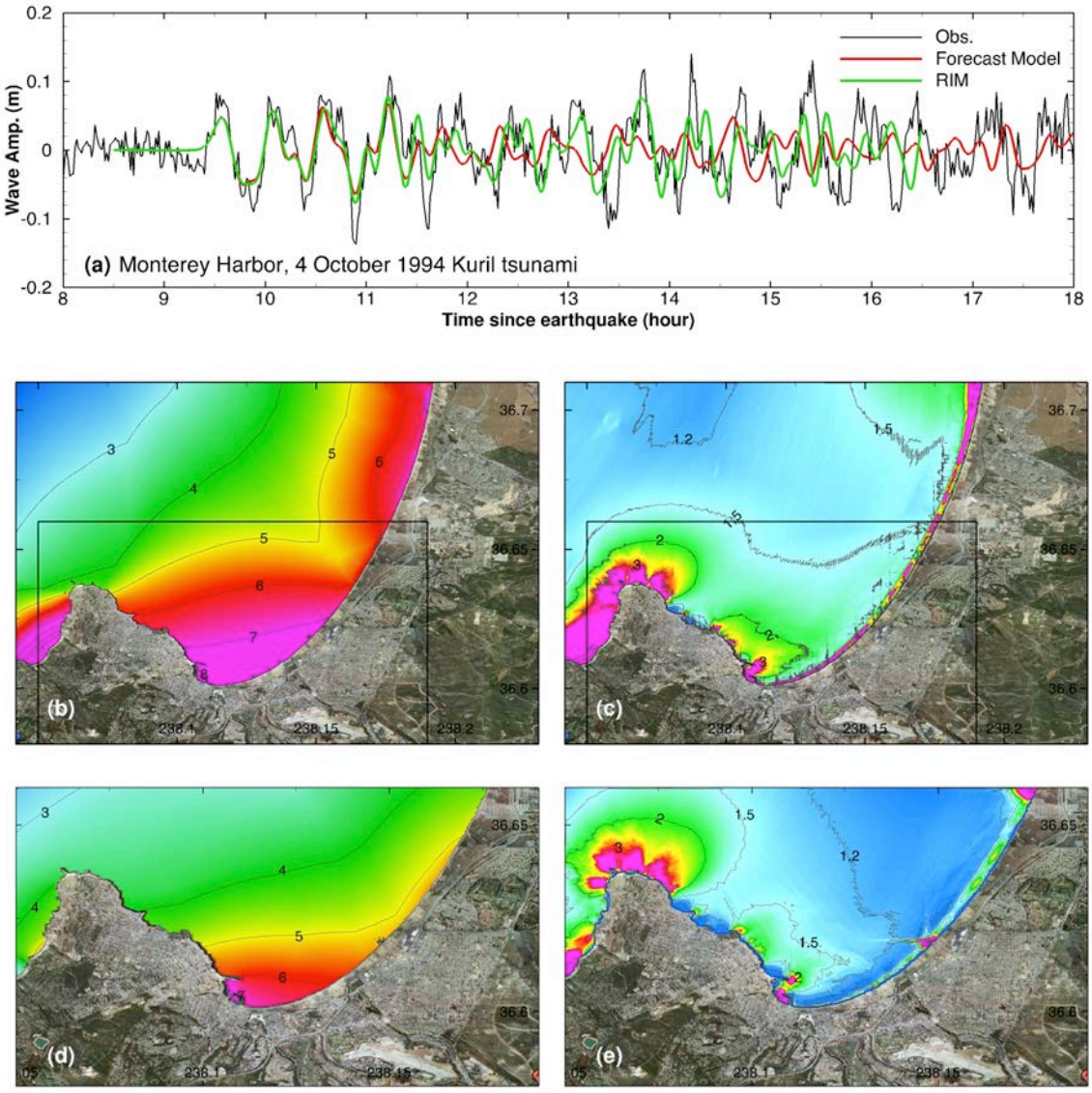

Figure 13 Model validation at Monterey for 4 October 1994 Kuril Islands tsunami. (a) Computed and observed time series at the Monterey tide station; (b) Computed maximum wave amplitude in C grid of the reference model; (c) Computed maximum current speed in C grid of the reference model; (d) Computed maximum wave amplitude in C grid of forecast model; (e) Computed current speed in C grid of forecast model. The black rectangular in (b) and (c) indicates the computational domain of forecast model C grid in (d) and (e).

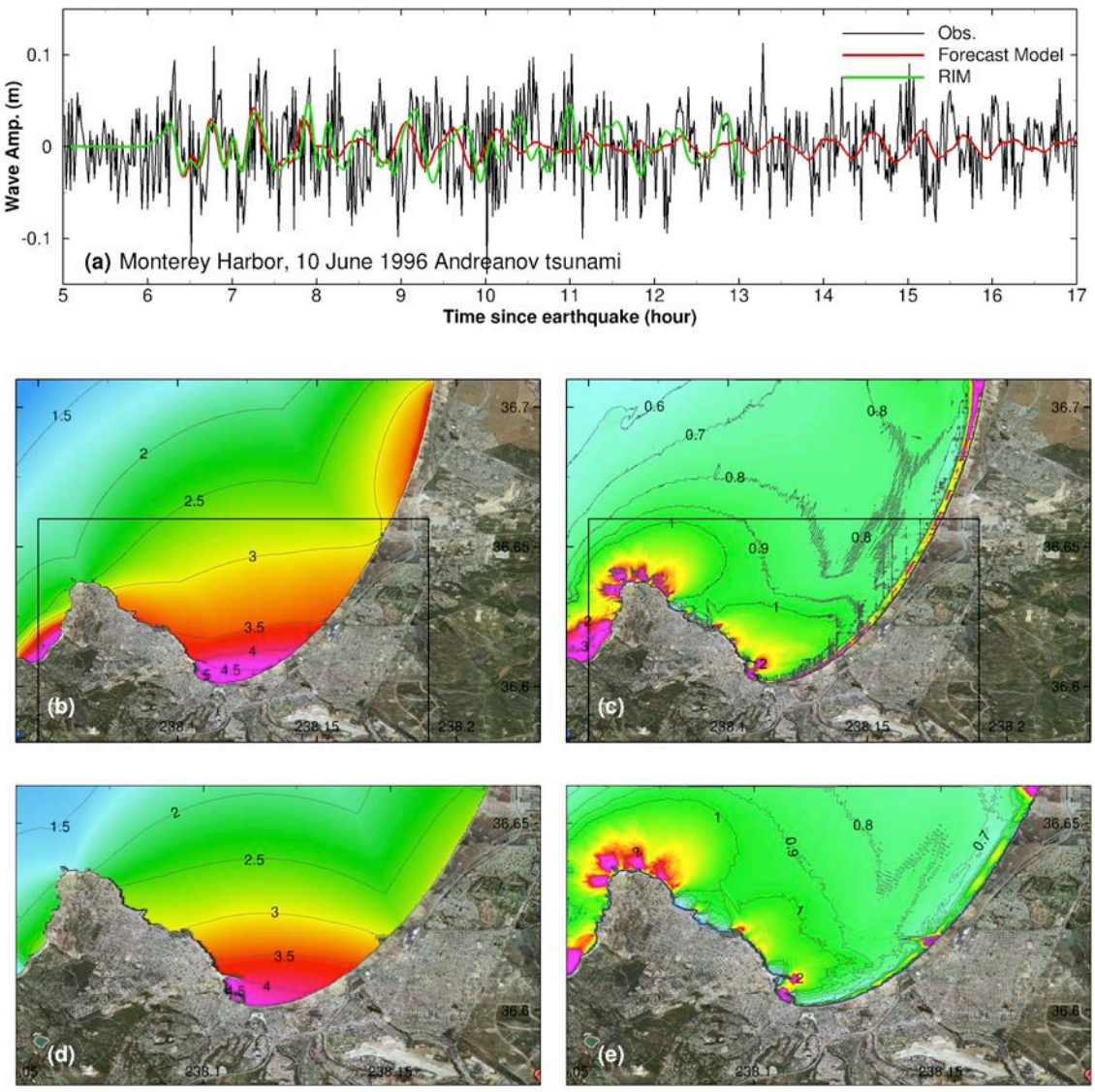

Figure 14 Model validation at Monterey for 4 October 1994 Kuril Islands tsunami. (a) Computed and observed time series at the Monterey tide station; (b) Computed maximum wave amplitude in C grid of the reference model; (c) Computed maximum current speed in C grid of the reference model; (d) Computed maximum wave amplitude in C grid of forecast model; (e) Computed current speed in C grid of forecast model. The black rectangular in (b) and (c) indicates the computational domain of forecast model C grid in (d) and (e).

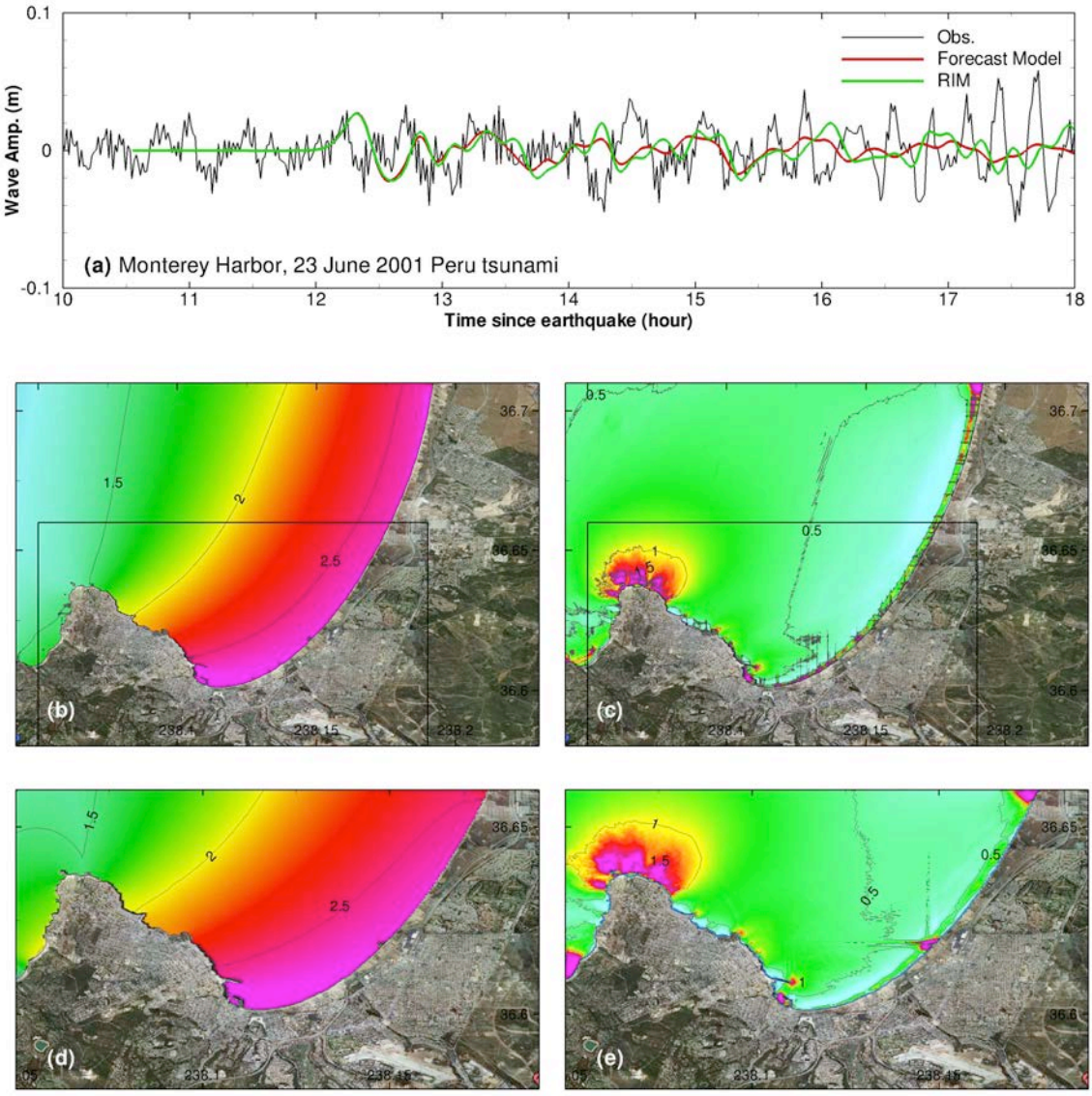

Figure 15 Model validation at Monterey for 23 June 2001 Peru tsunami. (a) Computed and observed time series at the Monterey tide station; (b) Computed maximum wave amplitude in C grid of the reference model; (c) Computed maximum current speed in C grid of the reference model; (d) Computed maximum wave amplitude in C grid of forecast model; (e) Computed current speed in C grid of forecast model. The black rectangular in (b) and (c) indicates the computational domain of forecast model C grid in (d) and (e).

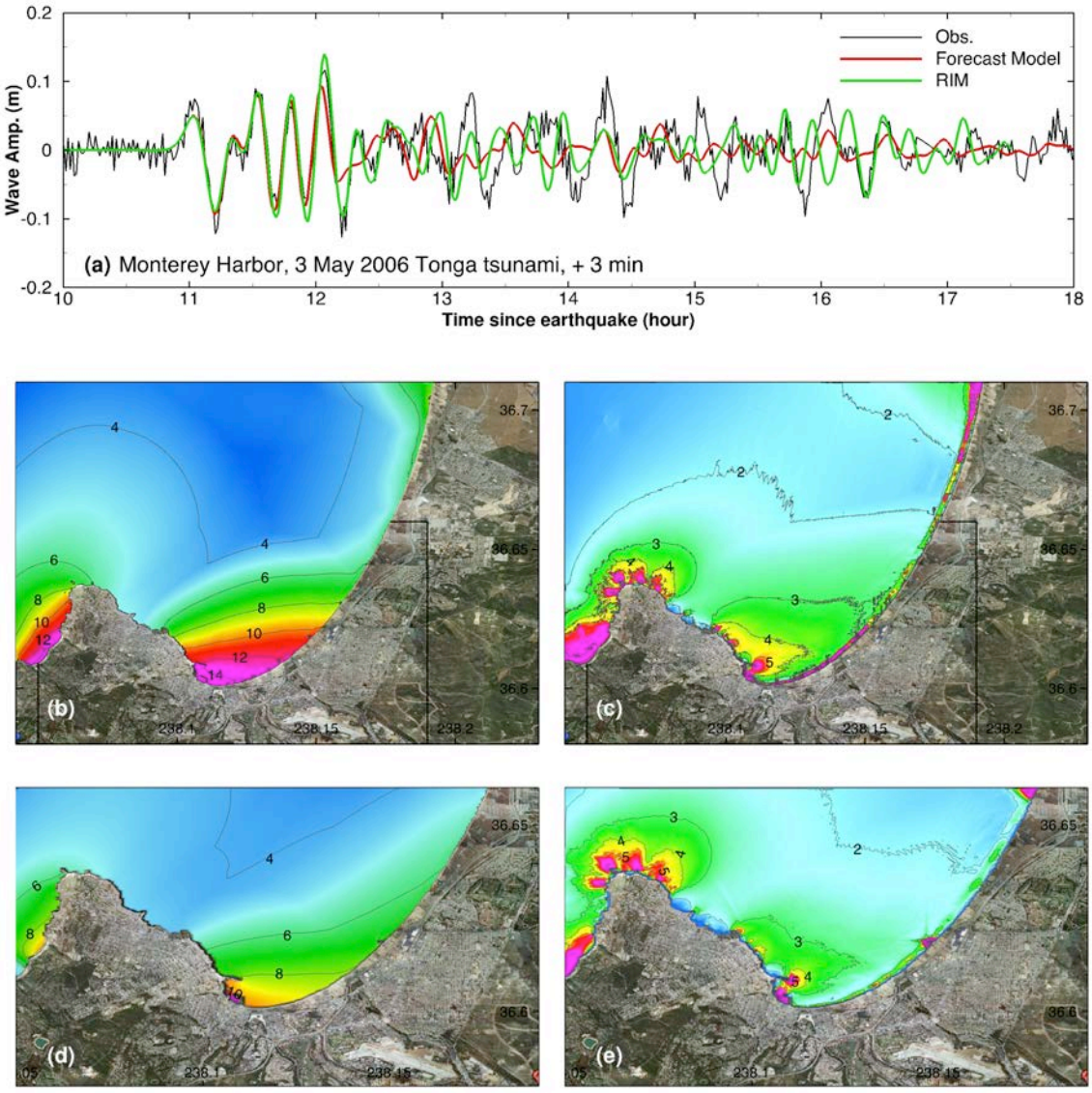

Figure 16 Model validation at Monterey for 3 May 2006 Tonga tsunami. (a) Computed and observed time series at the Monterey tide station; (b) Computed maximum wave amplitude in C grid of the reference model; (c) Computed maximum current speed in C grid of the reference model; (d) Computed maximum wave amplitude in C grid of forecast model; (e) Computed current speed in C grid of forecast model. The black rectangular in (b) and (c) indicates the computational domain of forecast model C grid in (d) and (e).

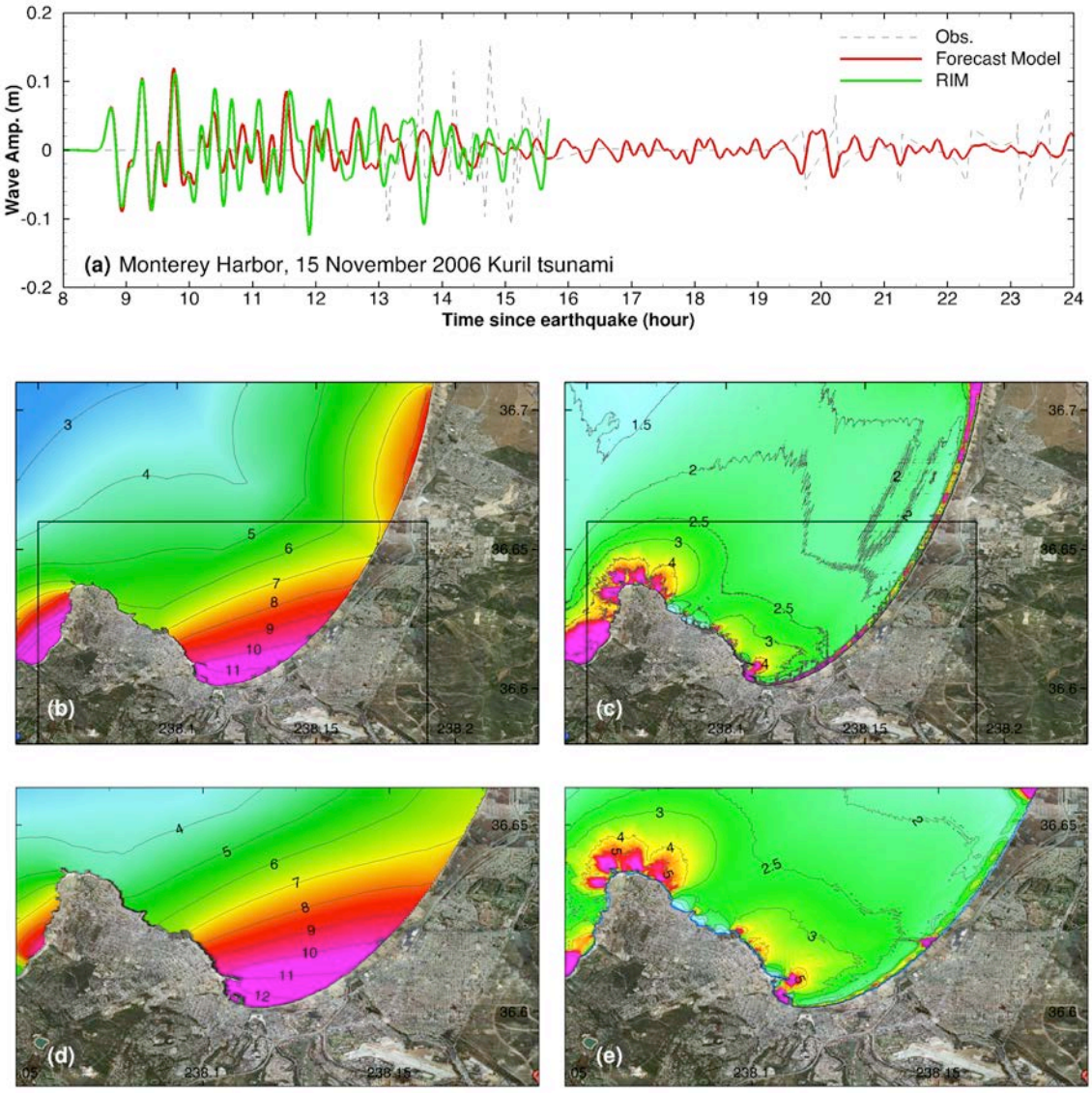

Figure 17 Model validation at Monterey for 11 November 2006 Kuril Islands tsunami. (a) Computed and observed time series at the Monterey tide station; (b) Computed maximum wave amplitude in C grid of the reference model; (c) Computed maximum current speed in C grid of the reference model; (d) Computed maximum wave amplitude in C grid of forecast model; (e) Computed current speed in C grid of forecast model. The black rectangular in (b) and (c) indicates the computational domain of forecast model C grid in (d) and (e).

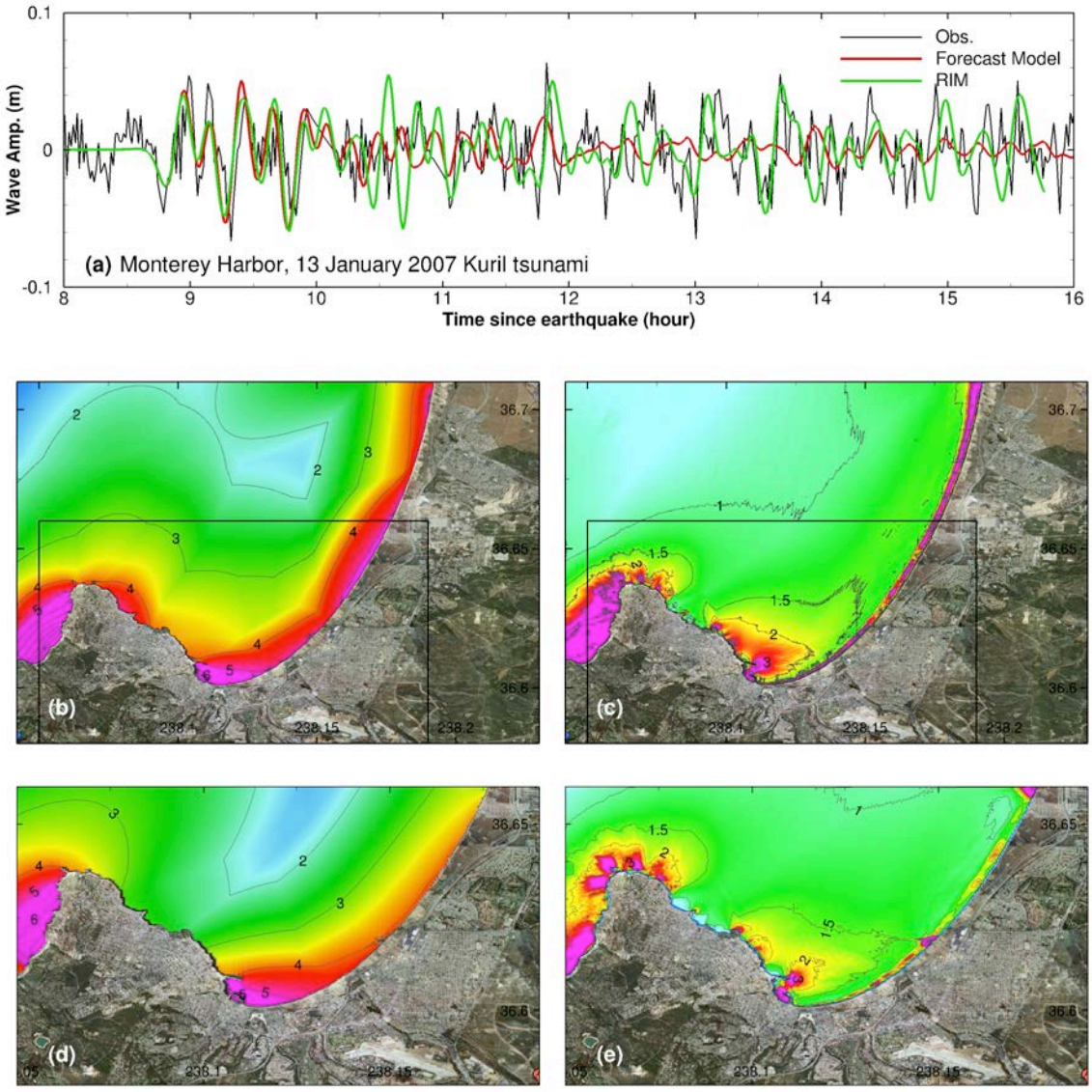

Figure 18 Model validation at Monterey for 13 January 2007 Kuril Islands tsunami. (a) Computed and observed time series at the Monterey tide station; (b) Computed maximum wave amplitude in C grid of the reference model; (c) Computed maximum current speed in C grid of the reference model; (d) Computed maximum wave amplitude in C grid of forecast model; (e) Computed current speed in C grid of forecast model. The black rectangular in (b) and (c) indicates the computational domain of forecast model C grid in (d) and (e).

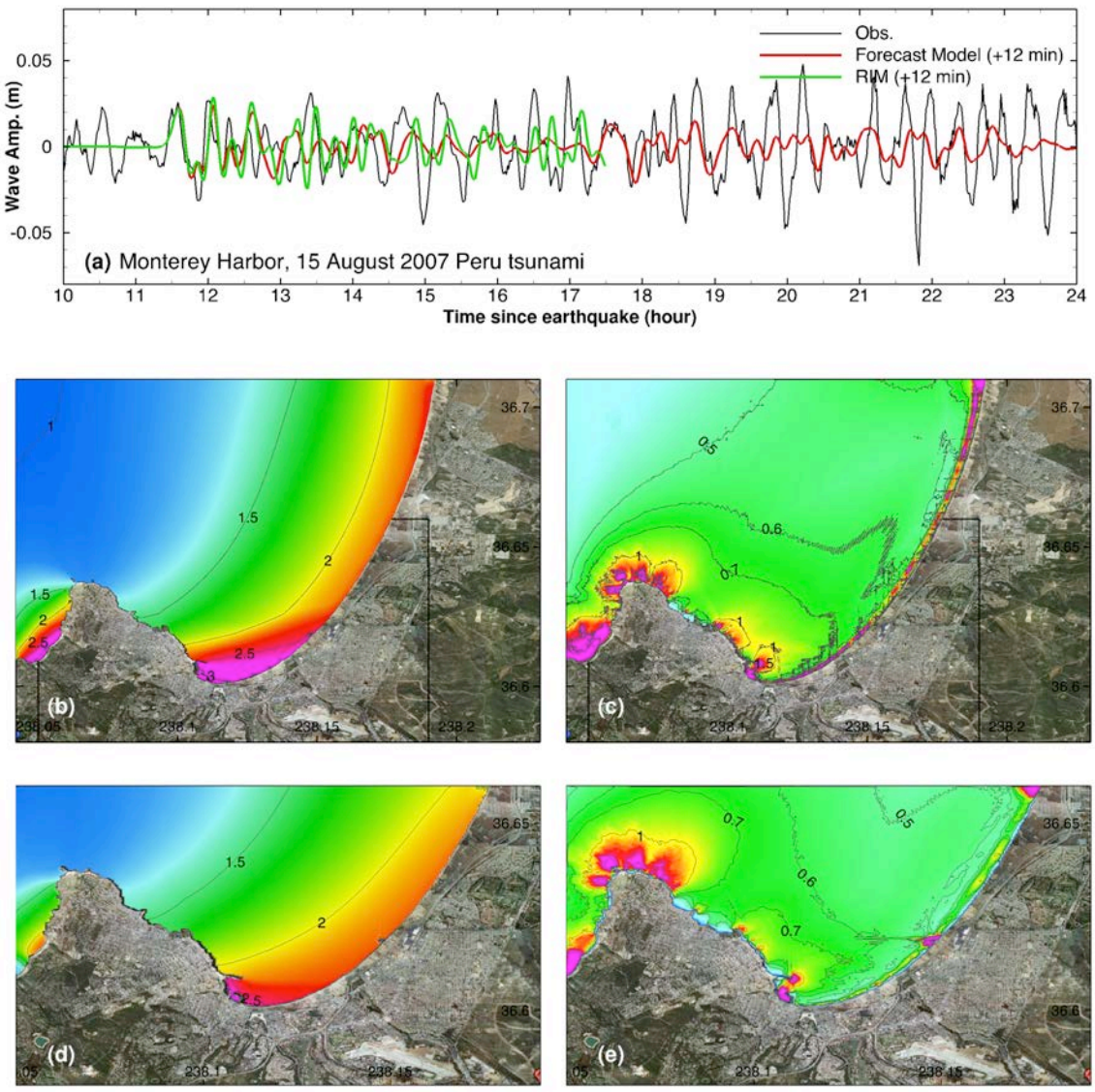

Figure 19 Model validation at Monterey for 15 August 2007 Peru tsunami. (a) Computed and observed time series at the Monterey tide station; (b) Computed maximum wave amplitude in C grid of the reference model; (c) Computed maximum current speed in C grid of the reference model; (d) Computed maximum wave amplitude in C grid of forecast model; (e) Computed current speed in C grid of forecast model. The black rectangular in (b) and (c) indicates the computational domain of forecast model C grid in (d) and (e).

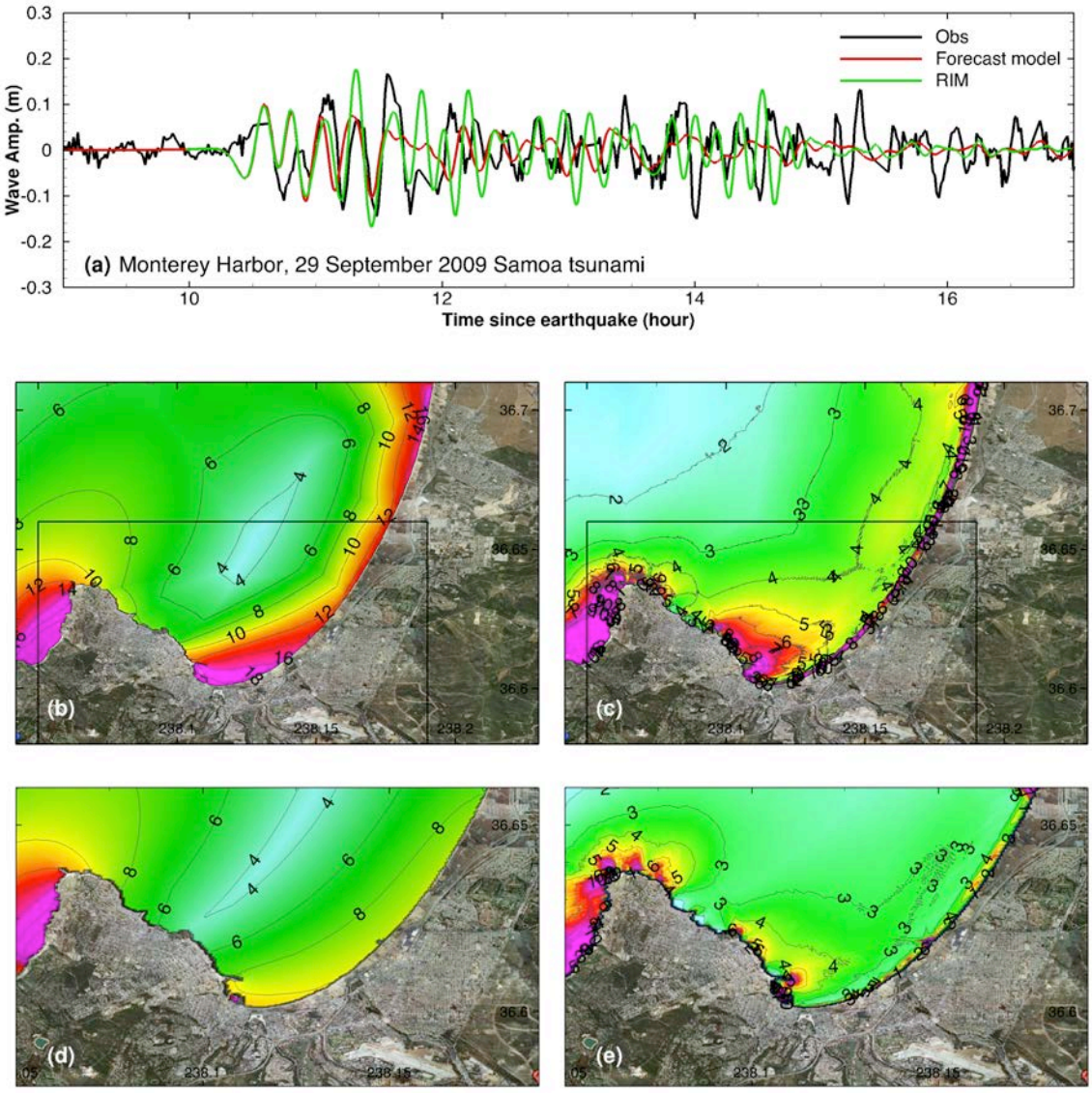

Figure 20 Model validation at Monterey for 29 September 2009 Samoa tsunami. (a) Computed and observed time series at the Monterey tide station; (b) Computed maximum wave amplitude in C grid of the reference model; (c) Computed maximum current speed in C grid of the reference model; (d) Computed maximum wave amplitude in C grid of forecast model; (e) Computed current speed in C grid of forecast model. The black rectangular in (b) and (c) indicates the computational domain of forecast model C grid in (d) and (e).

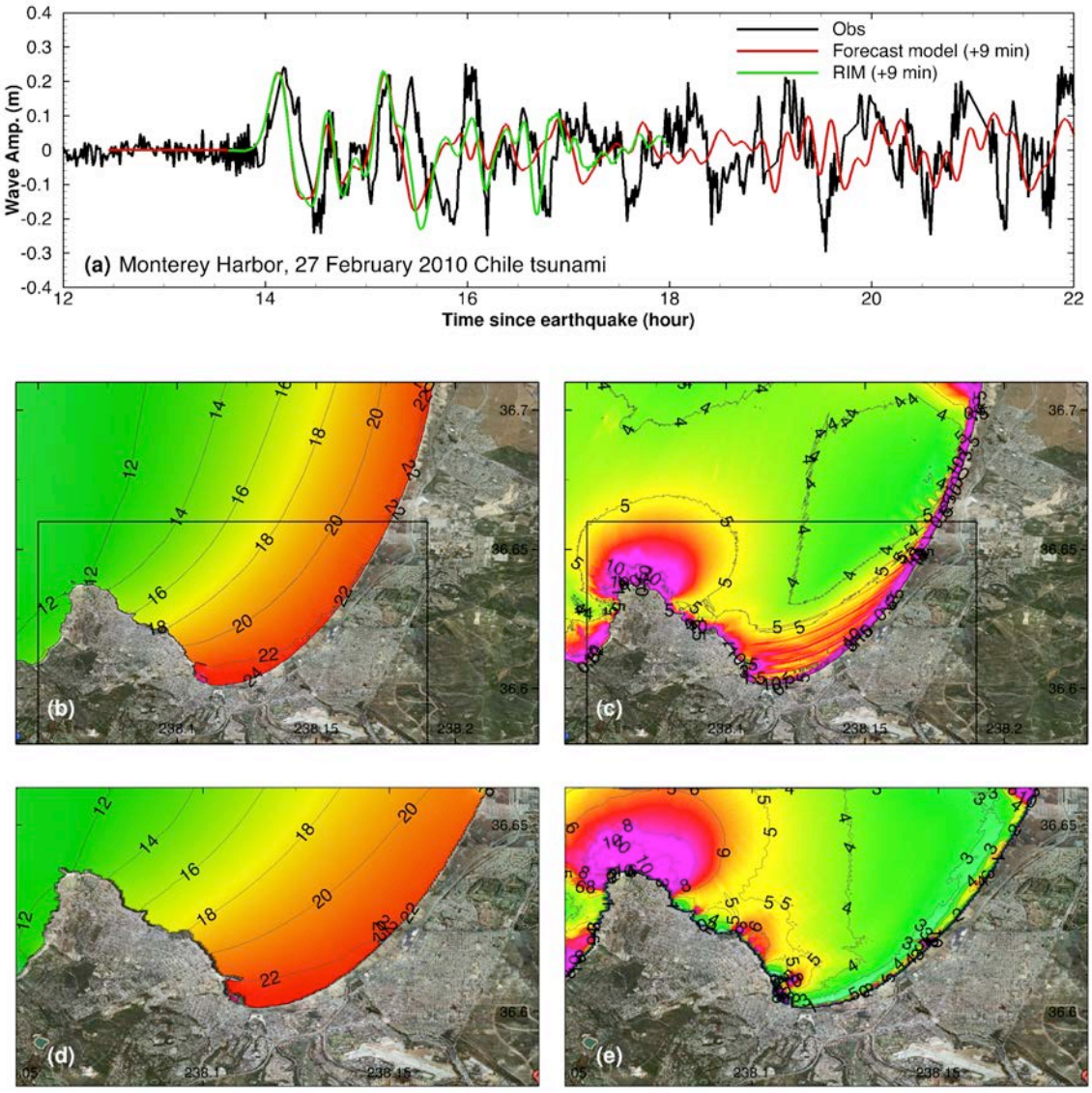

Figure 21 Model validation at Monterey for 27 February 2010 Chile tsunami. (a) Computed and observed time series at the Monterey tide station; (b) Computed maximum wave amplitude in C grid of the reference model; (c) Computed maximum current speed in C grid of the reference model; (d) Computed maximum wave amplitude in C grid of forecast model; (e) Computed current speed in C grid of forecast model. The black rectangular in (b) and (c) indicates the computational domain of forecast model C grid in (d) and (e).

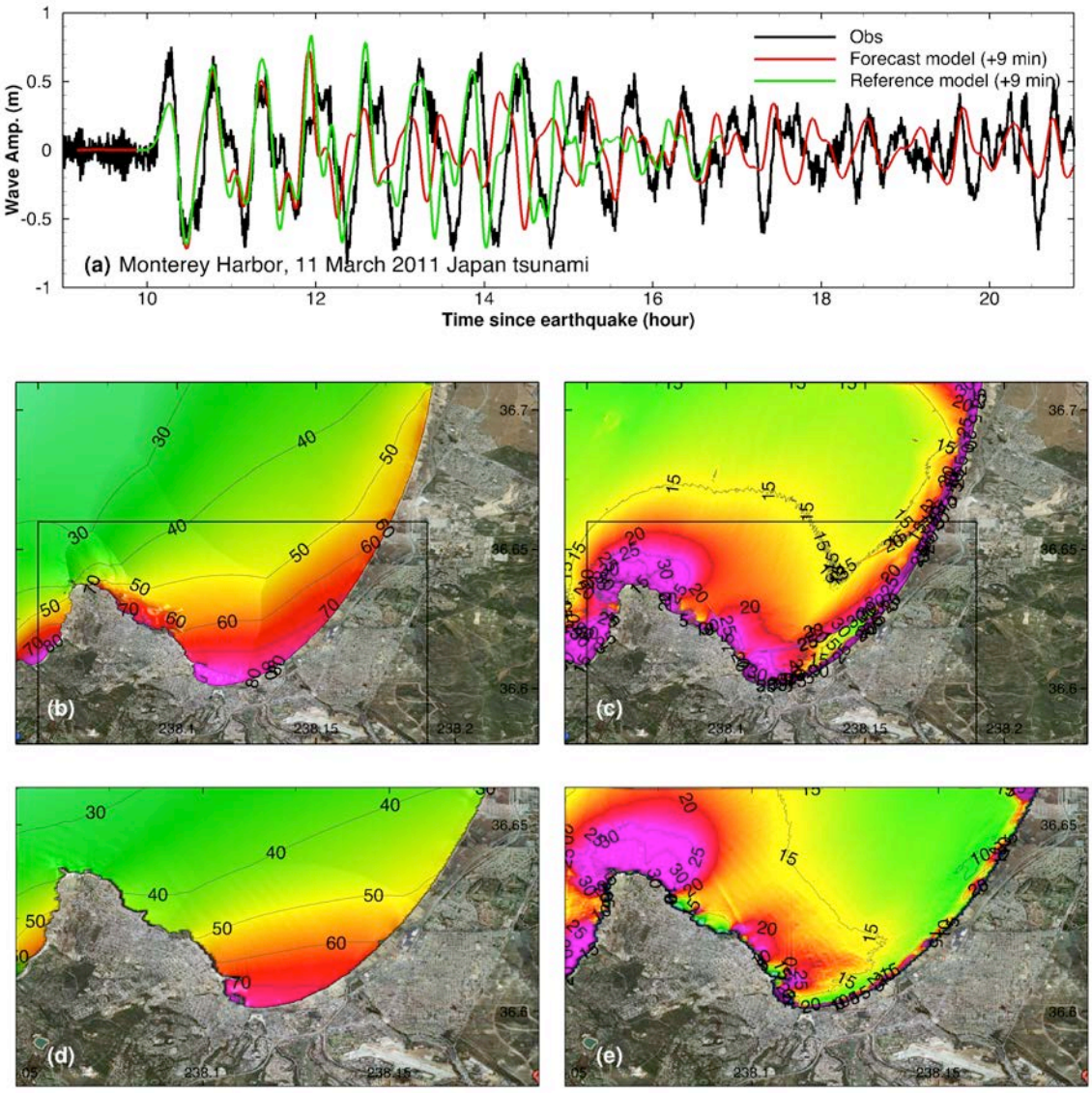

Figure 22 Model validation at Monterey for 11 March 2011 Japan tsunami. (a) Computed and observed time series at the Monterey tide station; (b) Computed maximum wave amplitude in C grid of the reference model; (c) Computed maximum current speed in C grid of the reference model; (d) Computed maximum wave amplitude in C grid of forecast model; (e) Computed current speed in C grid of forecast model. The black rectangular in (b) and (c) indicates the computational domain of forecast model C grid in (d) and (e).

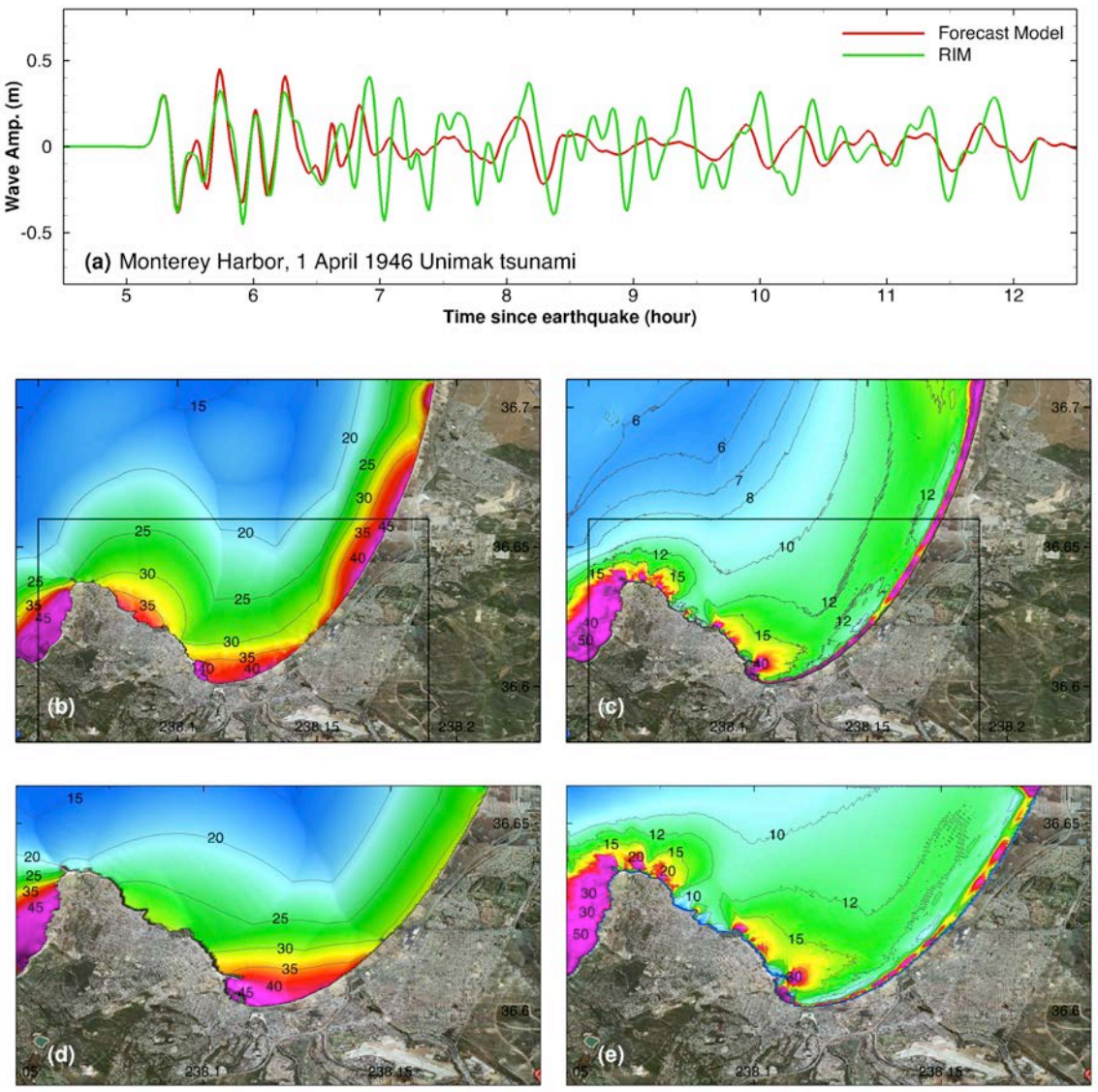

Figure 23 Model results at Monterey for 1 April 1946 Alaska tsunami. (a) Computed and observed time series at the Monterey tide station; (b) Computed maximum wave amplitude in C grid of the reference model; (c) Computed maximum current speed in C grid of the reference model; (d) Computed maximum wave amplitude in C grid of forecast model; (e) Computed current speed in C grid of forecast model. The black rectangular in (b) and (c) indicates the computational domain of forecast model C grid in (d) and (e).

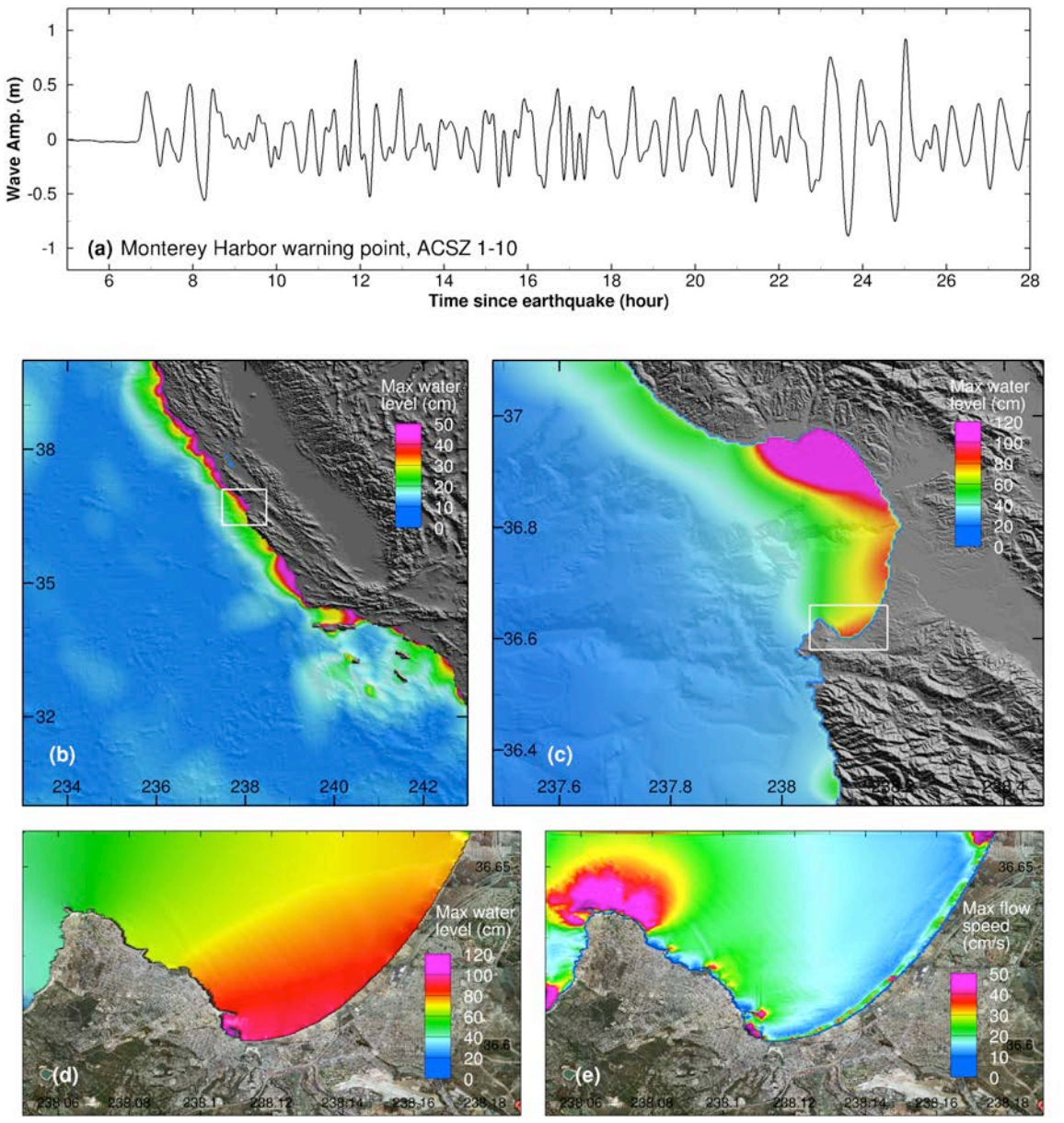

Figure 24 Model stability testing results at Monterey for synthetic mega tsunami scenario ACSZ 1-10. (a) Computed time series at the Monterey warning point; (b) Computed maximum wave amplitude in A grid of the forecast model; (c) Computed maximum current speed in B grid of the forecast model; (d) Computed maximum wave amplitude in C grid of the forecast model; (e) Computed current speed in C grid of the forecast model.

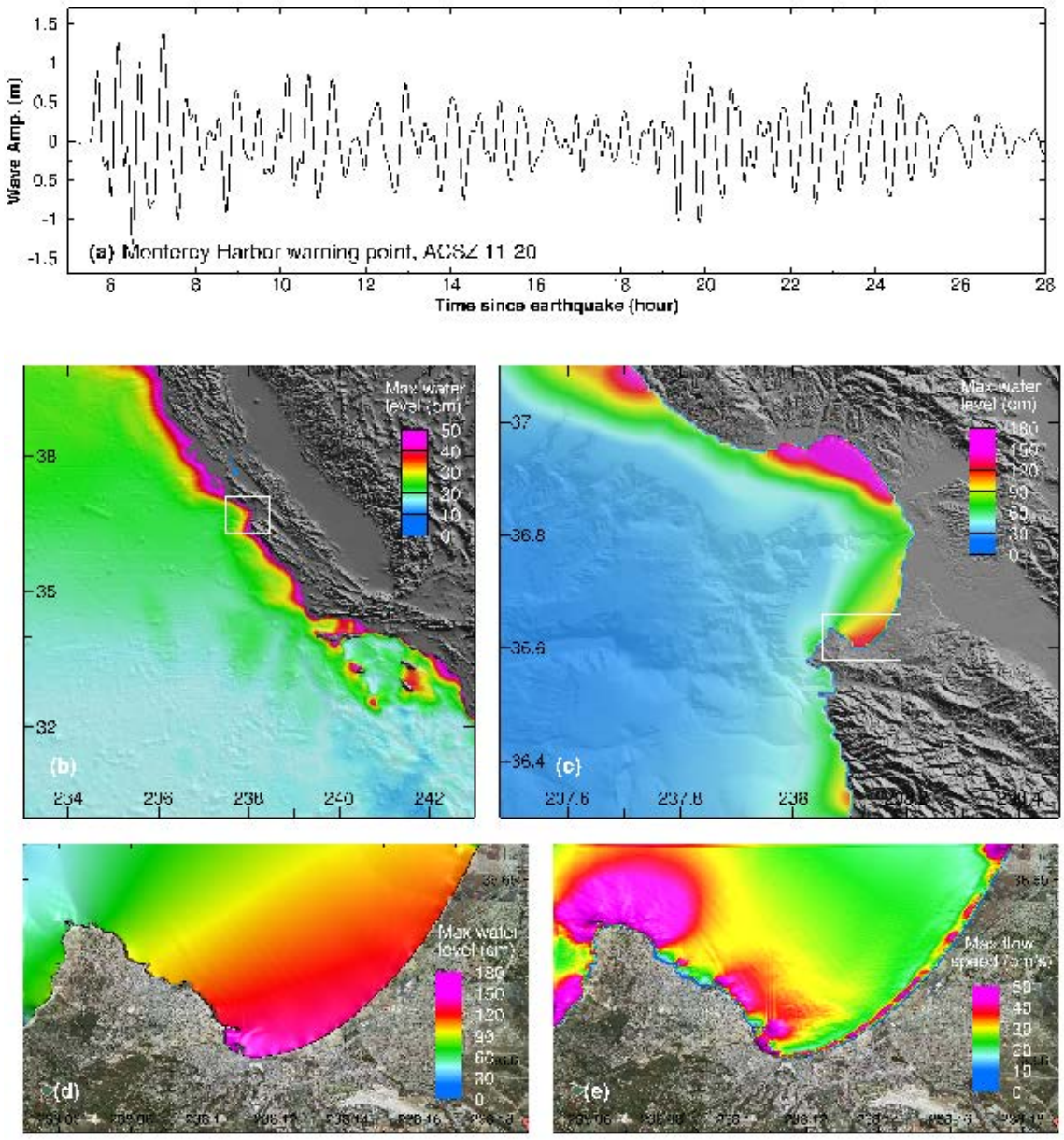

Figure 25 Model stability testing results at Monterey for synthetic mega tsunami scenario ACSZ 11-20. (a) Computed time series at the Monterey warning point; (b) Computed maximum wave amplitude in A grid of the forecast model; (c) Computed maximum current speed in B grid of the forecast model; (d) Computed maximum wave amplitude in C grid of the forecast model; (e) Computed current speed in C grid of the forecast model.

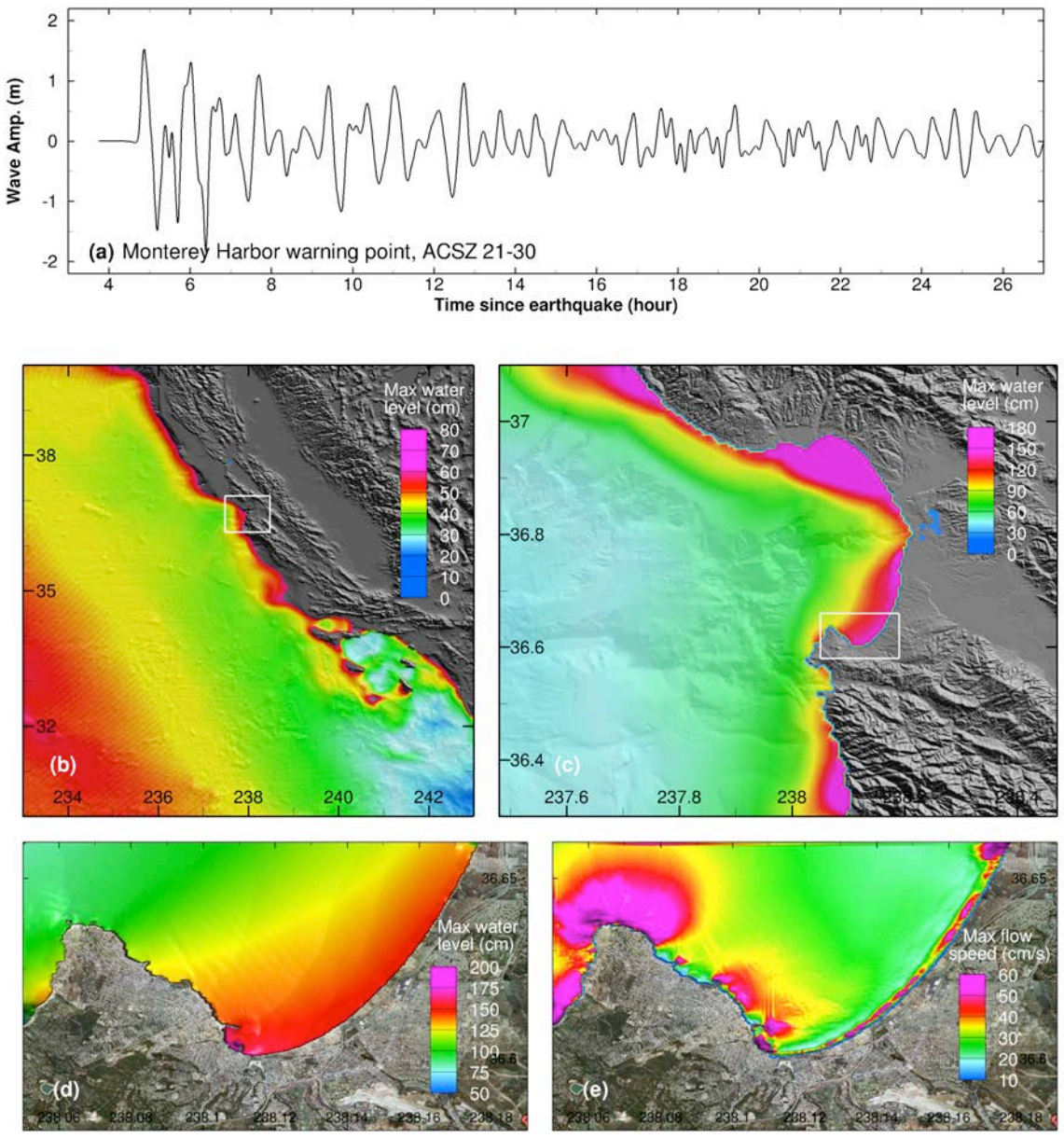

Figure 26 Model stability testing results at Monterey for synthetic mega tsunami scenario ACSZ 21-30. (a) Computed time series at the Monterey warning point; (b) Computed maximum wave amplitude in A grid of the forecast model; (c) Computed maximum current speed in B grid of the forecast model; (d) Computed maximum wave amplitude in C grid of the forecast model; (e) Computed current speed in C grid of the forecast model.

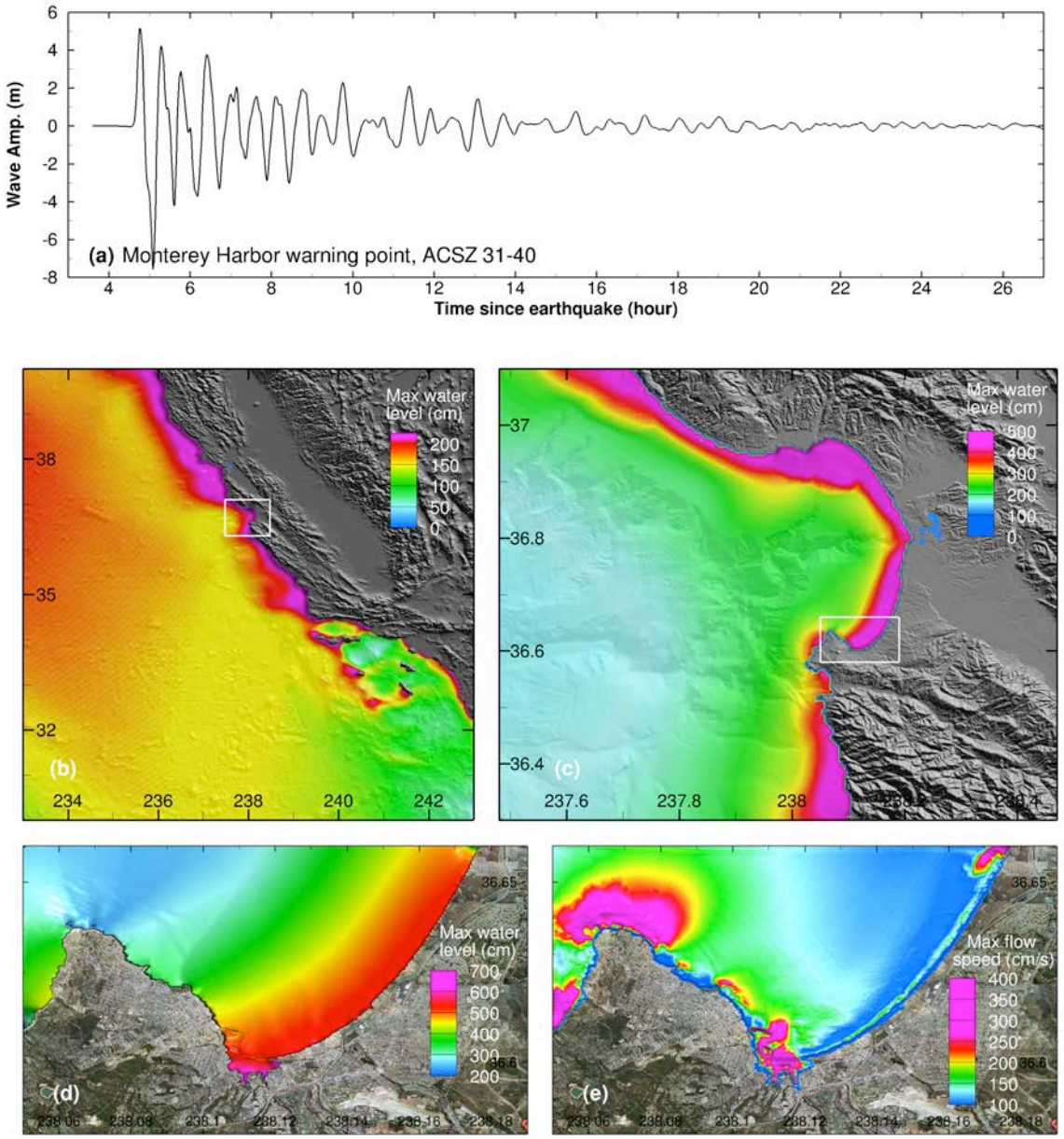

Figure 27 Model stability testing results at Monterey for synthetic mega tsunami scenario ACSZ 31-40. (a) Computed time series at the Monterey warning point; (b) Computed maximum wave amplitude in A grid of the forecast model; (c) Computed maximum current speed in B grid of the forecast model; (d) Computed maximum wave amplitude in C grid of the forecast model; (e) Computed current speed in C grid of the forecast model.

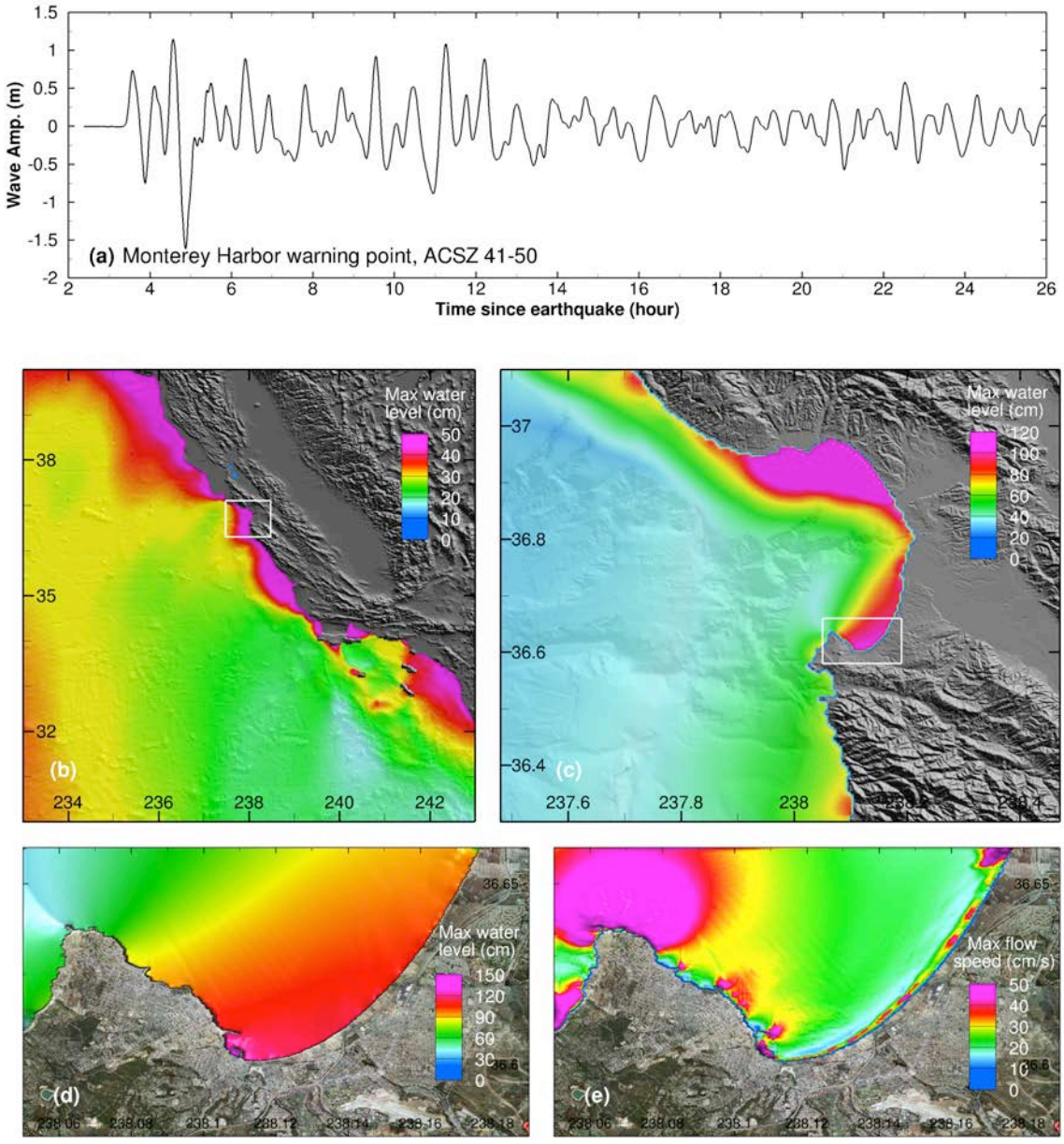

Figure 28 Model stability testing results at Monterey for synthetic mega tsunami scenario ACSZ 41-50. (a) Computed time series at the Monterey warning point; (b) Computed maximum wave amplitude in A grid of the forecast model; (c) Computed maximum current speed in B grid of the forecast model; (d) Computed maximum wave amplitude in C grid of the forecast model; (e) Computed current speed in C grid of the forecast model.

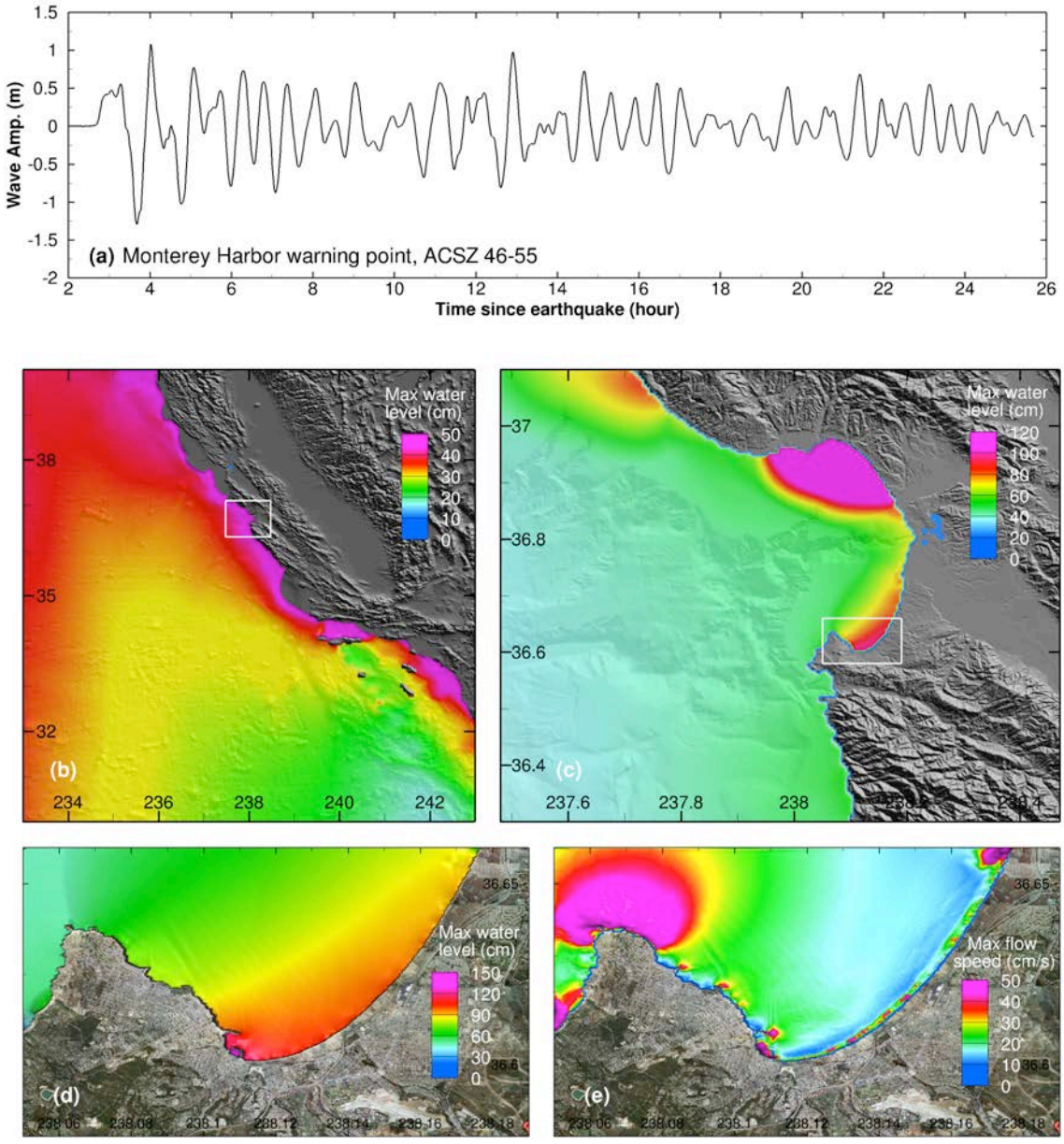

Figure 29 Model stability testing results at Monterey for synthetic mega tsunami scenario ACSZ 46-55. (a) Computed time series at the Monterey warning point; (b) Computed maximum wave amplitude in A grid of the forecast model; (c) Computed maximum current speed in B grid of the forecast model; (d) Computed maximum wave amplitude in C grid of the forecast model; (e) Computed current speed in C grid of the forecast model.

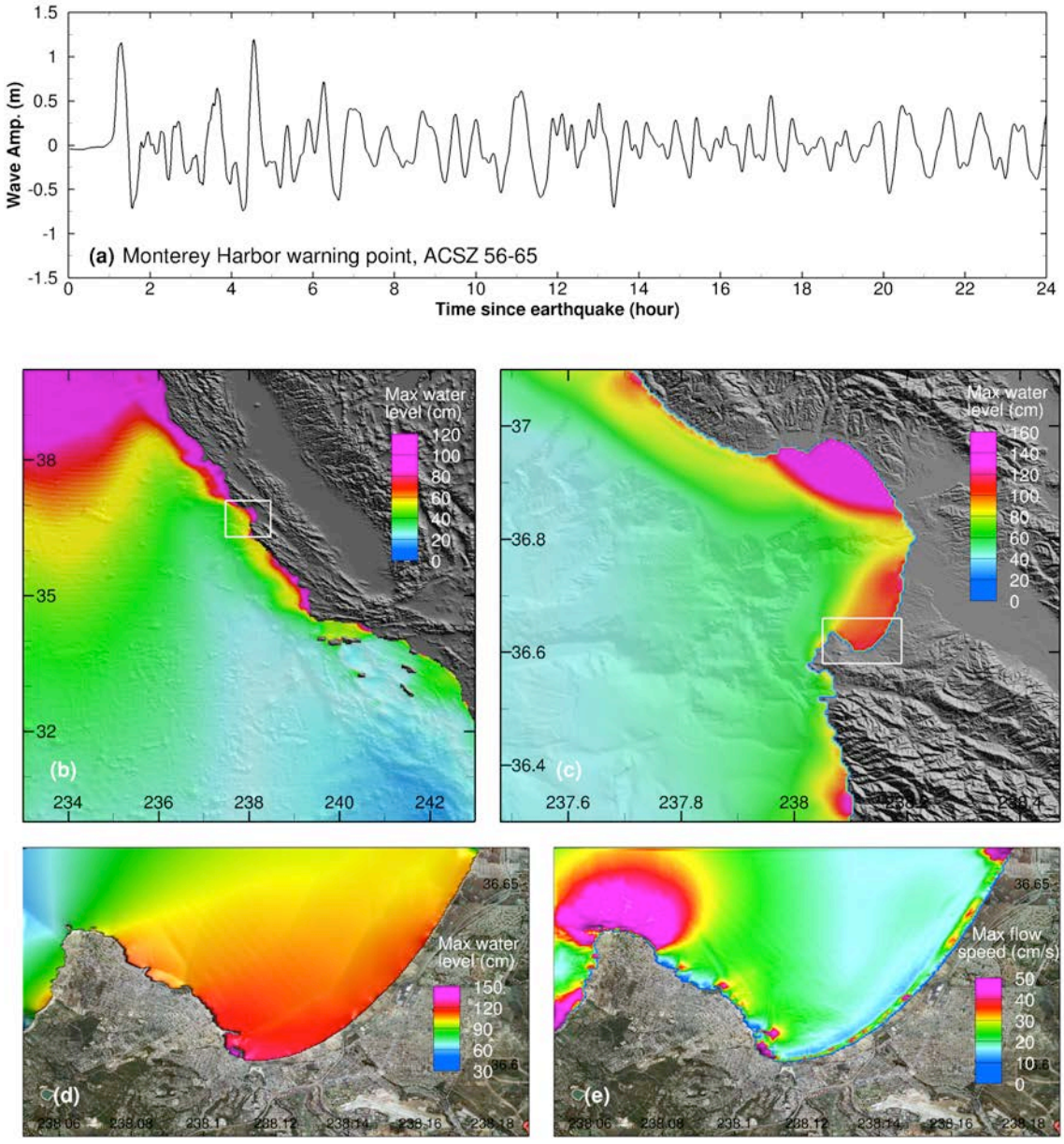

Figure 30 Model stability testing results at Monterey for synthetic mega tsunami scenario ACSZ 56-65. (a) Computed time series at the Monterey warning point; (b) Computed maximum wave amplitude in A grid of the forecast model; (c) Computed maximum current speed in B grid of the forecast model; (d) Computed maximum wave amplitude in C grid of the forecast model; (e) Computed current speed in C grid of the forecast model.

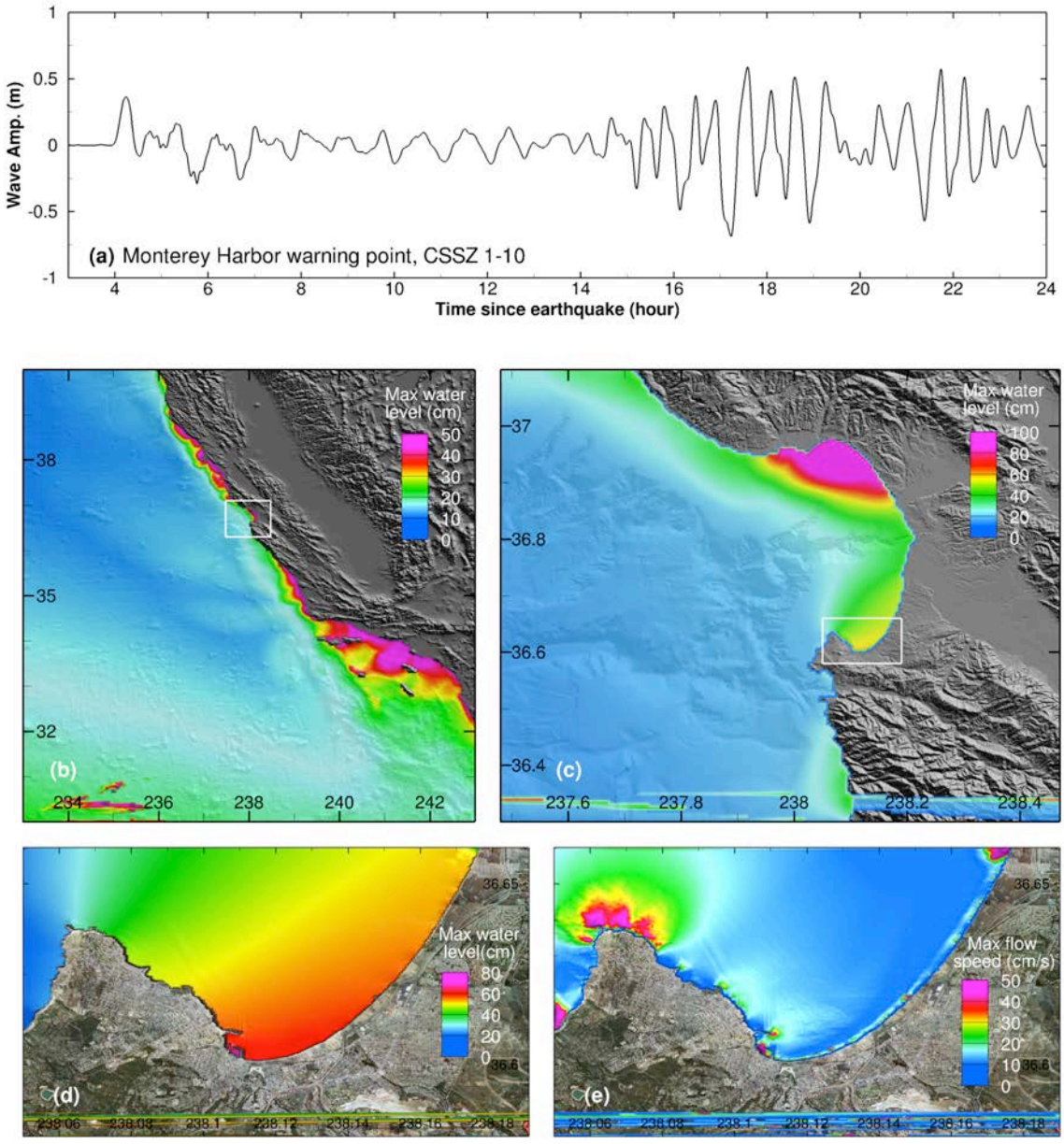

Figure 31 Model stability testing results at Monterey for synthetic mega tsunami scenario CSSZ 1-10. (a) Computed time series at the Monterey warning point; (b) Computed maximum wave amplitude in A grid of the forecast model; (c) Computed maximum current speed in B grid of the forecast model; (d) Computed maximum wave amplitude in C grid of the forecast model; (e) Computed current speed in C grid of the forecast model.

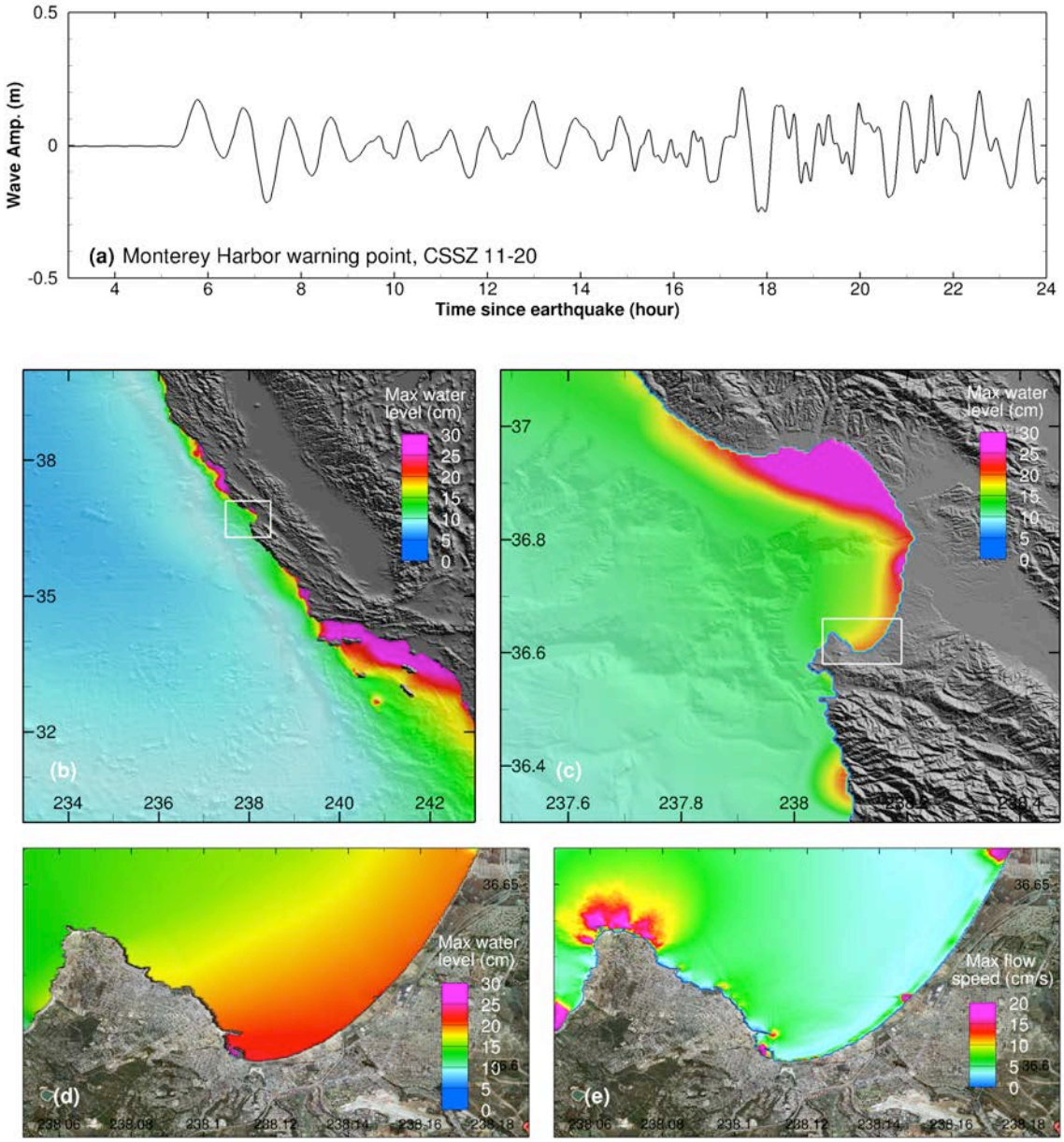

Figure 32 Model stability testing results at Monterey for synthetic mega tsunami scenario CSSZ 11-20. (a) Computed time series at the Monterey warning point; (b) Computed maximum wave amplitude in A grid of the forecast model; (c) Computed maximum current speed in B grid of the forecast model; (d) Computed maximum wave amplitude in C grid of the forecast model; (e) Computed current speed in C grid of the forecast model.

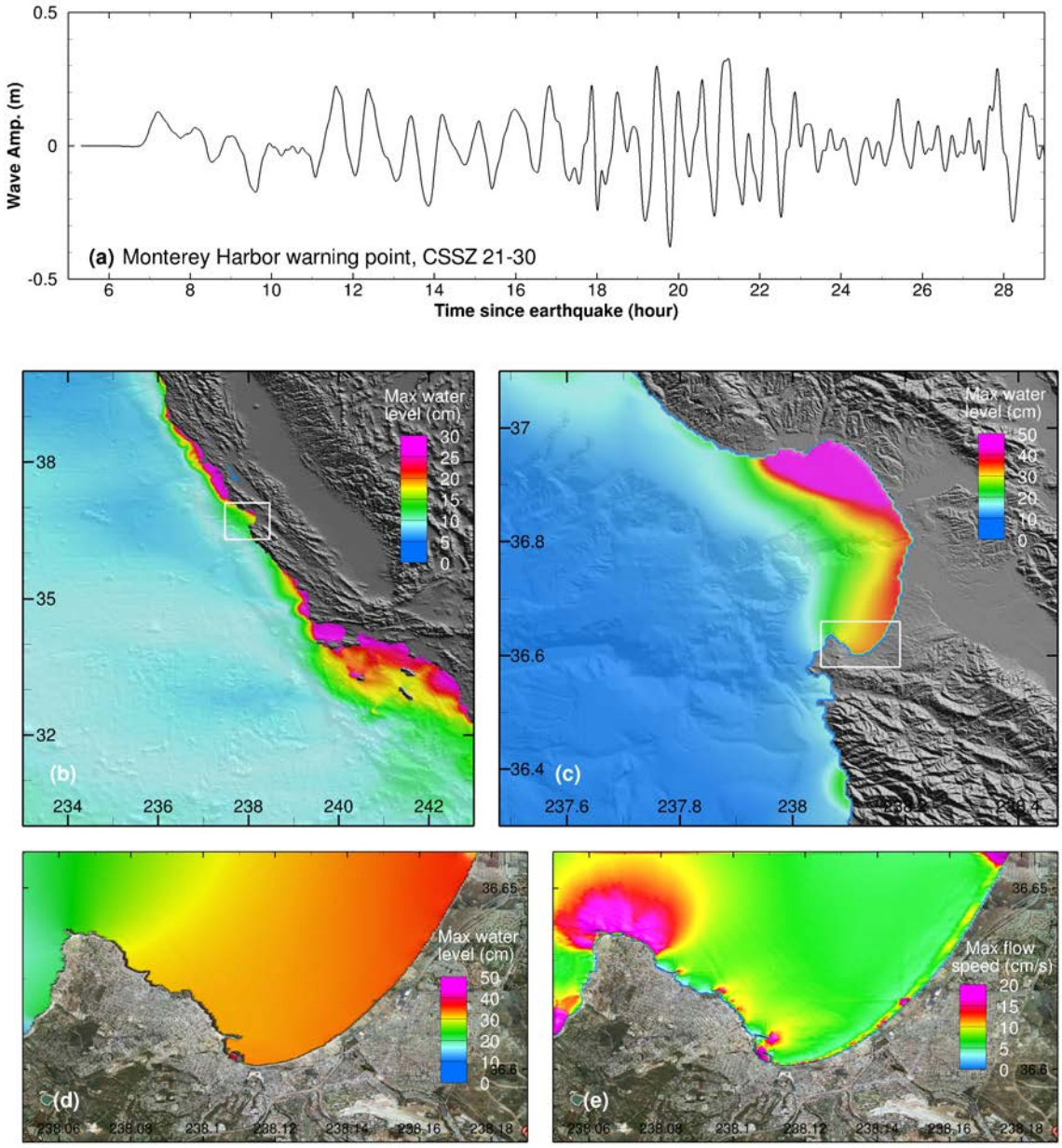

Figure 33 Model stability testing results at Monterey for synthetic mega tsunami scenario CSSZ 21-30. (a) Computed time series at the Monterey warning point; (b) Computed maximum wave amplitude in A grid of the forecast model; (c) Computed maximum current speed in B grid of the forecast model; (d) Computed maximum wave amplitude in C grid of the forecast model; (e) Computed current speed in C grid of the forecast model.

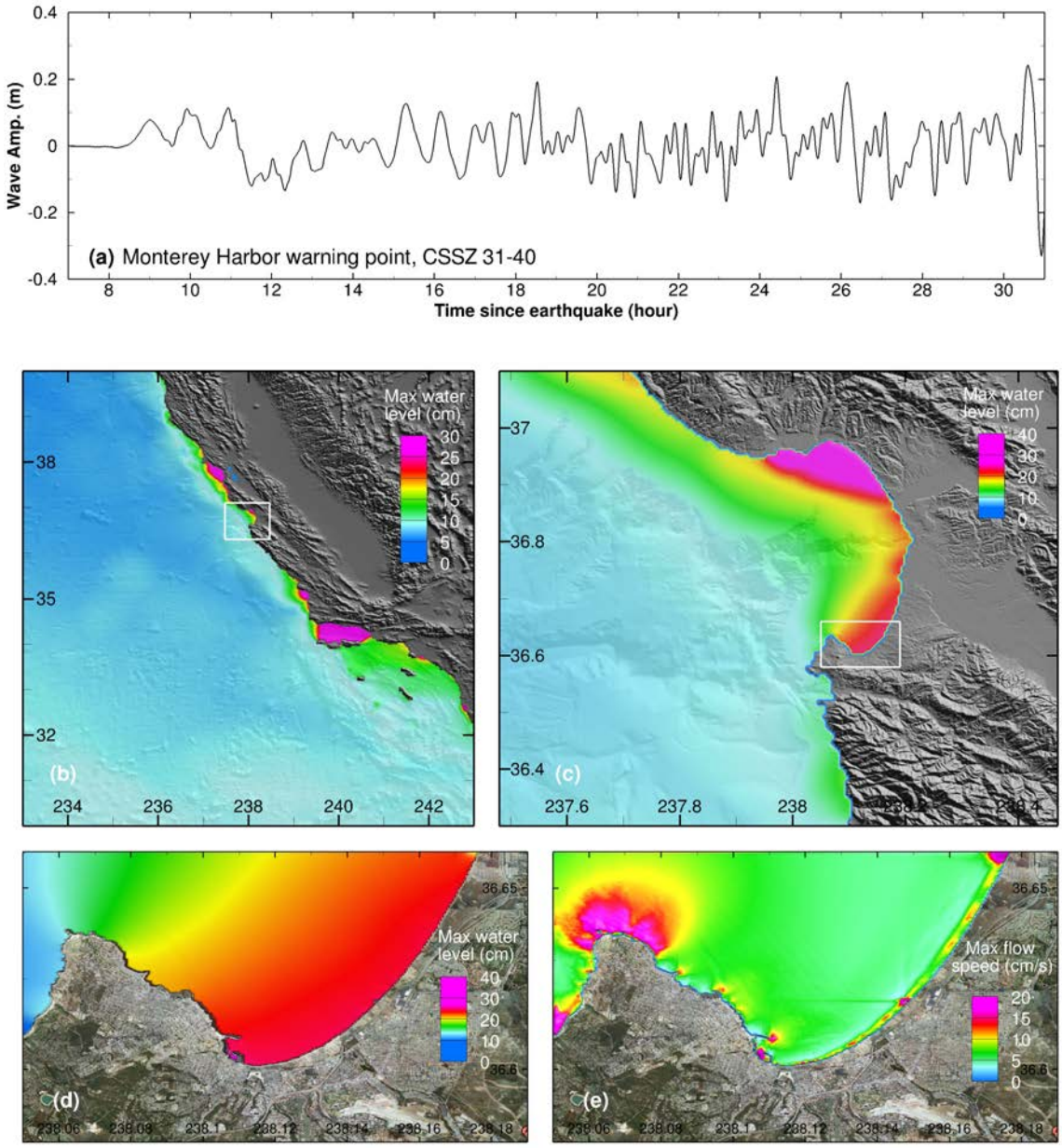

Figure 34 Model stability testing results at Monterey for synthetic mega tsunami scenario CSSZ 31-40. (a) Computed time series at the Monterey warning point; (b) Computed maximum wave amplitude in A grid of the forecast model; (c) Computed maximum current speed in B grid of the forecast model; (d) Computed maximum wave amplitude in C grid of the forecast model; (e) Computed current speed in C grid of the forecast model.

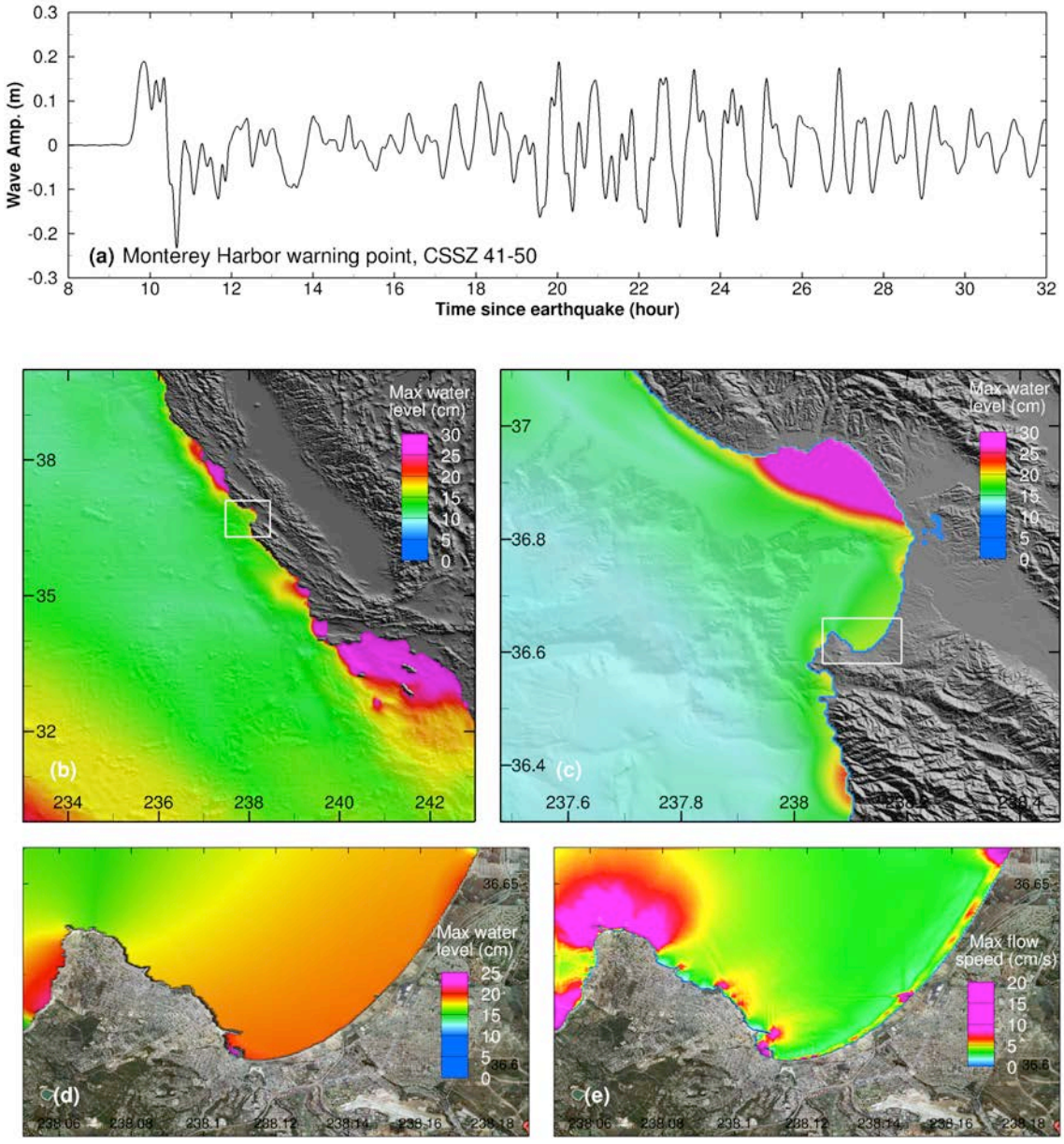

Figure 35 Model stability testing results at Monterey for synthetic mega tsunami scenario CSSZ 41-50. (a) Computed time series at the Monterey warning point; (b) Computed maximum wave amplitude in A grid of the forecast model; (c) Computed maximum current speed in B grid of the forecast model; (d) Computed maximum wave amplitude in C grid of the forecast model; (e) Computed current speed in C grid of the forecast model.

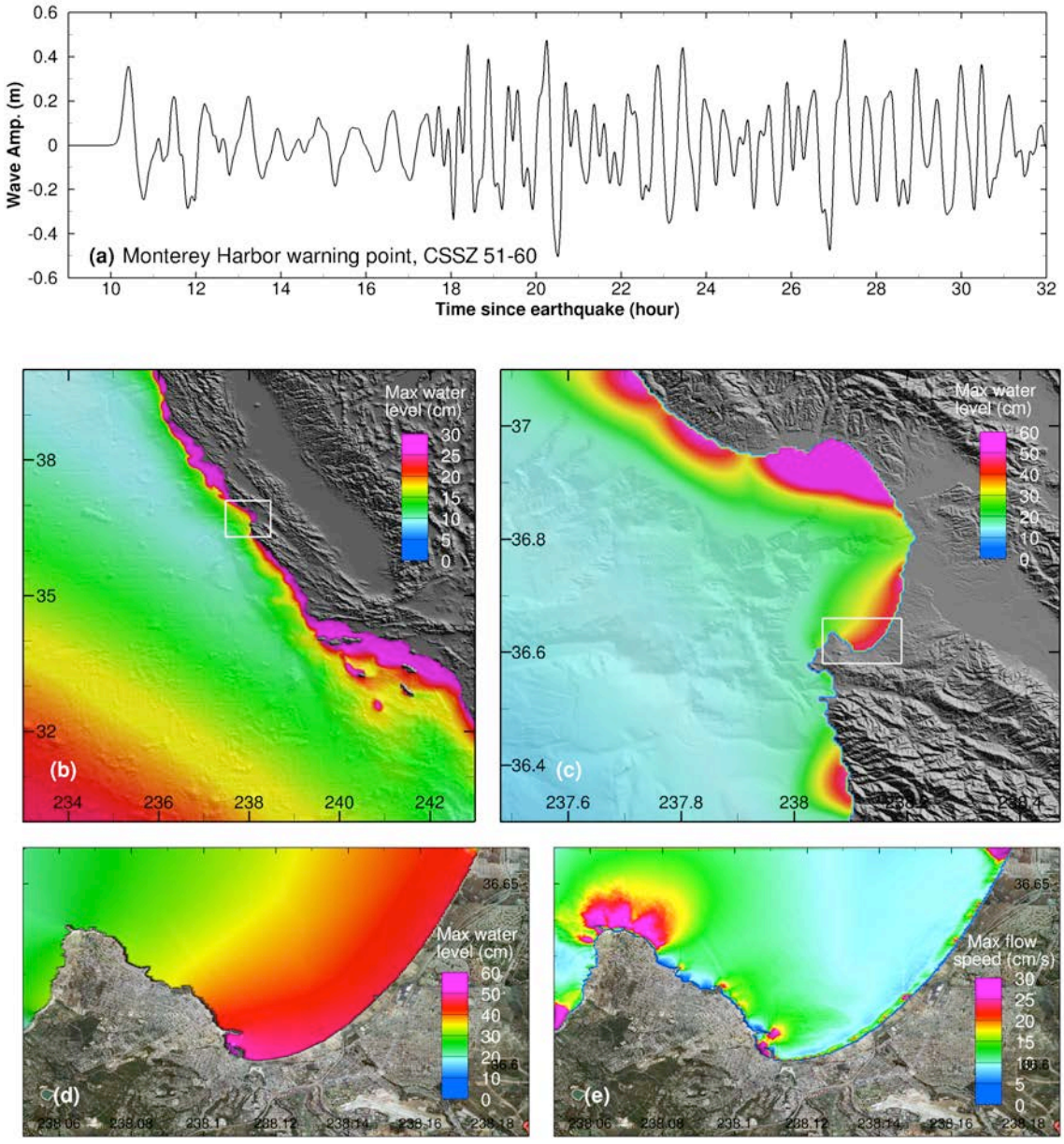

Figure 36 Model stability testing results at Monterey for synthetic mega tsunami scenario CSSZ 51-60. (a) Computed time series at the Monterey warning point; (b) Computed maximum wave amplitude in A grid of the forecast model; (c) Computed maximum current speed in B grid of the forecast model; (d) Computed maximum wave amplitude in C grid of the forecast model; (e) Computed current speed in C grid of the forecast model.

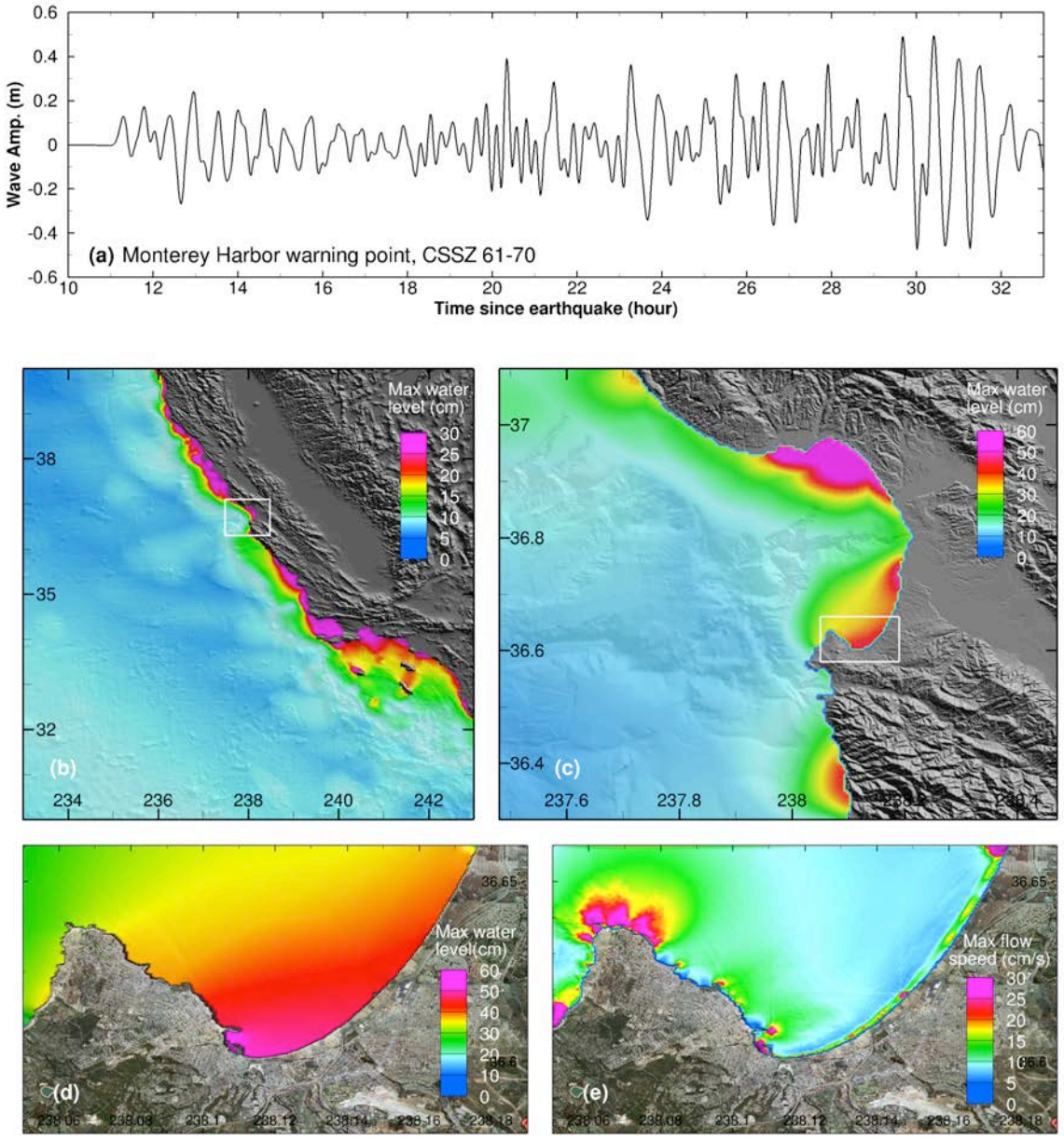

Figure 37 Model stability testing results at Monterey for synthetic mega tsunami scenario CSSZ 61-70. (a) Computed time series at the Monterey warning point; (b) Computed maximum wave amplitude in A grid of the forecast model; (c) Computed maximum current speed in B grid of the forecast model; (d) Computed maximum wave amplitude in C grid of the forecast model; (e) Computed current speed in C grid of the forecast model.

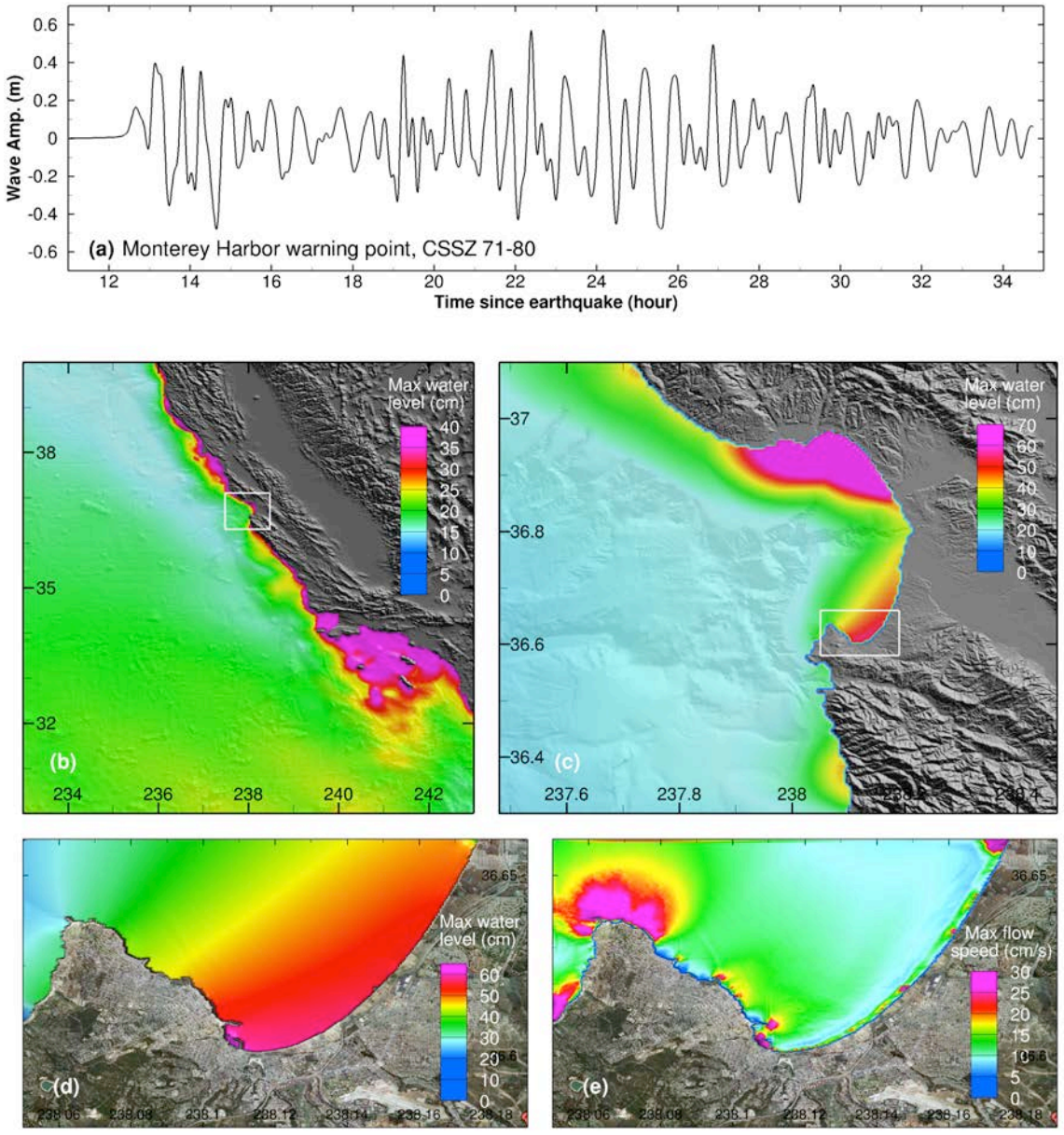

Figure 38 Model stability testing results at Monterey for synthetic mega tsunami scenario CSSZ 71-80. (a) Computed time series at the Monterey warning point; (b) Computed maximum wave amplitude in A grid of the forecast model; (c) Computed maximum current speed in B grid of the forecast model; (d) Computed maximum wave amplitude in C grid of the forecast model; (e) Computed current speed in C grid of the forecast model.

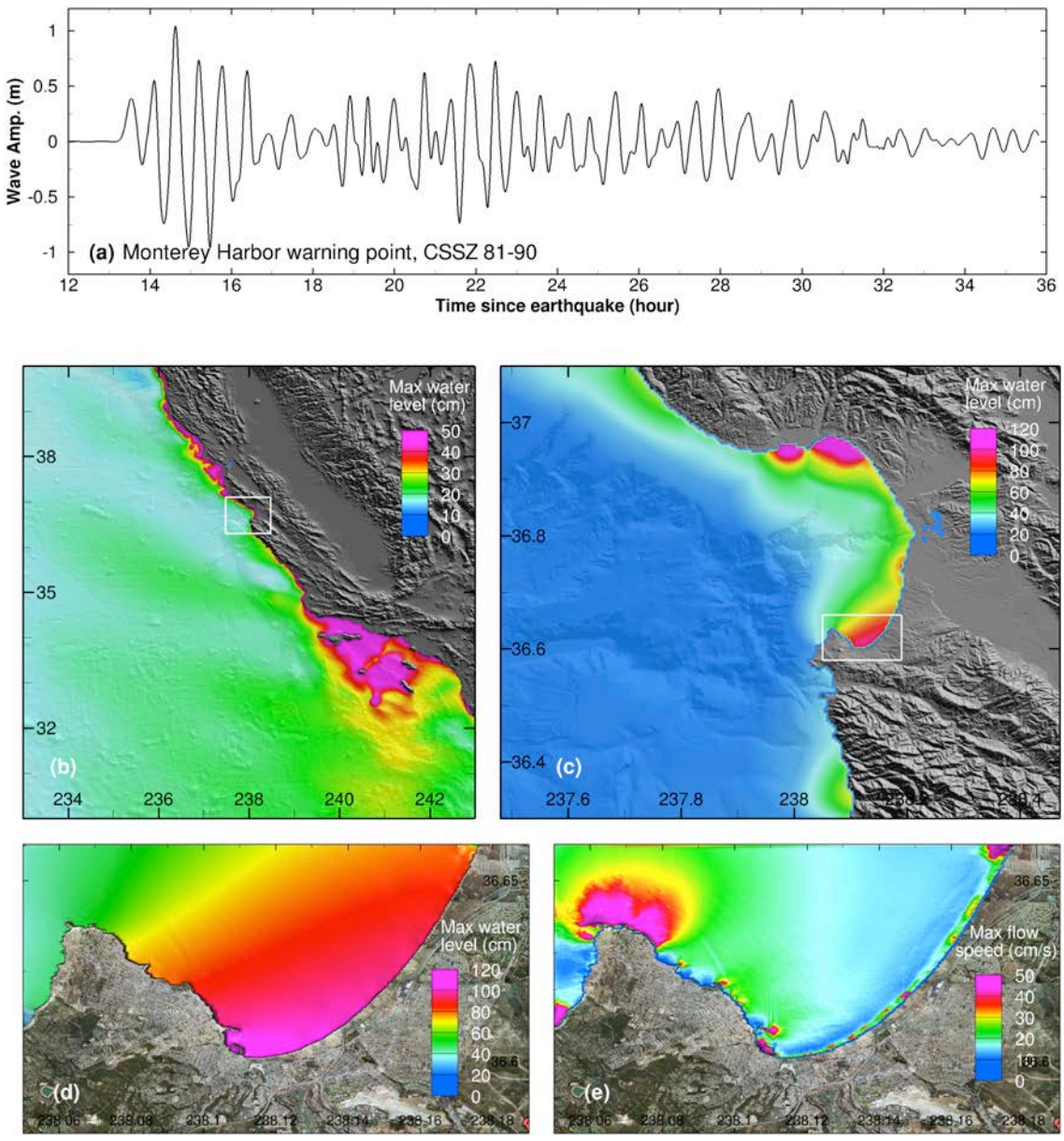

Figure 39 Model stability testing results at Monterey for synthetic mega tsunami scenario CSSZ 81-90. (a) Computed time series at the Monterey warning point; (b) Computed maximum wave amplitude in A grid of the forecast model; (c) Computed maximum current speed in B grid of the forecast model; (d) Computed maximum wave amplitude in C grid of the forecast model; (e) Computed current speed in C grid of the forecast model.

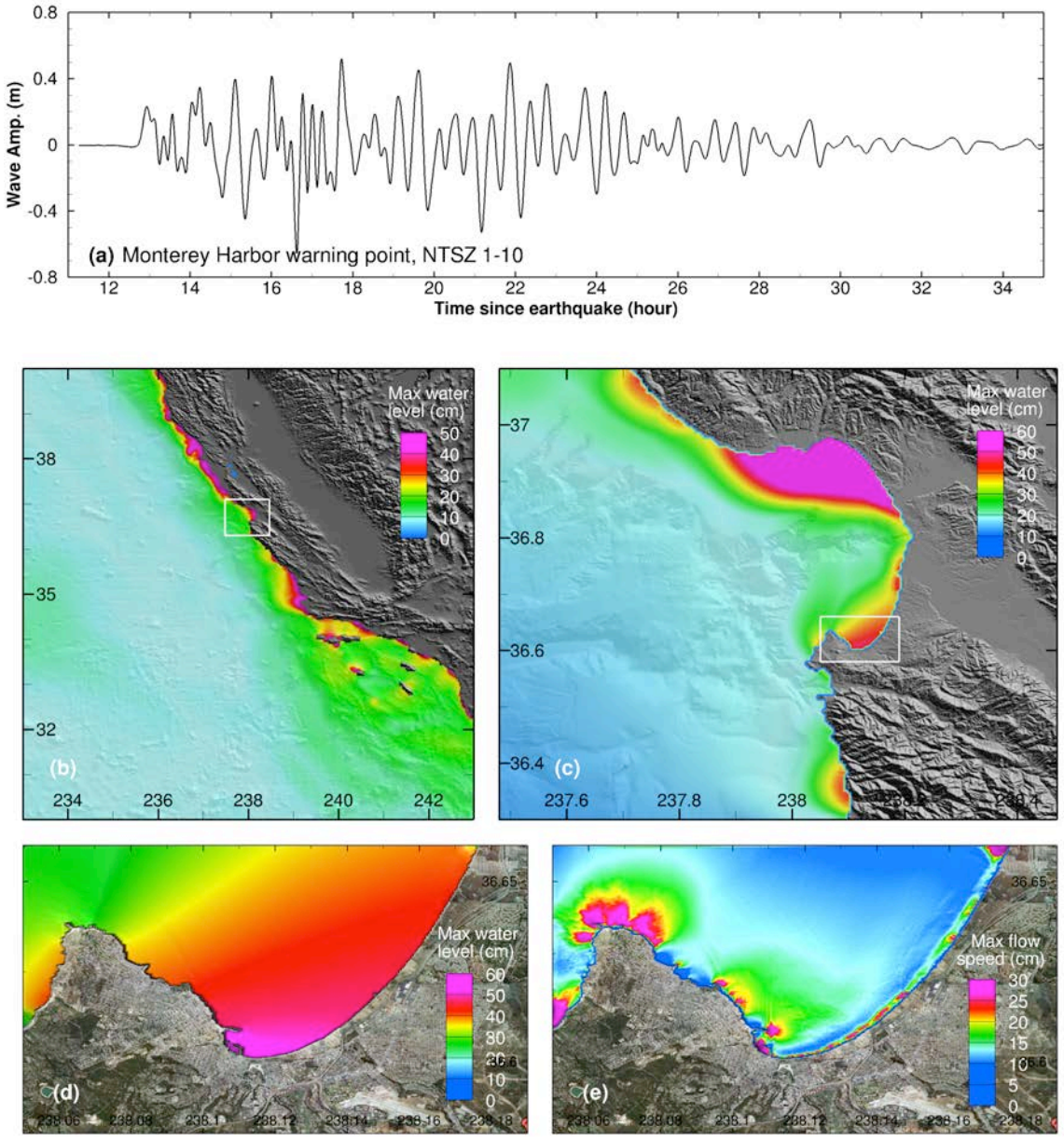

Figure 40 Model stability testing results at Monterey for synthetic mega tsunami scenario NTSZ 1-10. (a) Computed time series at the Monterey warning point; (b) Computed maximum wave amplitude in A grid of the forecast model; (c) Computed maximum current speed in B grid of the forecast model; (d) Computed maximum wave amplitude in C grid of the forecast model; (e) Computed current speed in C grid of the forecast model.

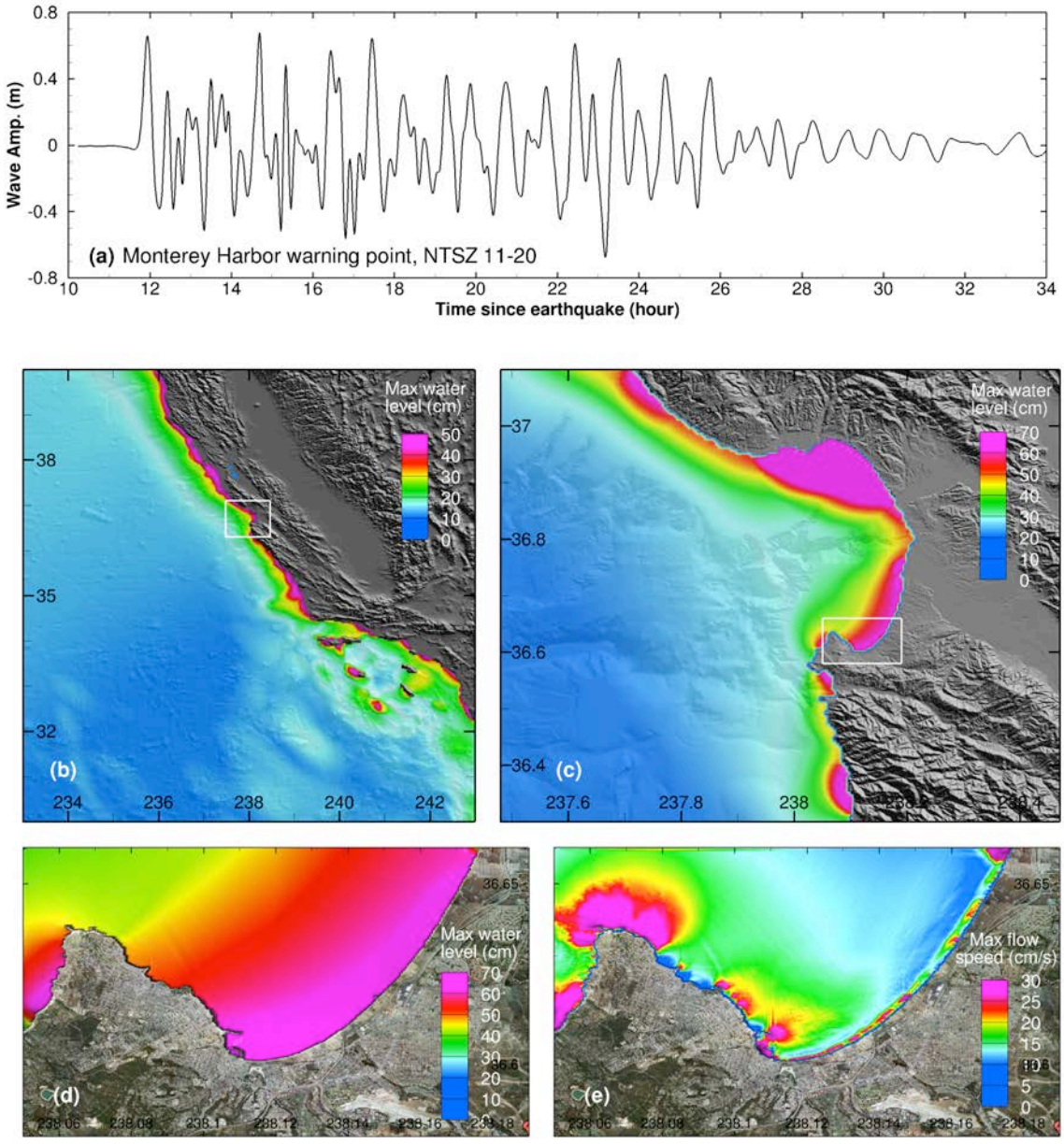

Figure 41 Model stability testing results at Monterey for synthetic mega tsunami scenario NTSZ 11-20. (a) Computed time series at the Monterey warning point; (b) Computed maximum wave amplitude in A grid of the forecast model; (c) Computed maximum current speed in B grid of the forecast model; (d) Computed maximum wave amplitude in C grid of the forecast model; (e) Computed current speed in C grid of the forecast model.

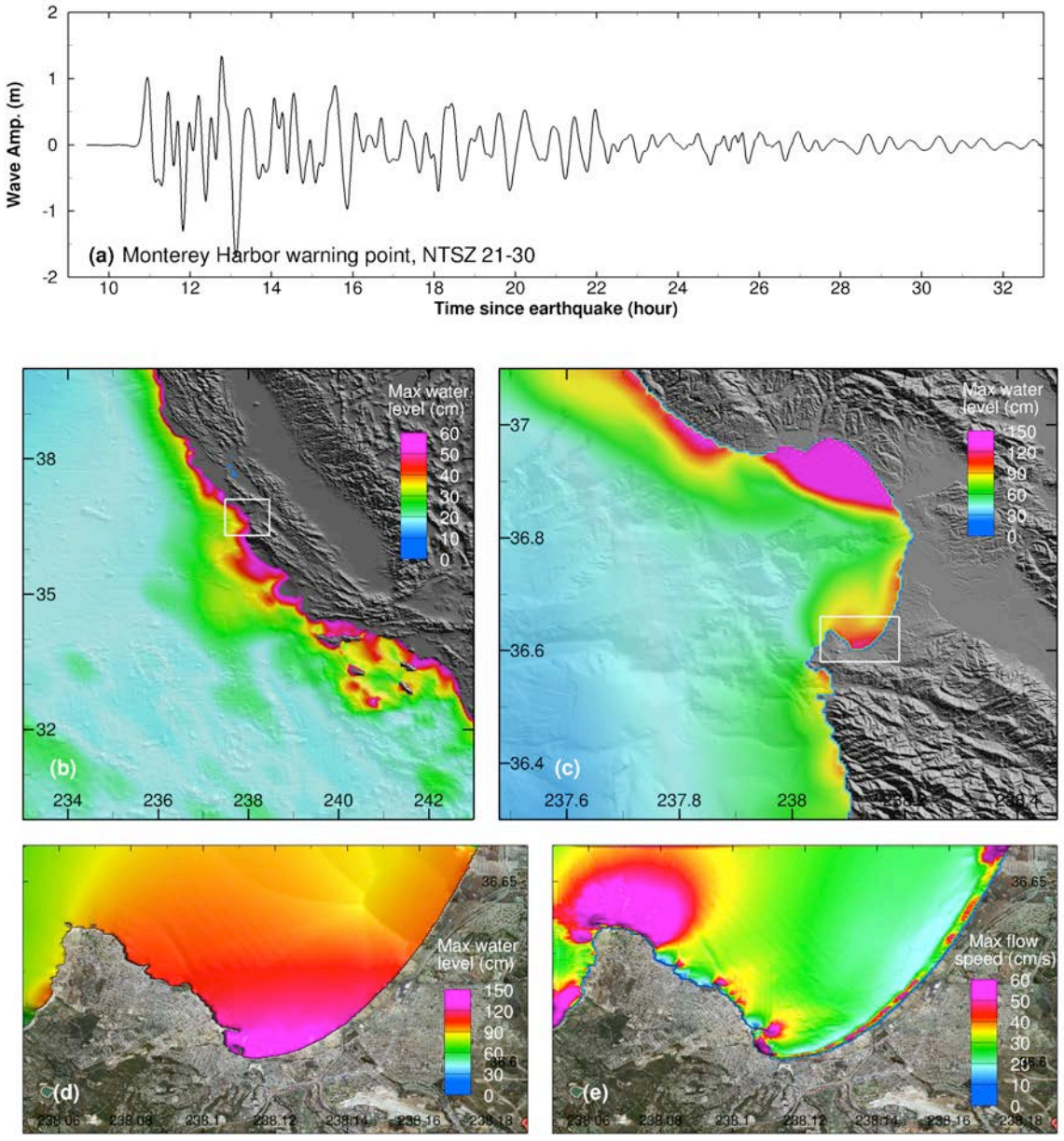

Figure 42 Model stability testing results at Monterey for synthetic mega tsunami scenario NTSZ 21-30. (a) Computed time series at the Monterey warning point; (b) Computed maximum wave amplitude in A grid of the forecast model; (c) Computed maximum current speed in B grid of the forecast model; (d) Computed maximum wave amplitude in C grid of the forecast model; (e) Computed current speed in C grid of the forecast model.

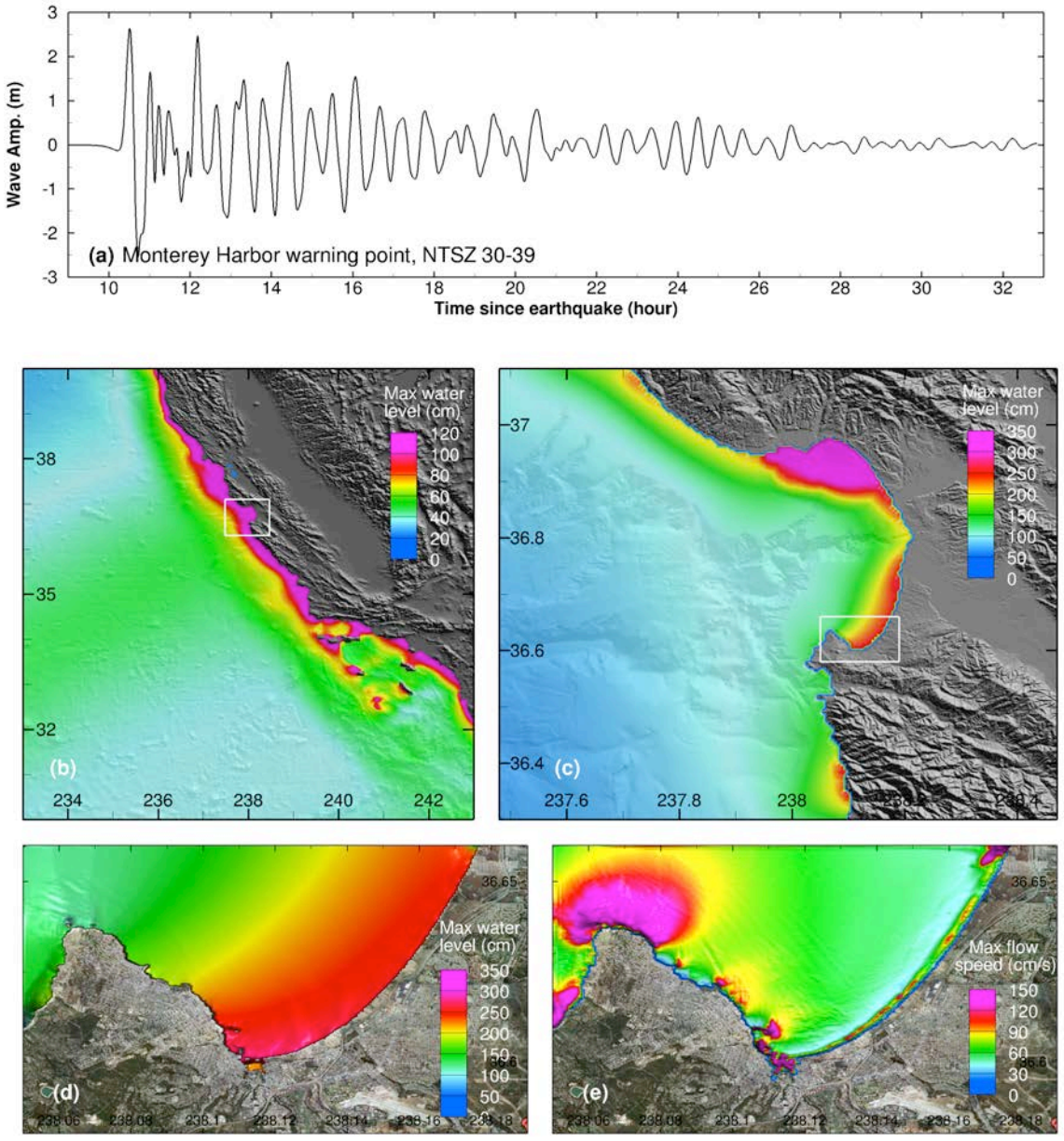

Figure 43 (a) Computed time series at the Monterey warning point; (b) Computed maximum wave amplitude in A grid of the forecast model; (c) Computed maximum current speed in B grid of the forecast model; (d) Computed maximum wave amplitude in C grid of the forecast model; (e) Computed current speed in C grid of the forecast model.

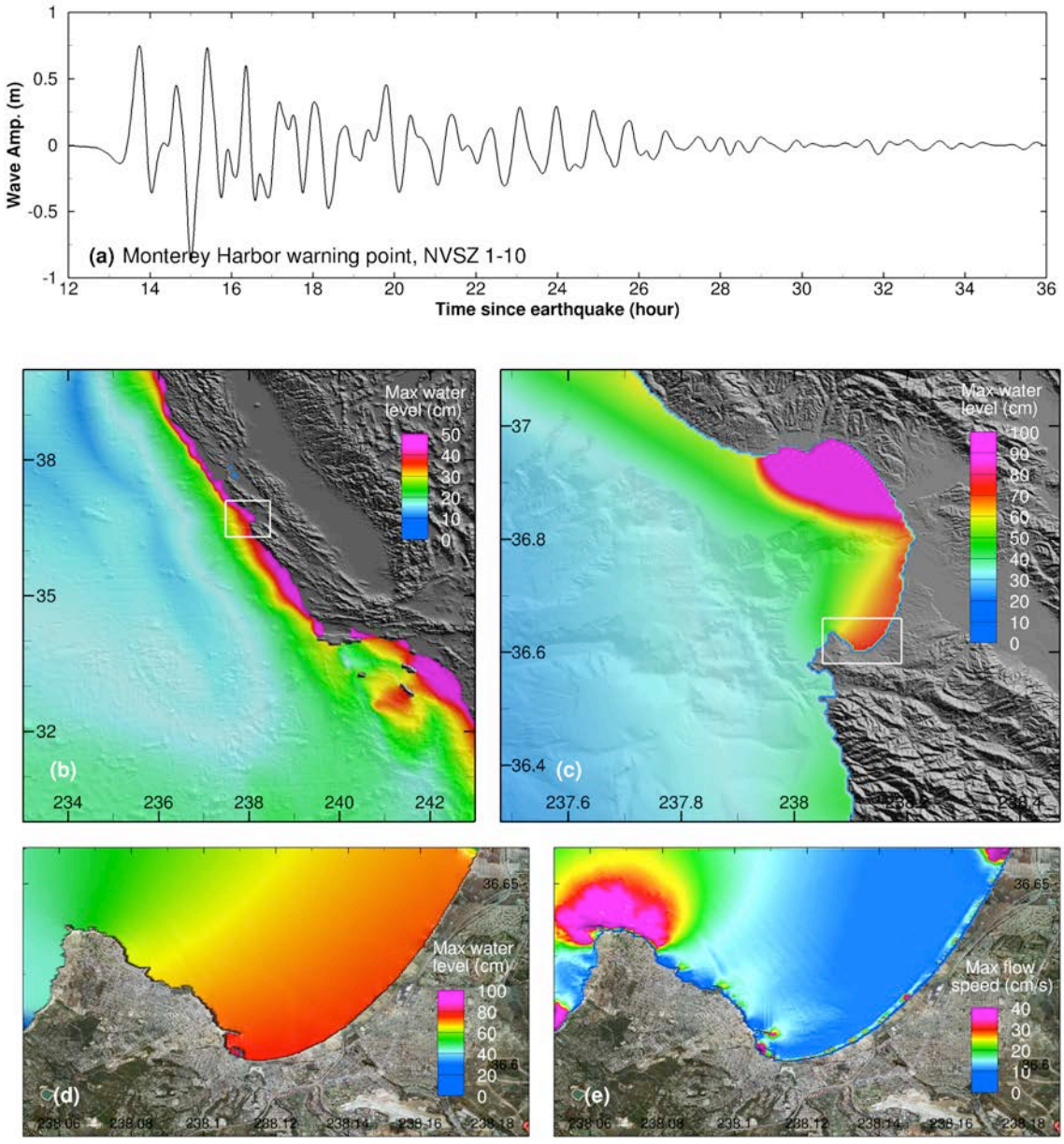

Figure 44 (a) Computed time series at the Monterey warning point; (b) Computed maximum wave amplitude in A grid of the forecast model; (c) Computed maximum current speed in B grid of the forecast model; (d) Computed maximum wave amplitude in C grid of the forecast model; (e) Computed current speed in C grid of the forecast model.

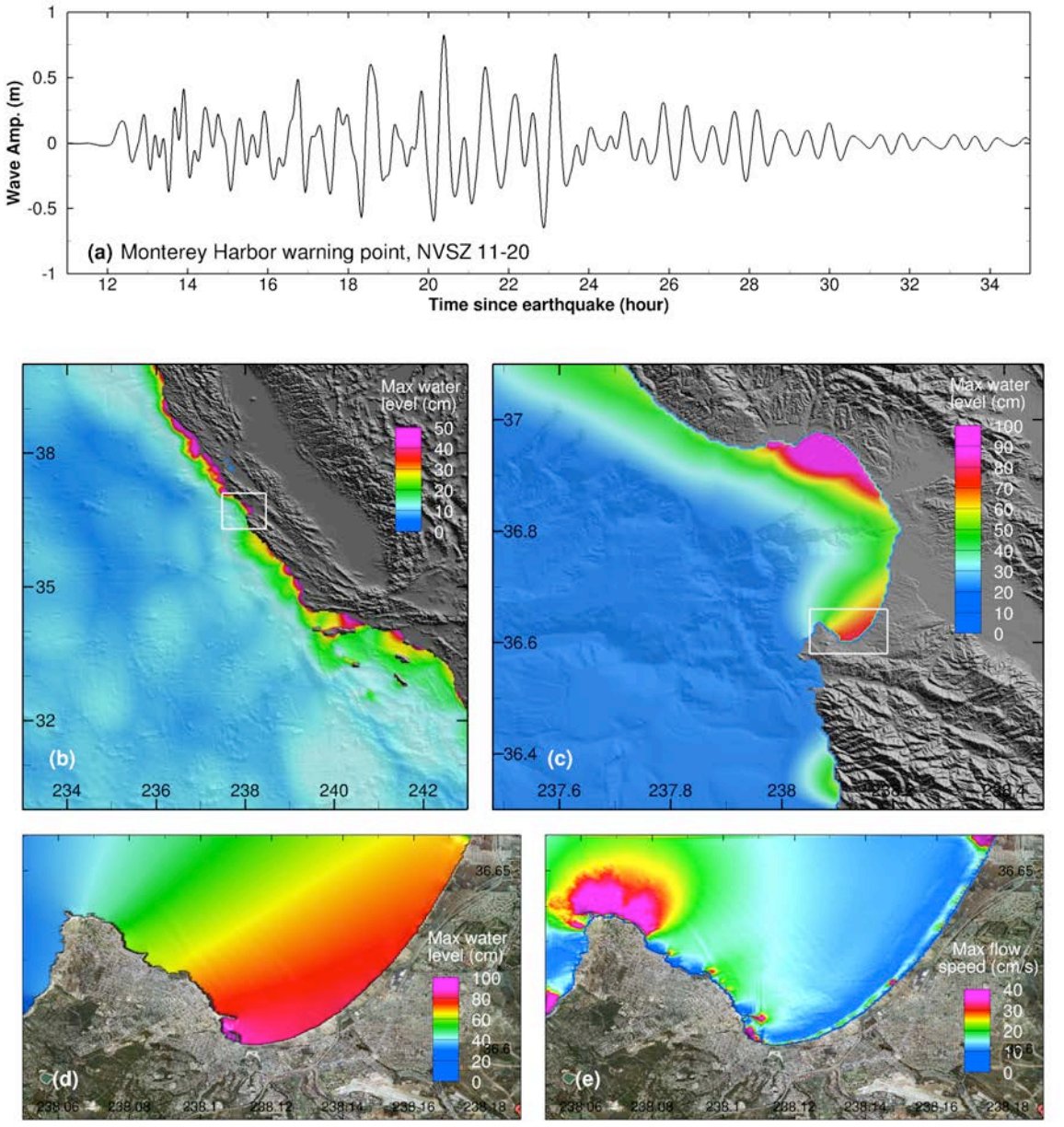

Figure 45 Model stability testing results at Monterey for synthetic mega tsunami scenario NVSZ 11-20. (a) Computed time series at the Monterey warning point; (b) Computed maximum wave amplitude in A grid of the forecast model; (c) Computed maximum current speed in B grid of the forecast model; (d) Computed maximum wave amplitude in C grid of the forecast model; (e) Computed current speed in C grid of the forecast model.

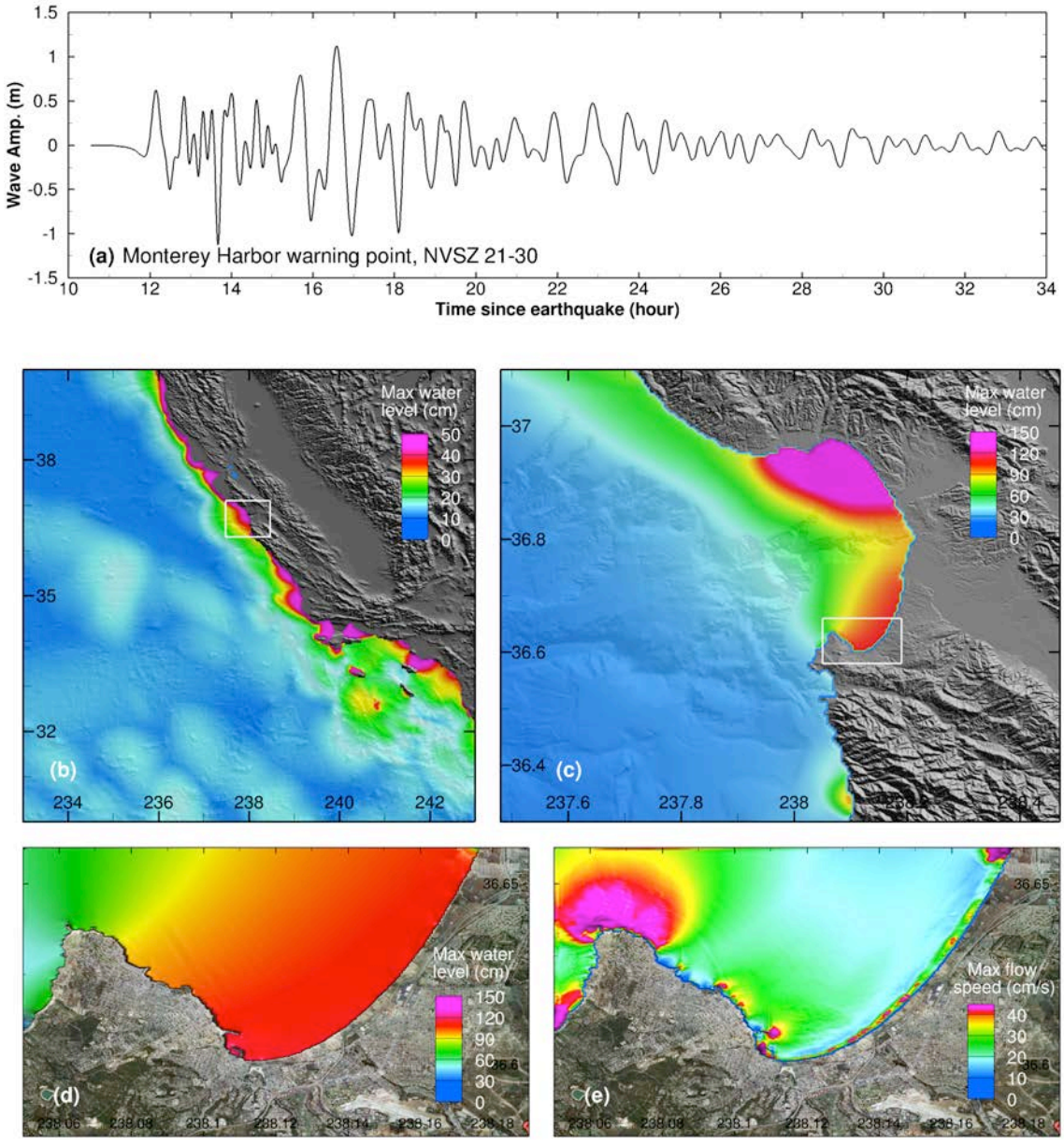

Figure 46 Model stability testing results at Monterey for synthetic mega tsunami scenario NVSZ 21-30. (a) Computed time series at the Monterey warning point; (b) Computed maximum wave amplitude in A grid of the forecast model; (c) Computed maximum current speed in B grid of the forecast model; (d) Computed maximum wave amplitude in C grid of the forecast model; (e) Computed current speed in C grid of the forecast model.

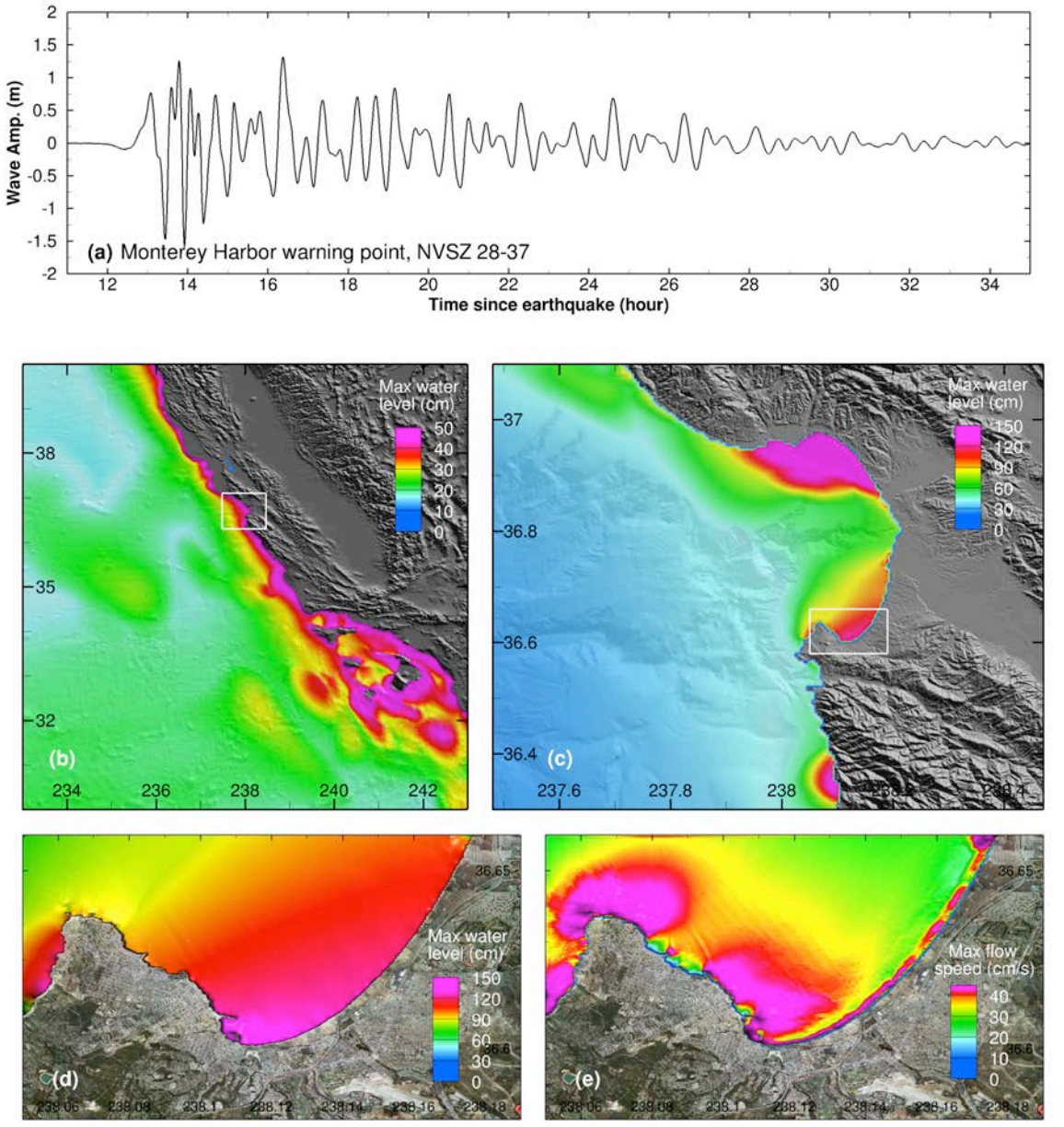

Figure 47 Model stability testing results at Monterey for synthetic mega tsunami scenario NVSZ 28-37. (a) Computed time series at the Monterey warning point; (b) Computed maximum wave amplitude in A grid of the forecast model; (c) Computed maximum current speed in B grid of the forecast model; (d) Computed maximum wave amplitude in C grid of the forecast model; (e) Computed current speed in C grid of the forecast model.

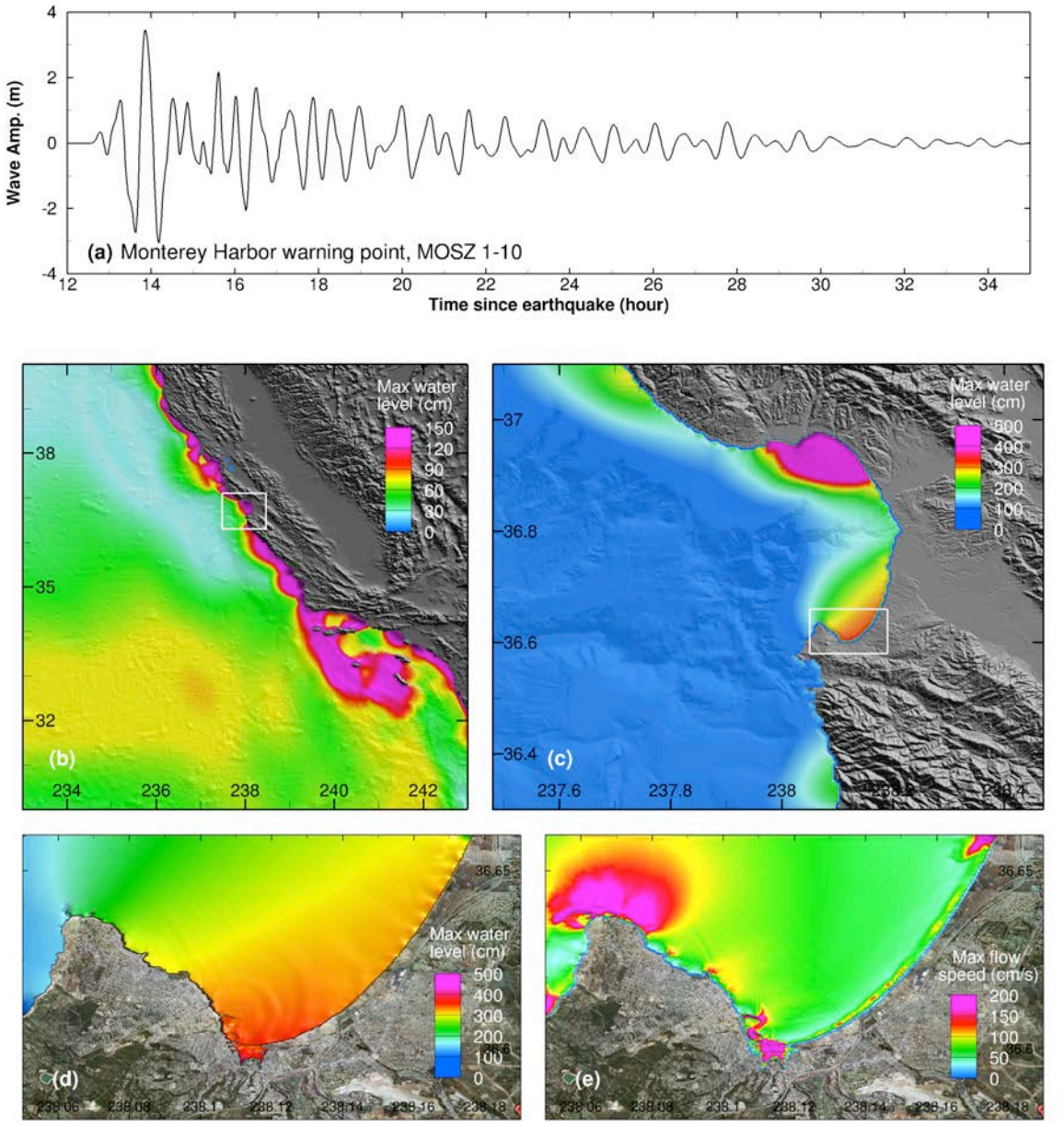

Figure 48 Model stability testing results at Monterey for synthetic mega tsunami scenario MOSZ 1-10. (a) Computed time series at the Monterey warning point; (b) Computed maximum wave amplitude in A grid of the forecast model; (c) Computed maximum current speed in B grid of the forecast model; (d) Computed maximum wave amplitude in C grid of the forecast model; (e) Computed current speed in C grid of the forecast model.

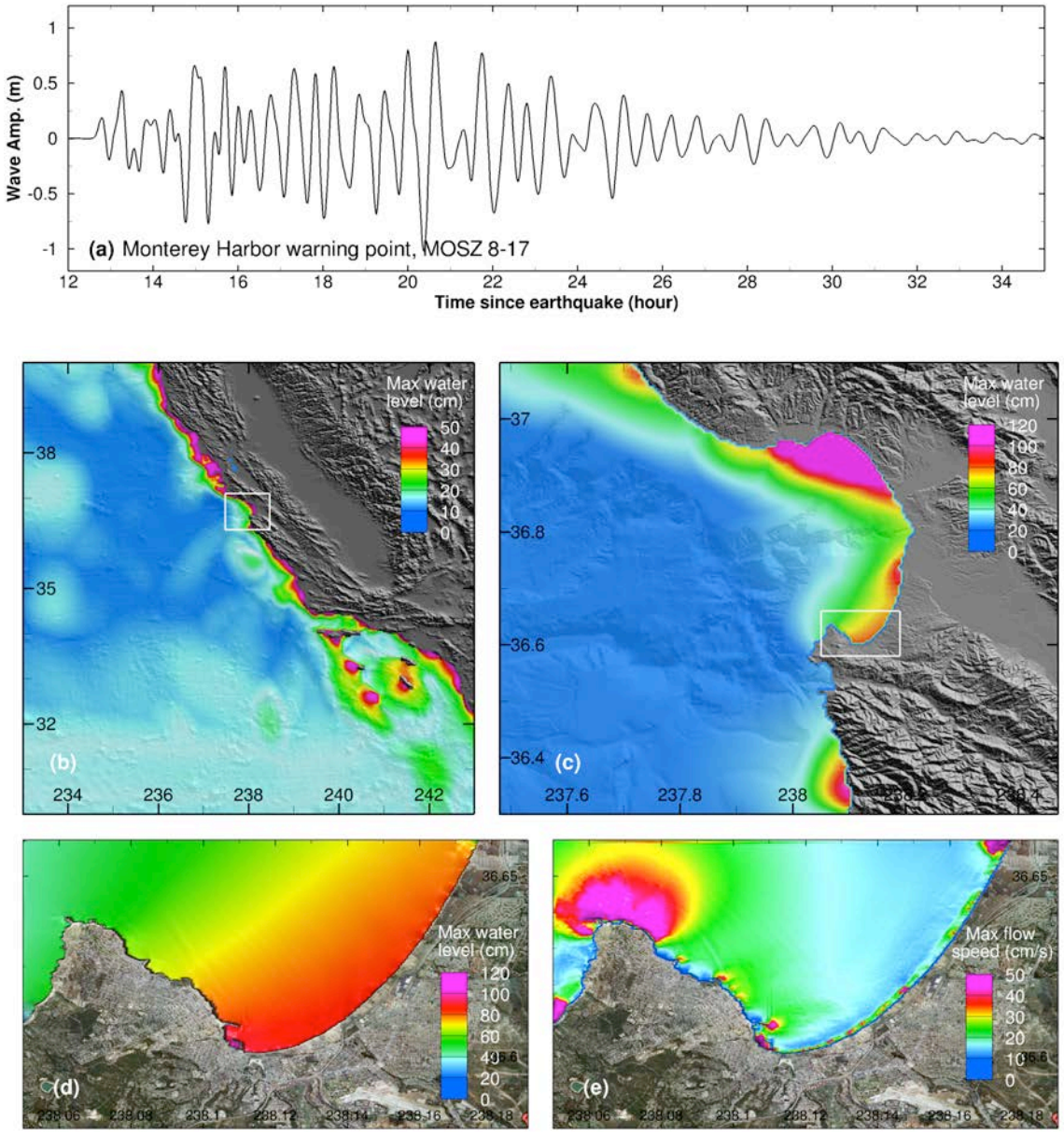

Figure 49 Model stability testing results at Monterey for synthetic mega tsunami scenario MOSZ 8-17. (a) Computed time series at the Monterey warning point; (b) Computed maximum wave amplitude in A grid of the forecast model; (c) Computed maximum current speed in B grid of the forecast model; (d) Computed maximum wave amplitude in C grid of the forecast model; (e) Computed current speed in C grid of the forecast model.

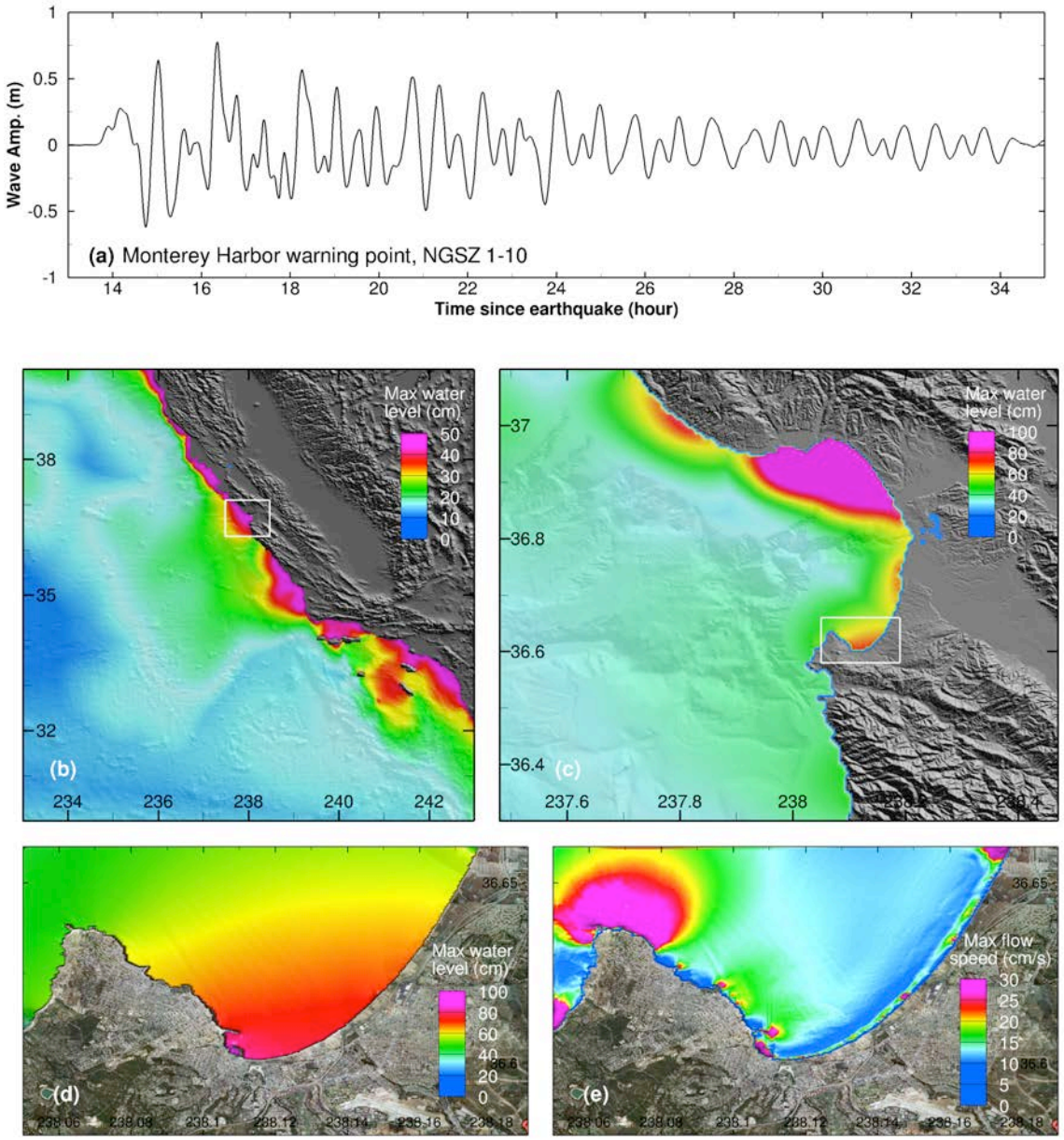

Figure 50 Model stability testing results at Monterey for synthetic mega tsunami scenario NGSZ 1-10. (a) Computed time series at the Monterey warning point; (b) Computed maximum wave amplitude in A grid of the forecast model; (c) Computed maximum current speed in B grid of the forecast model; (d) Computed maximum wave amplitude in C grid of the forecast model; (e) Computed current speed in C grid of the forecast model.

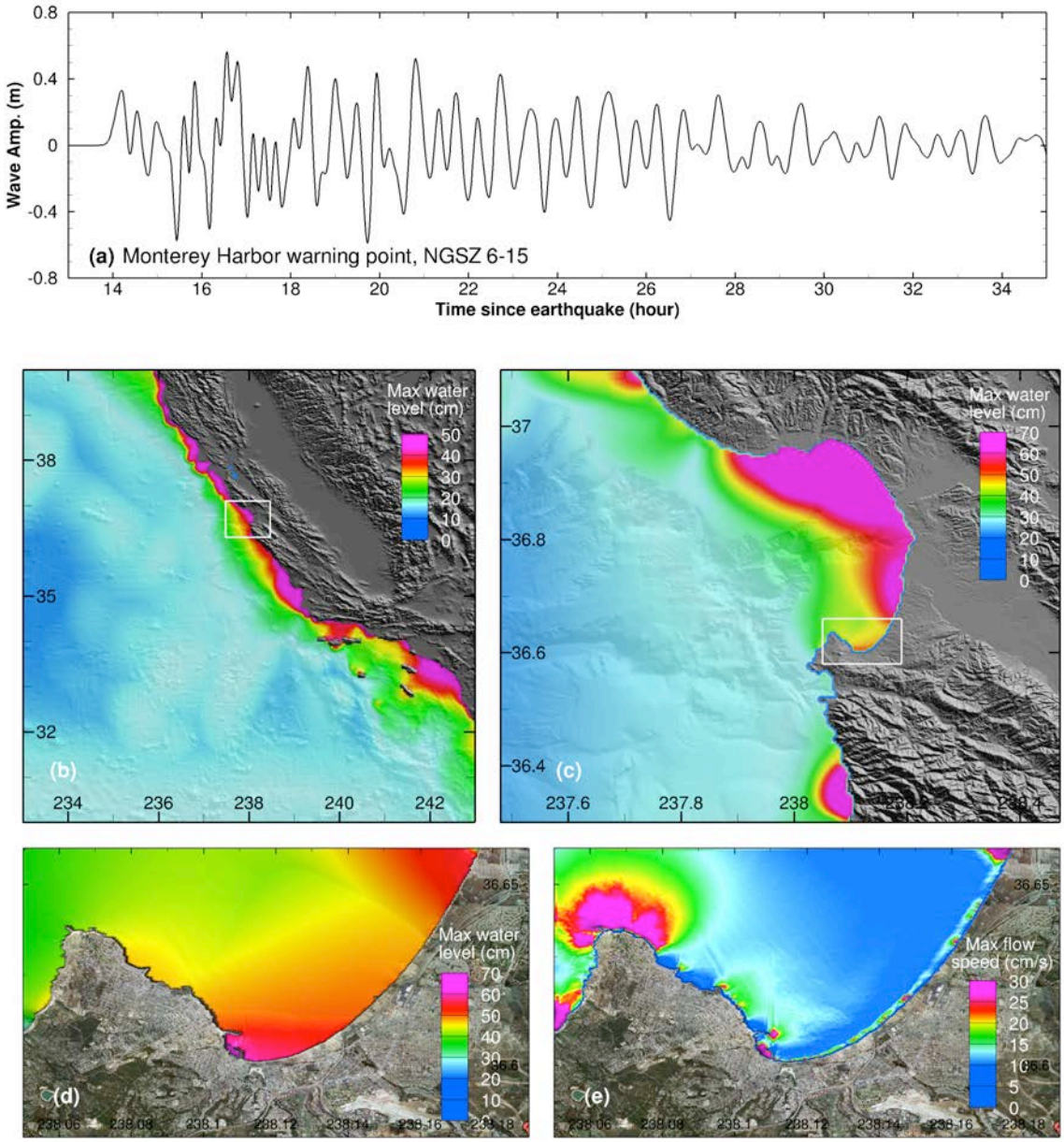

Figure 51 Model stability testing results at Monterey for synthetic mega tsunami scenario NGSZ 6-15. (a) Computed time series at the Monterey warning point; (b) Computed maximum wave amplitude in A grid of the forecast model; (c) Computed maximum current speed in B grid of the forecast model; (d) Computed maximum wave amplitude in C grid of the forecast model; (e) Computed current speed in C grid of the forecast model.

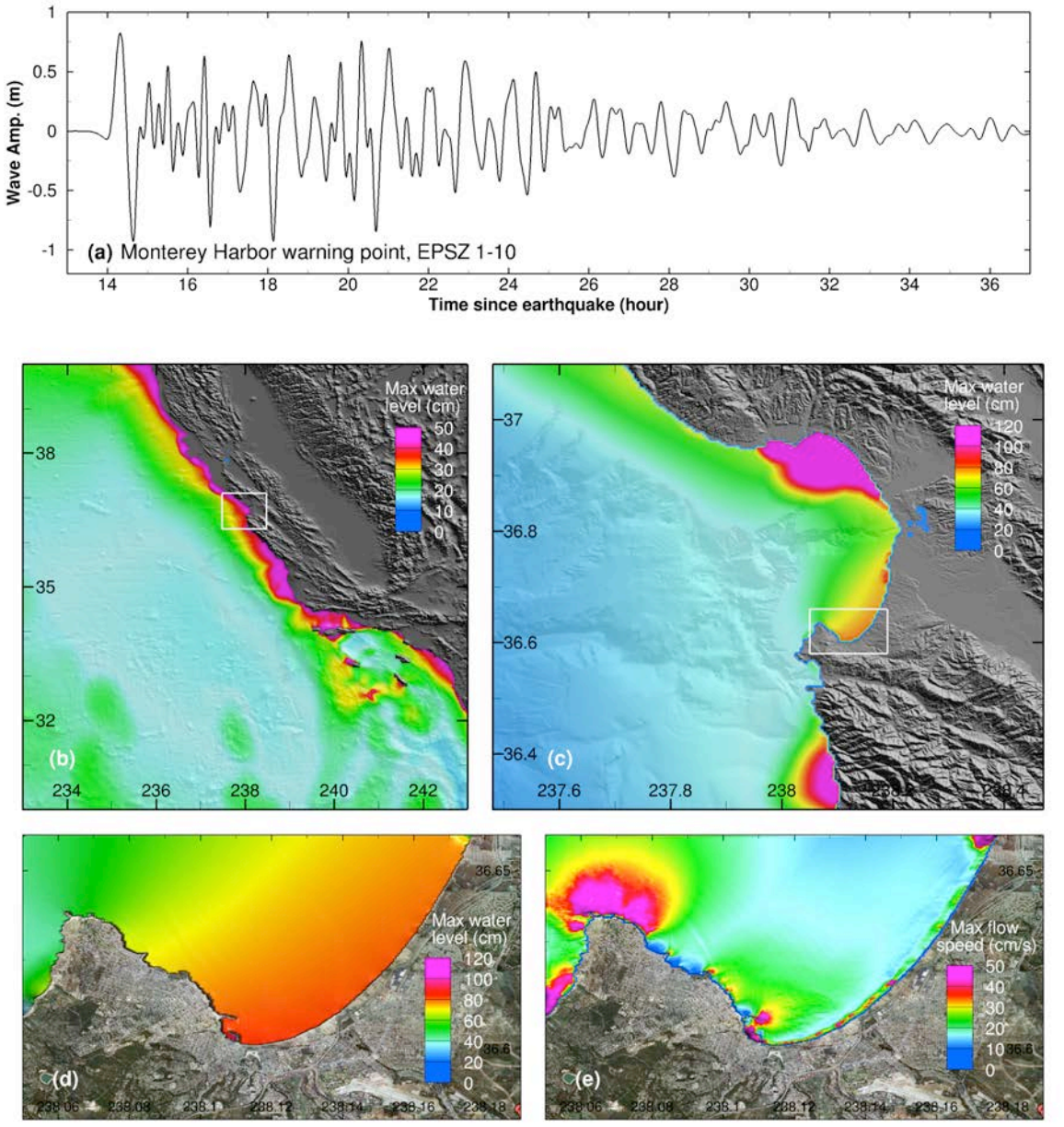

Figure 52 Model stability testing results at Monterey for synthetic mega tsunami scenario EPSZ 1-10. (a) Computed time series at the Monterey warning point; (b) Computed maximum wave amplitude in A grid of the forecast model; (c) Computed maximum current speed in B grid of the forecast model; (d) Computed maximum wave amplitude in C grid of the forecast model; (e) Computed current speed in C grid of the forecast model.

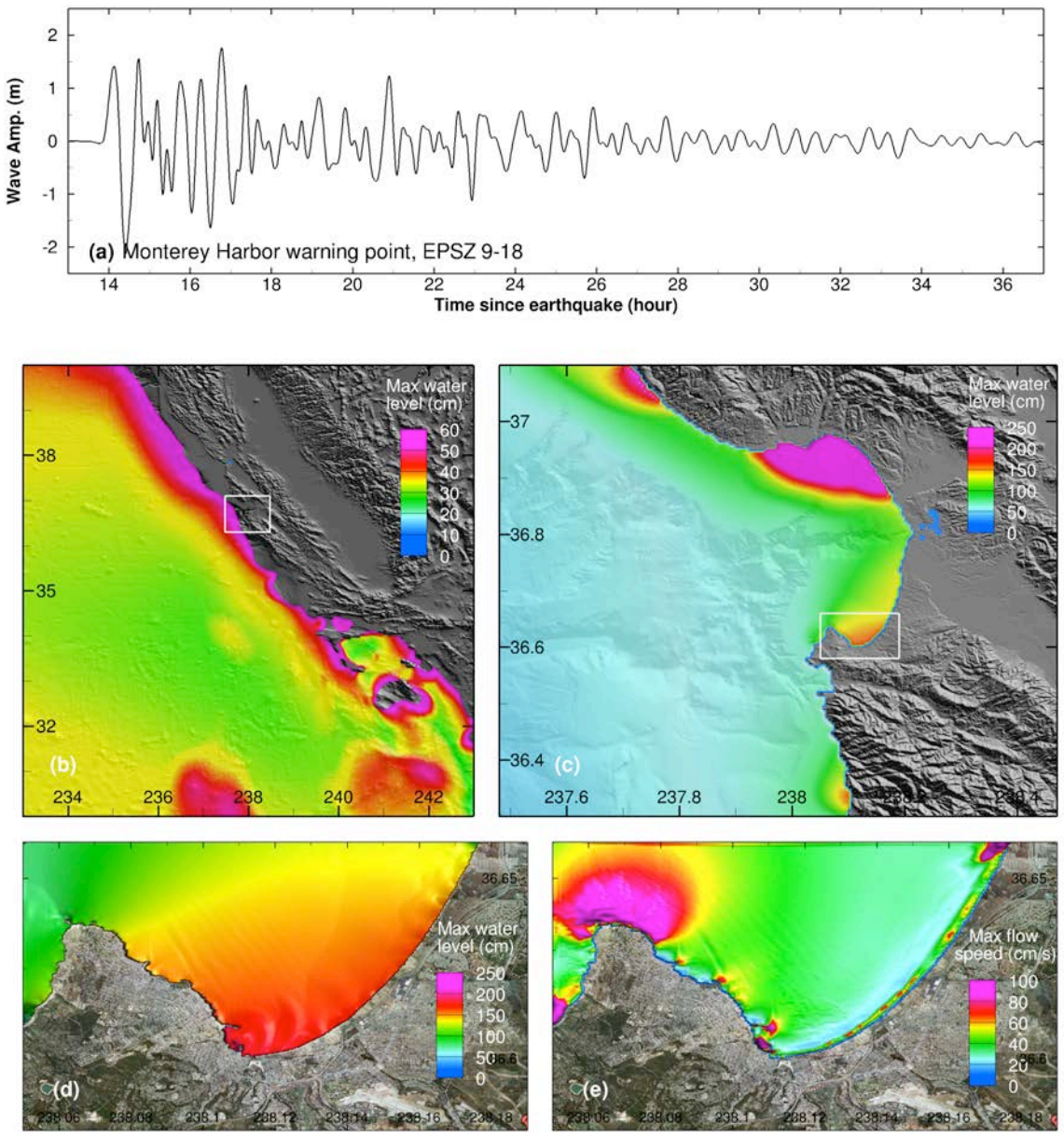

Figure 53 Model stability testing results at Monterey for synthetic mega tsunami scenario EPSZ 9-18. (a) Computed time series at the Monterey warning point; (b) Computed maximum wave amplitude in A grid of the forecast model; (c) Computed maximum current speed in B grid of the forecast model; (d) Computed maximum wave amplitude in C grid of the forecast model; (e) Computed current speed in C grid of the forecast model.

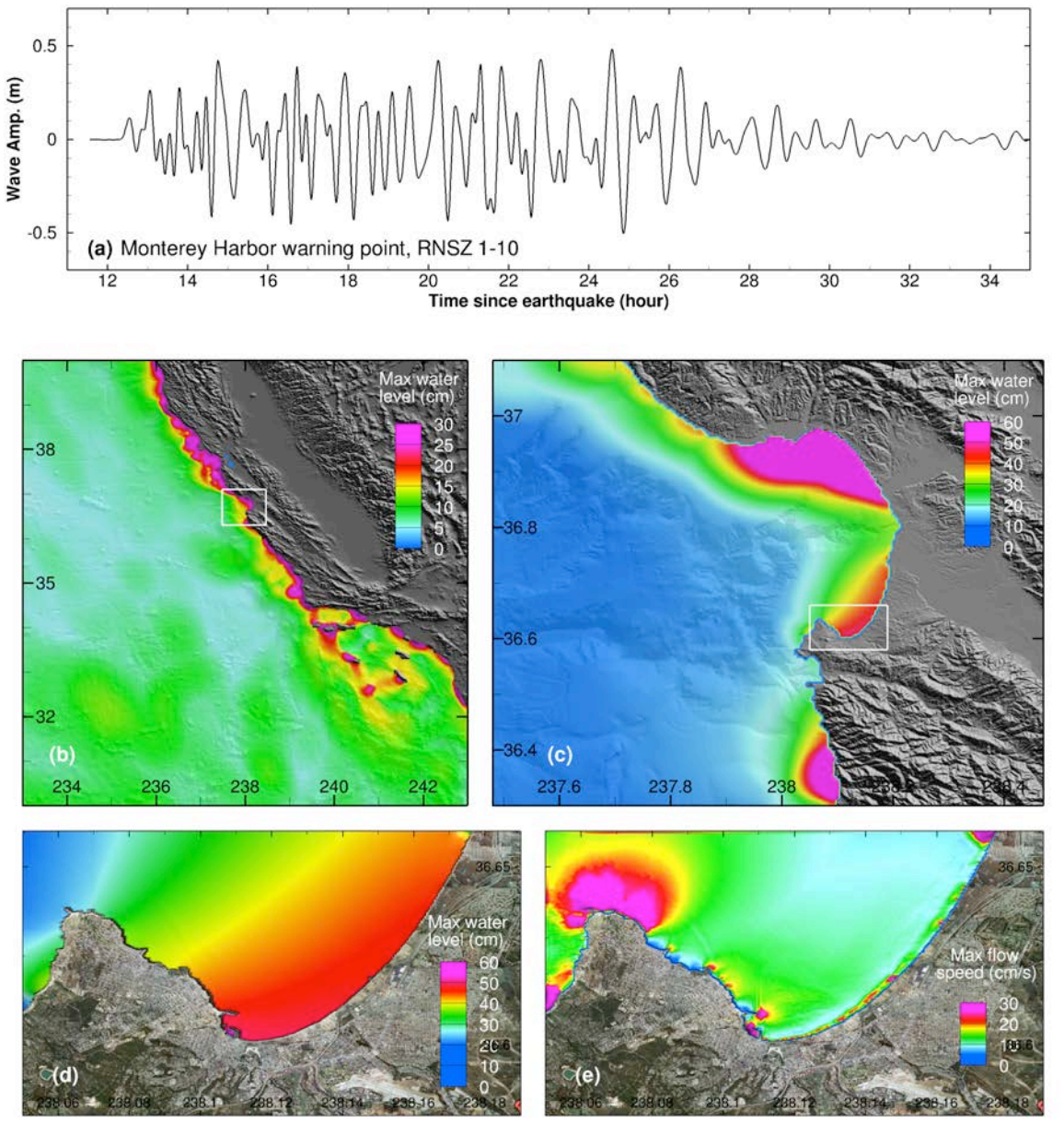

Figure 54 Model stability testing results at Monterey for synthetic mega tsunami scenario RNSZ 1-10. (a) Computed time series at the Monterey warning point; (b) Computed maximum wave amplitude in A grid of the forecast model; (c) Computed maximum current speed in B grid of the forecast model; (d) Computed maximum wave amplitude in C grid of the forecast model; (e) Computed current speed in C grid of the forecast model.

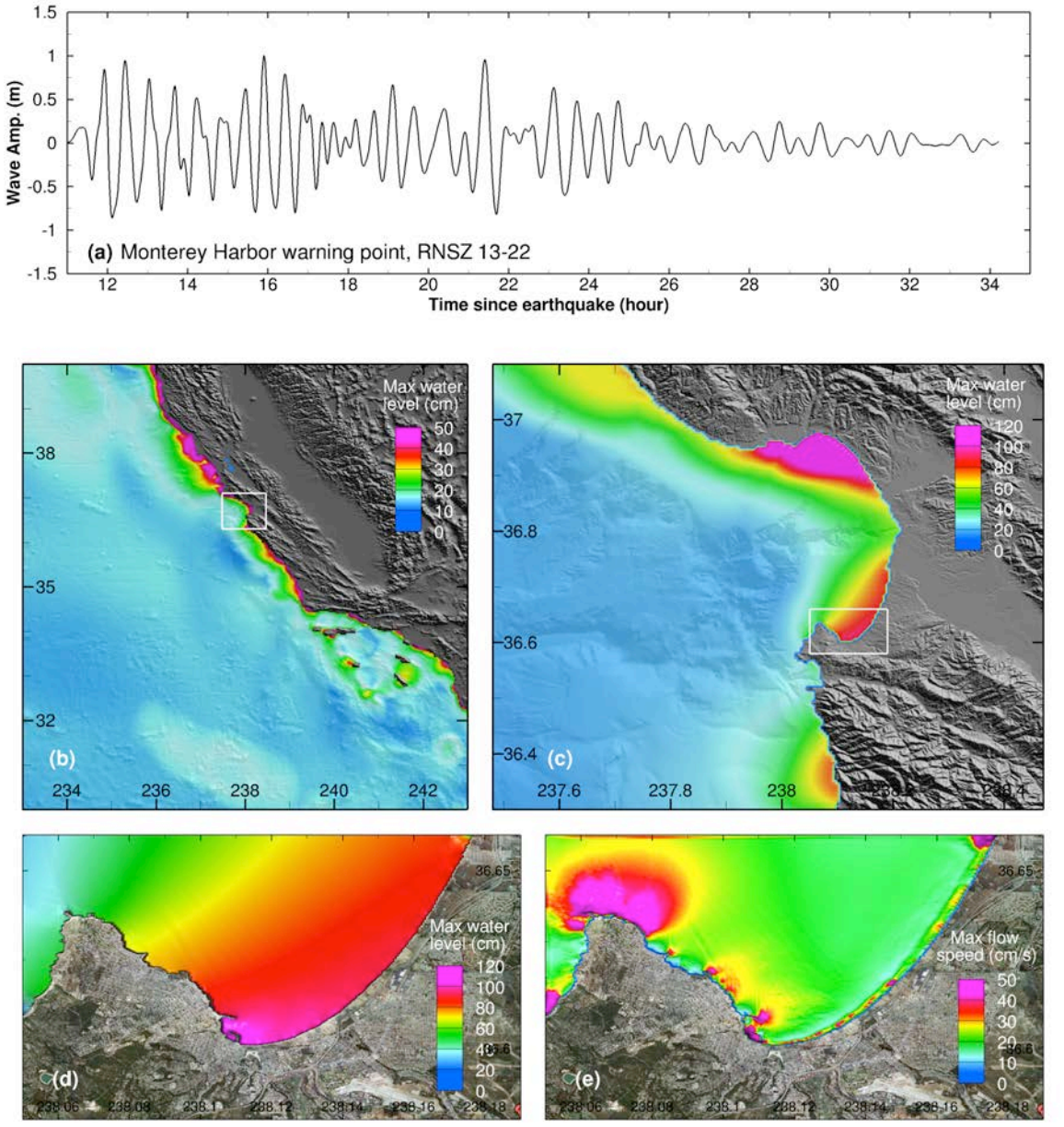

Figure 55 Model stability testing results at Monterey for synthetic mega tsunami scenario RNSZ 13-22. (a) Computed time series at the Monterey warning point; (b) Computed maximum wave amplitude in A grid of the forecast model; (c) Computed maximum current speed in B grid of the forecast model; (d) Computed maximum wave amplitude in C grid of the forecast model; (e) Computed current speed in C grid of the forecast model.

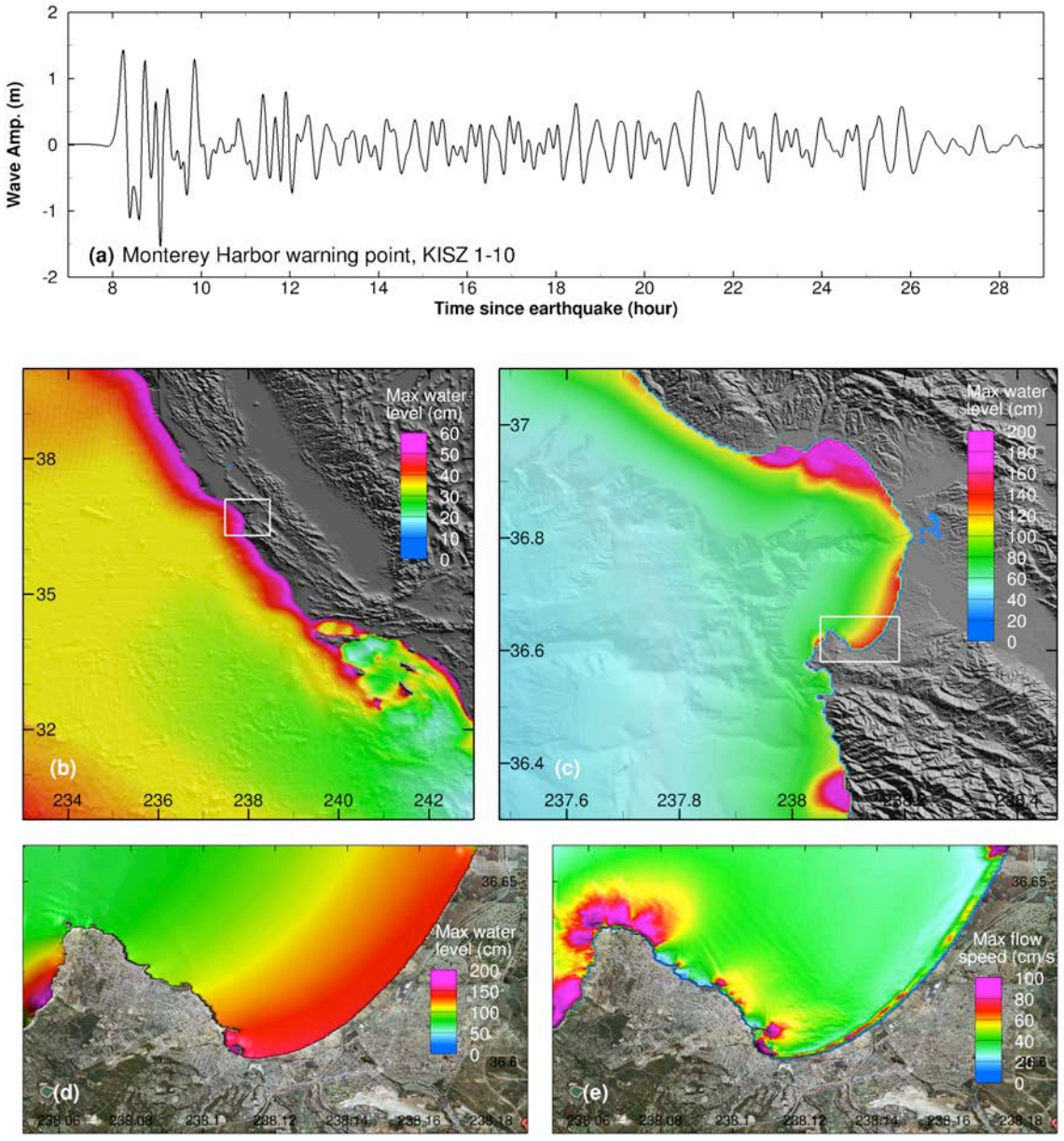

Figure 56 Model stability testing results at Monterey for synthetic mega tsunami scenario KISZ 1-10. (a) Computed time series at the Monterey warning point; (b) Computed maximum wave amplitude in A grid of the forecast model; (c) Computed maximum current speed in B grid of the forecast model; (d) Computed maximum wave amplitude in C grid of the forecast model; (e) Computed current speed in C grid of the forecast model.

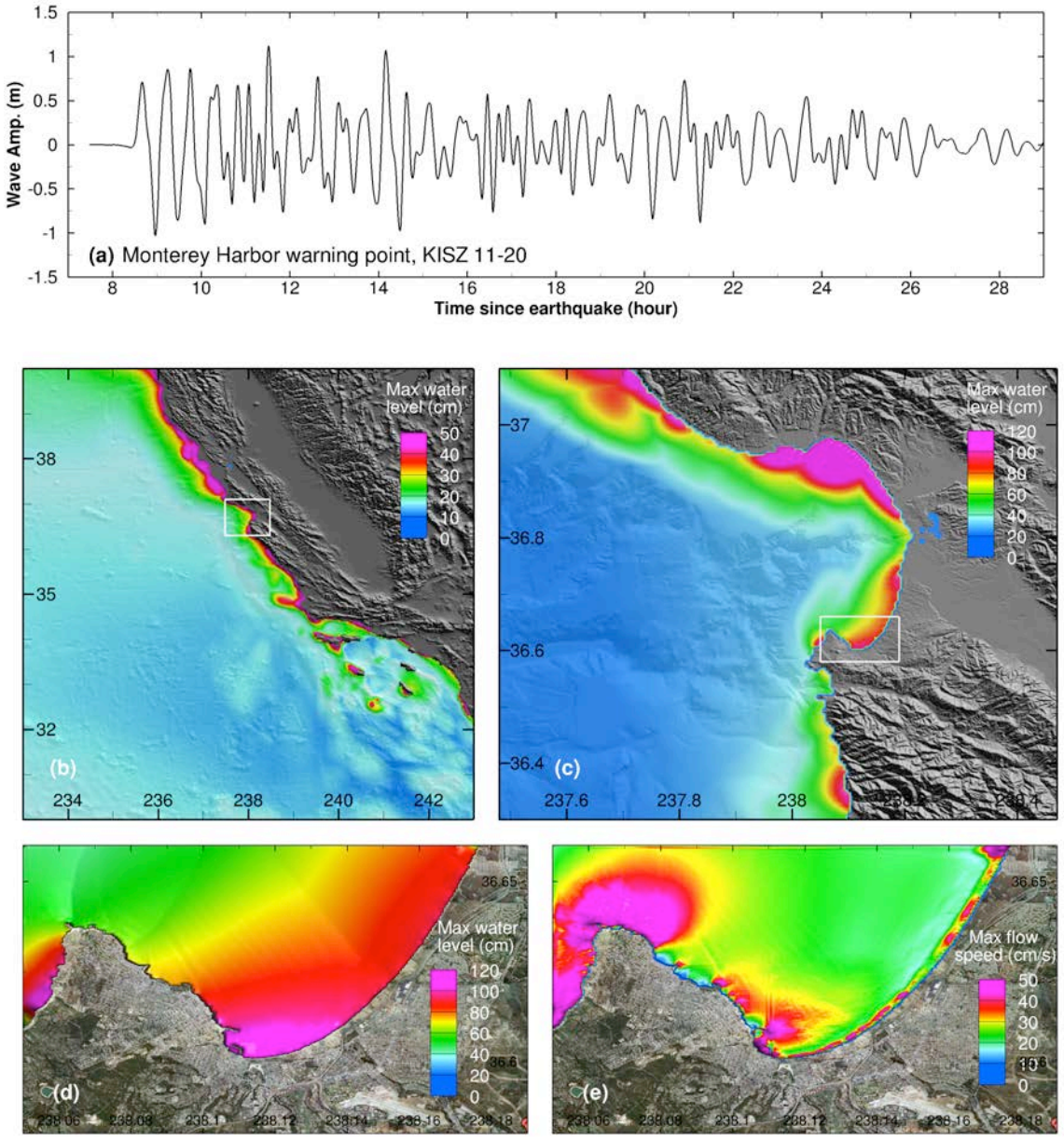

Figure 57 Model stability testing results at Monterey for synthetic mega tsunami scenario KISZ 11-20. (a) Computed time series at the Monterey warning point; (b) Computed maximum wave amplitude in A grid of the forecast model; (c) Computed maximum current speed in B grid of the forecast model; (d) Computed maximum wave amplitude in C grid of the forecast model; (e) Computed current speed in C grid of the forecast model.

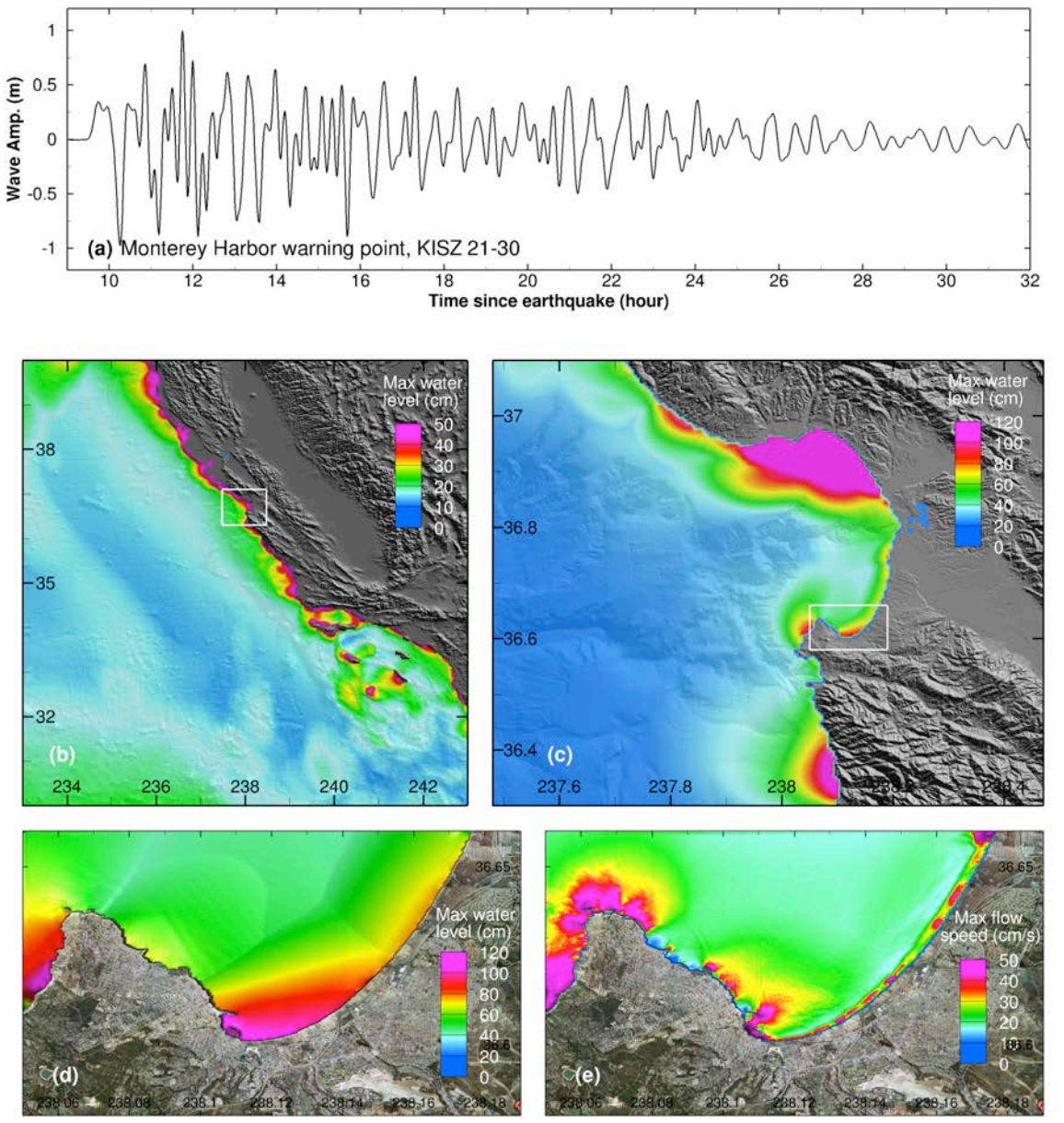

Figure 58 Model stability testing results at Monterey for synthetic mega tsunami scenario KISZ 21-30. (a) Computed time series at the Monterey warning point; (b) Computed maximum wave amplitude in A grid of the forecast model; (c) Computed maximum current speed in B grid of the forecast model; (d) Computed maximum wave amplitude in C grid of the forecast model; (e) Computed current speed in C grid of the forecast model.

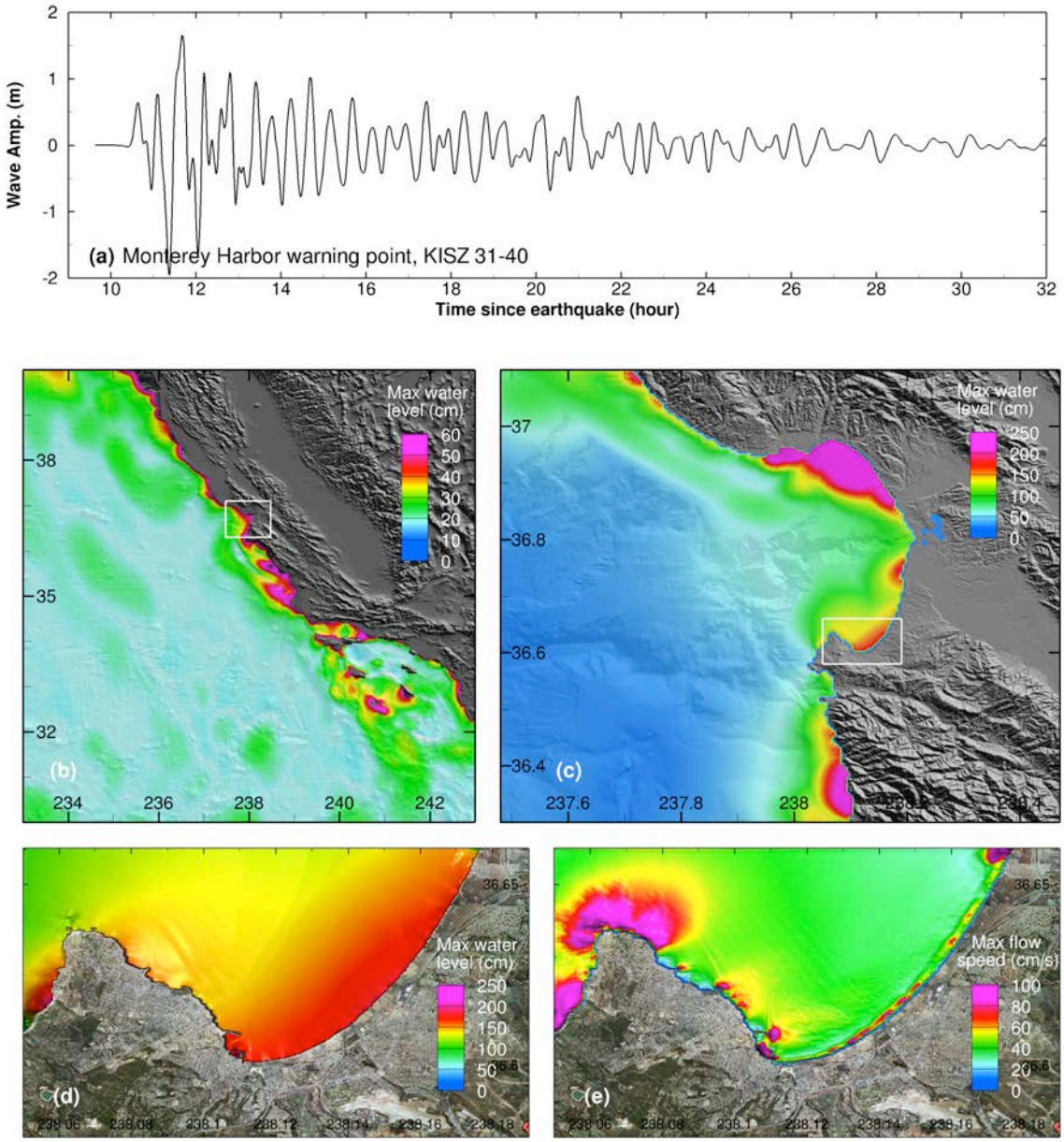

Figure 59 Model stability testing results at Monterey for synthetic mega tsunami scenario KISZ 31-40. (a) Computed time series at the Monterey warning point; (b) Computed maximum wave amplitude in A grid of the forecast model; (c) Computed maximum current speed in B grid of the forecast model; (d) Computed maximum wave amplitude in C grid of the forecast model; (e) Computed current speed in C grid of the forecast model.

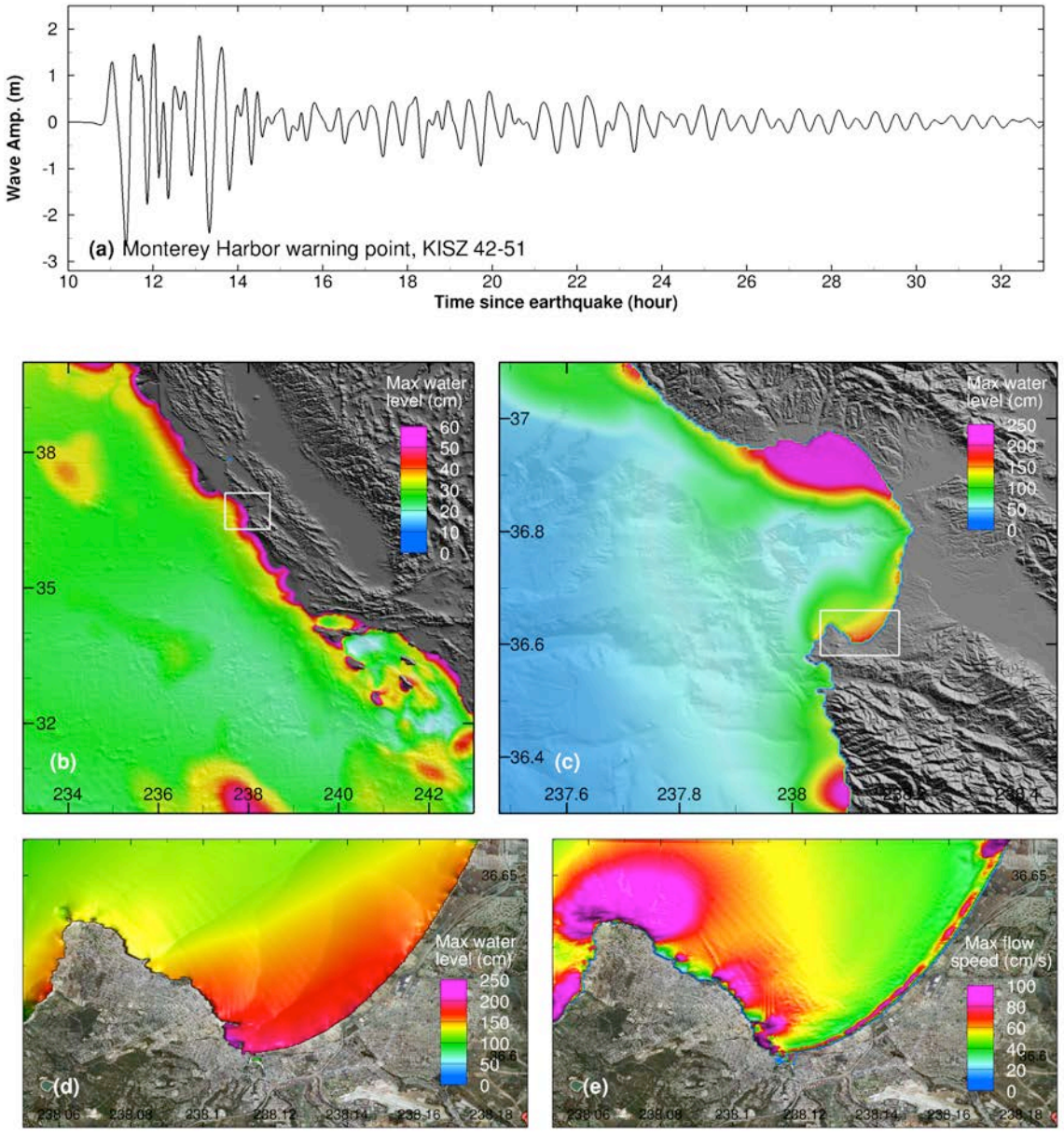

Figure 60 Model stability testing results at Monterey for synthetic mega tsunami scenario KISZ 42-51. (a) Computed time series at the Monterey warning point; (b) Computed maximum wave amplitude in A grid of the forecast model; (c) Computed maximum current speed in B grid of the forecast model; (d) Computed maximum wave amplitude in C grid of the forecast model; (e) Computed current speed in C grid of the forecast model.

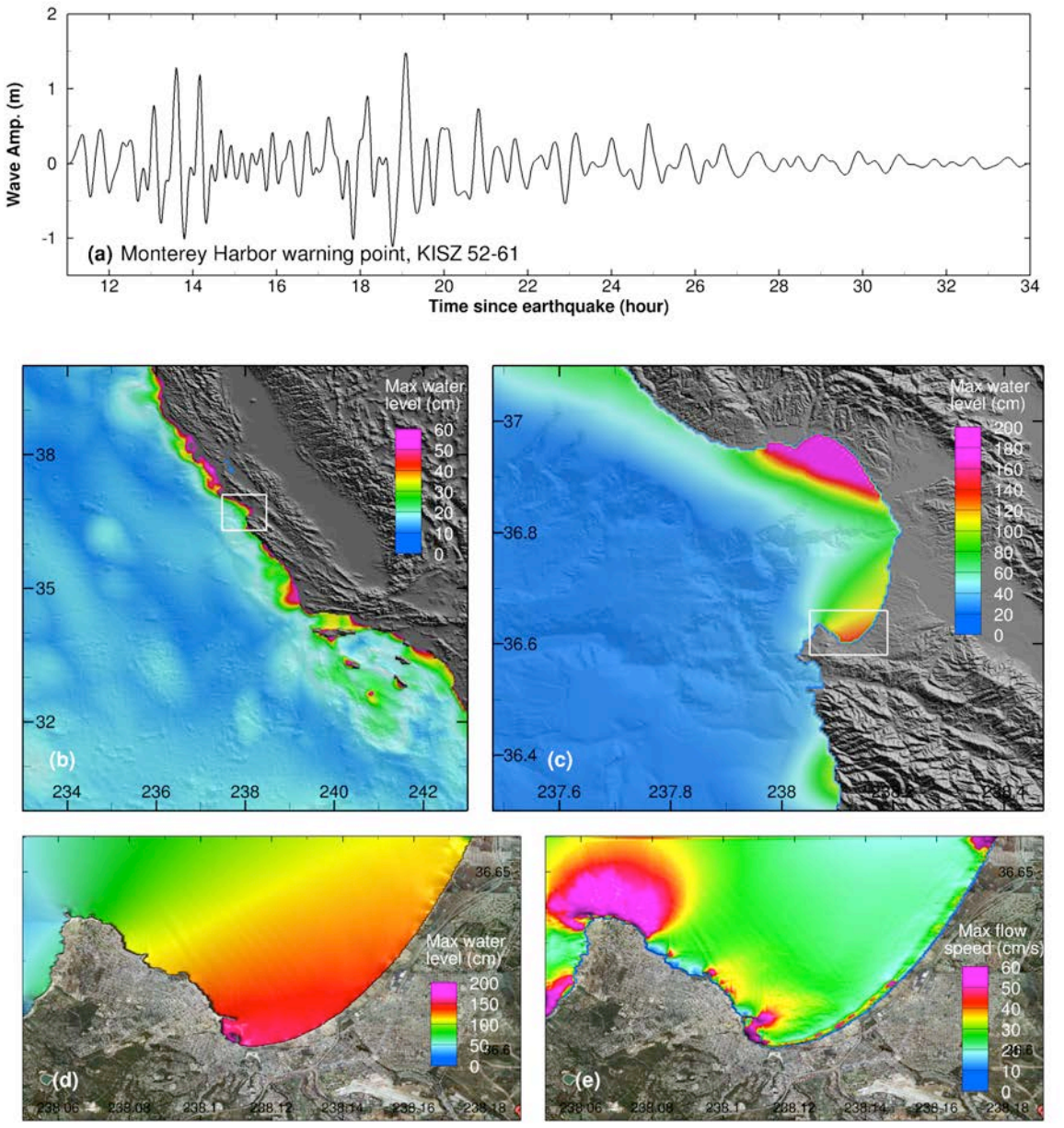

Figure 61 Model stability testing results at Monterey for synthetic mega tsunami scenario KISZ 52-61. (a) Computed time series at the Monterey warning point; (b) Computed maximum wave amplitude in A grid of the forecast model; (c) Computed maximum current speed in B grid of the forecast model; (d) Computed maximum wave amplitude in C grid of the forecast model; (e) Computed current speed in C grid of the forecast model.

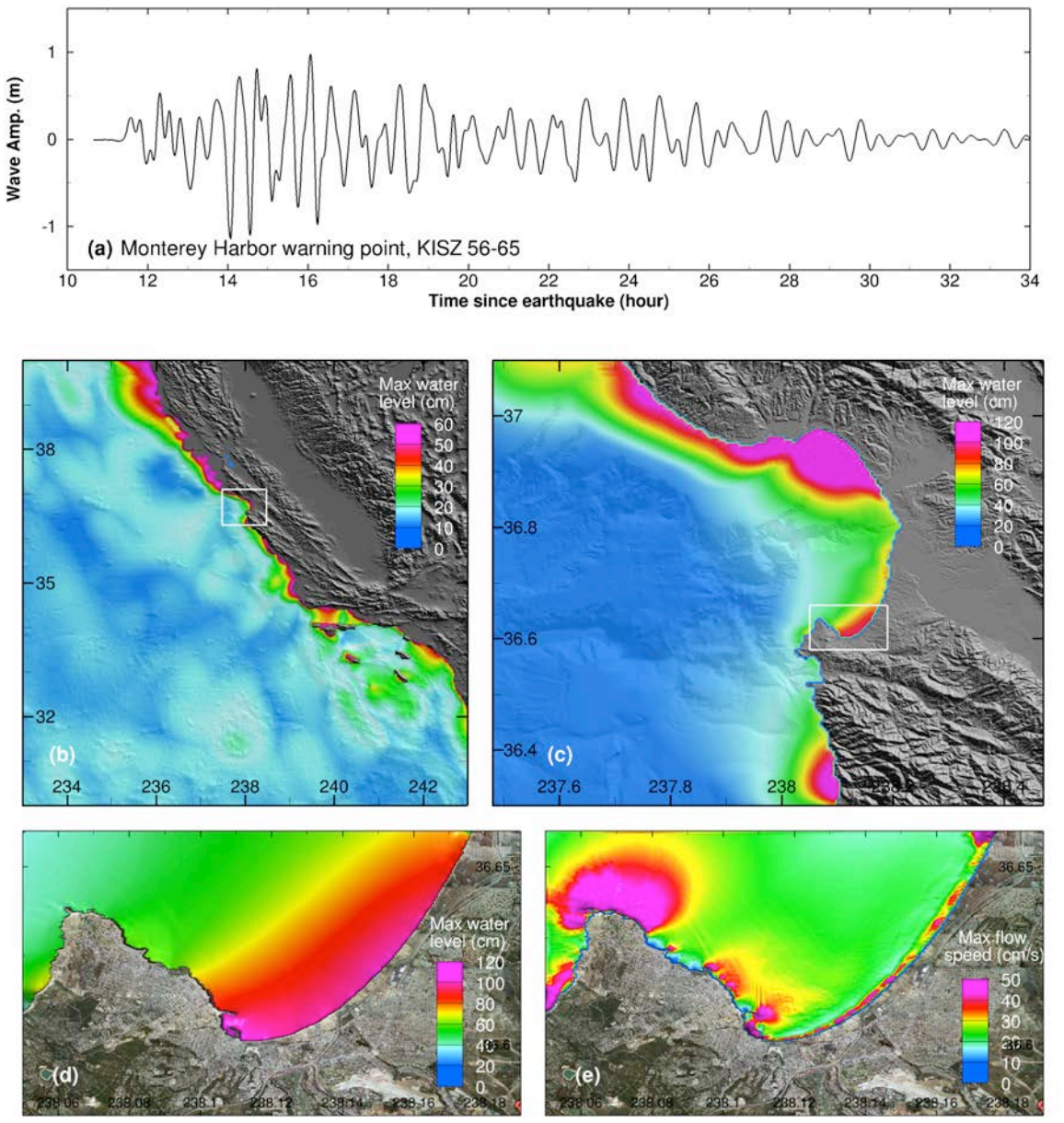

Figure 62 Model stability testing results at Monterey for synthetic mega tsunami scenario KISZ 56-65. (a) Computed time series at the Monterey warning point; (b) Computed maximum wave amplitude in A grid of the forecast model; (c) Computed maximum current speed in B grid of the forecast model; (d) Computed maximum wave amplitude in C grid of the forecast model; (e) Computed current speed in C grid of the forecast model.

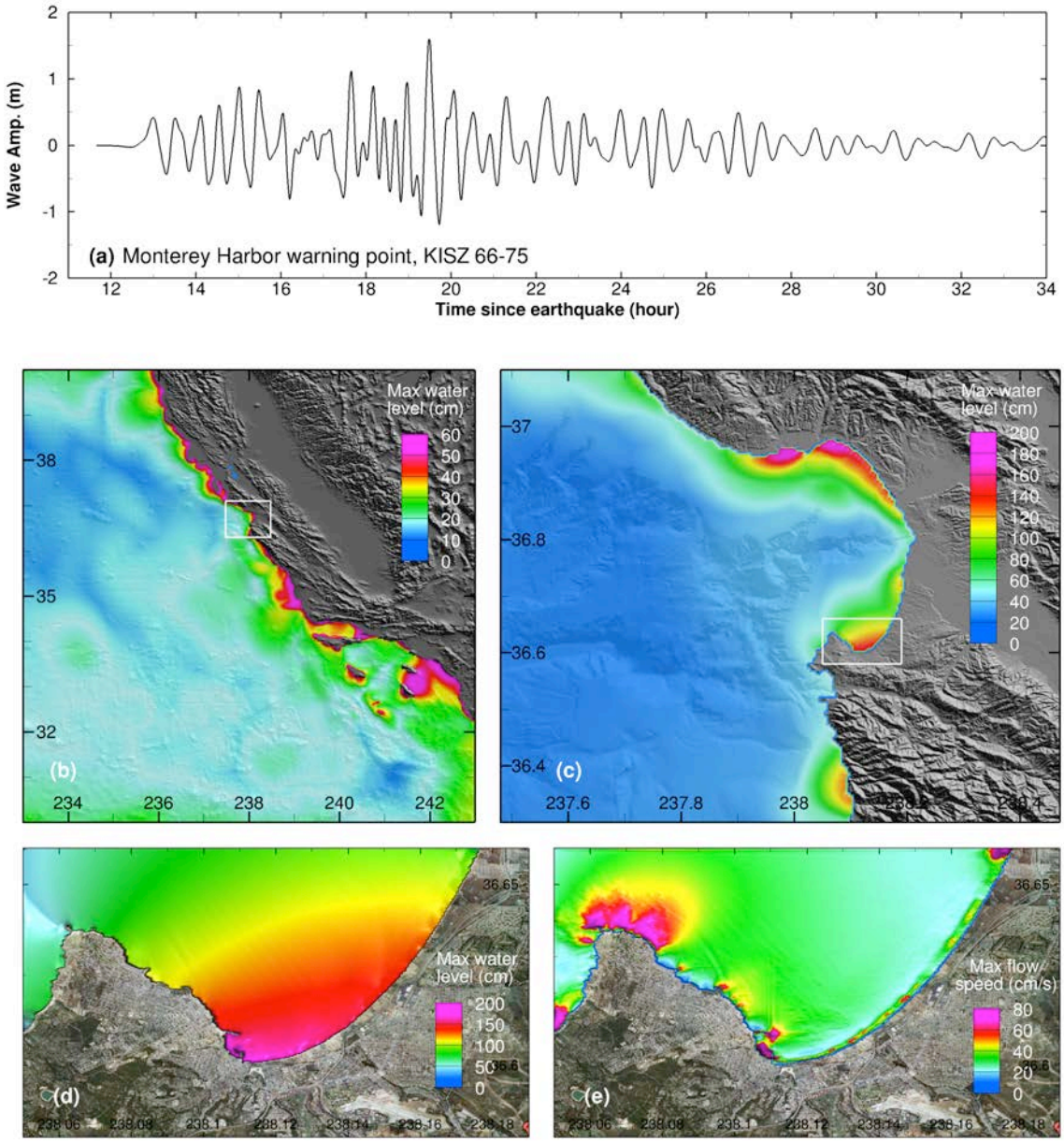

Figure 63 Model stability testing results at Monterey for synthetic mega tsunami scenario KISZ 66-75. (a) Computed time series at the Monterey warning point; (b) Computed maximum wave amplitude in A grid of the forecast model; (c) Computed maximum current speed in B grid of the forecast model; (d) Computed maximum wave amplitude in C grid of the forecast model; (e) Computed current speed in C grid of the forecast model.

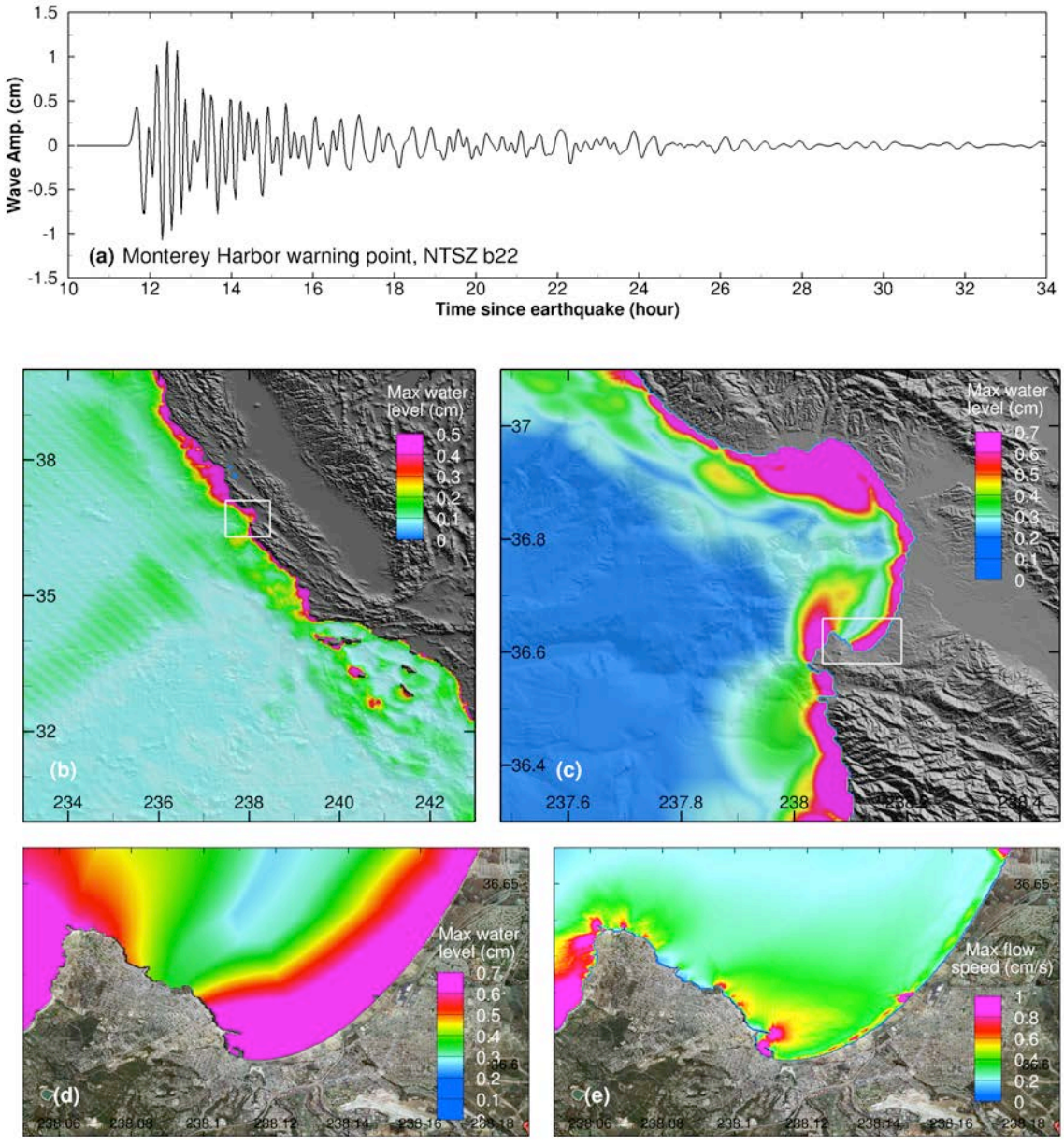

Figure 64 Model stability testing results at Monterey for synthetic tsunami scenario NTSZ b22. (a) Computed time series at the Monterey warning point; (b) Computed maximum wave amplitude in A grid of the forecast model; (c) Computed maximum current speed in B grid of the forecast model; (d) Computed maximum wave amplitude in C grid of the forecast model; (e) Computed current speed in C grid of the forecast model.

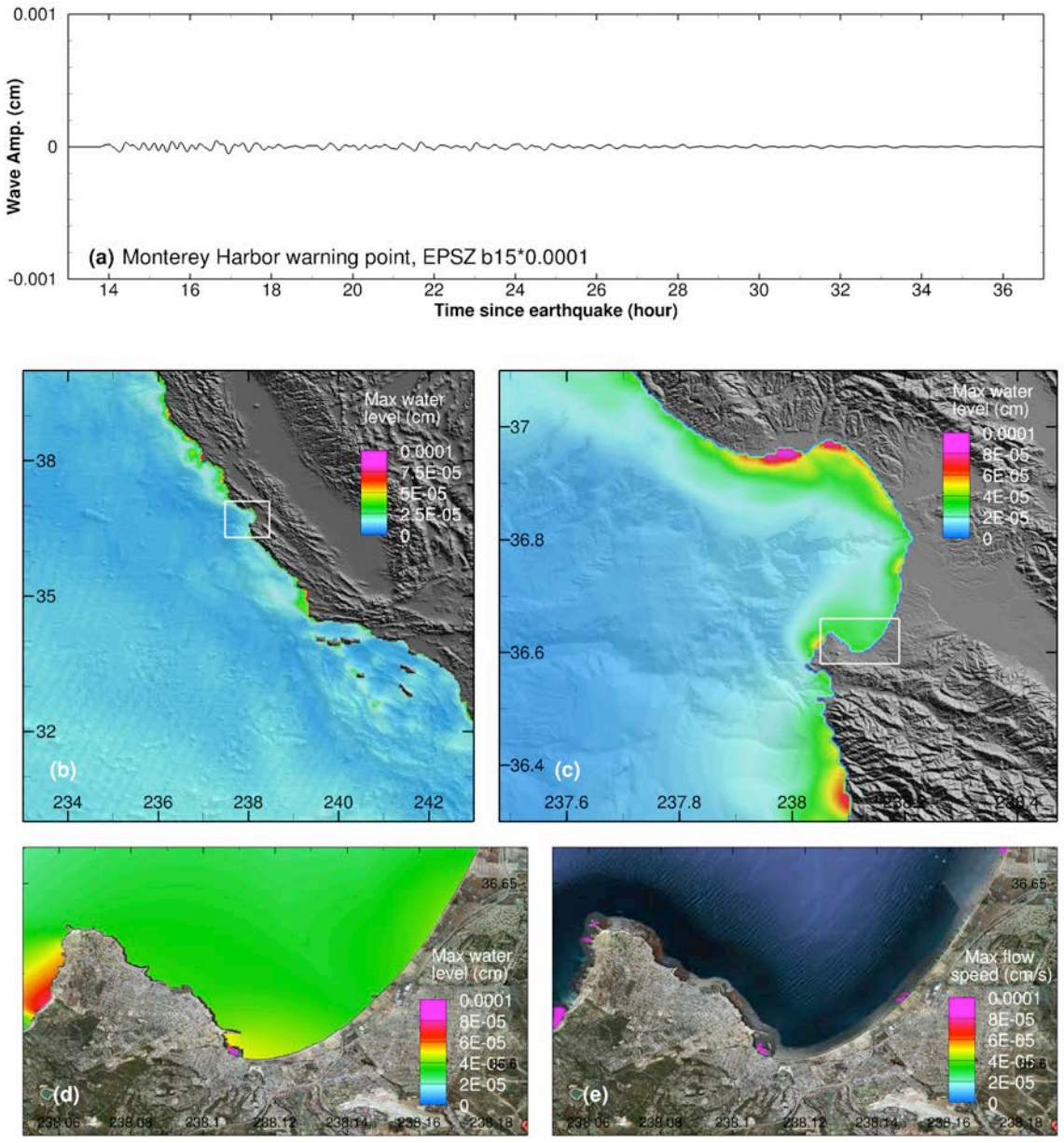

Figure 65 Model stability testing results at Monterey for synthetic micro tsunami scenario EPSZ b15. (a) Computed time series at the Monterey warning point; (b) Computed maximum wave amplitude in A grid of the forecast model; (c) Computed maximum current speed in B grid of the forecast model; (d) Computed maximum wave amplitude in C grid of the forecast model; (e) Computed current speed in C grid of the forecast model.

Tables:

Event	Date, Time (UTC), Epicenter	Mw	Earthquake source area	Max water elev. at Monterey, CA
1901 California	03 March 07:45:00 36.0ºN 120.5ºW	6.7	San Diego, California	observed
1946 Unimak	1 Apr. 12:28:56 53.32ºN 162.19ºW	8.1	Unimak Island, Alaska	0.91 m – 2.6 m at Monterey, 1.57 m at Pacific Grove.
1957 Alaska	9 Mar 14:22:31.9 51.292ºN, 175.629ºW	8.6	Alaska	0.6 m
1960 Chile	22 May 19:11:17 39.5ºS 74.5ºW	9.5	Valdivia, Chile	0.9 – 1.1 m
1964 Alaska	28 Mar. 03:36:14 61.04ºN, 147.73ºW	9.2	Prince William Sound, Alaska	Up to 2.6 m at Monterey, 1.4 m at Pacific Grove, and 4.5 m at Pebble Beach
1989 California	18 Oct. 00:04:15.2 37.036ºN, 121.883ºW	6.9	Loma Prieta, California	0.4 – 1.0 m
1992 California	25 Apr/ 18:06:4.2 40.368ºN, 124.316ºW	7.2	Humboldt County, California	0.03 m
1995 Chile	30 Jul. 05:11:23.6 23.34ºS, 70.294ºW	8.0	Antofagasta, Calama, and Mejillones, Chile	0.04 m
1995 Kuril	03 Dec. 18:01:8.9 44.63ºN, 149.3ºE	7.9	Kuril Islands	0.1 m
1996 Papua New Guinea	17 Feb. 05:59:30.5 0.891ºS, 136.953ºE	8.2	Papua New Guinea	0.05 m
1996 Andreanof	10 Jun. 04:03:35.4 51.564ºN, 177.632ºW	7.9	Andreanof Island, Alaska	observed
2001 Peru	23 Jun 20:33:14.1	8.4	Peru	0.08 m

	16.265ºS, 73.641ºW			
2003 Hokkaido	25 Sep 19:50:6.3 41.815ºN, 143.91ºE	8.3	Hokkaido, Japan	0.05 m
2004 Sumatra	26 Dec. 00:58:53.4 3.316ºN, 95.584ºE	9.1-9.3	Sumatra, Indonesia	0.1 m
2006 Kuril				
2007 Kuril				
2007 Peru	15 Aug. 23:40:57 13.354ºS, 76.509ºW	8.0	Central Peru	
2009 Samoa	29 Sep. 17:48:10.9 15.489ºS, 172.095ºW	8.0	Samoa Islands	0.15 m
2009 Vanuatu	7 Oct. 22:03:14.4 13.006ºS, 166.51ºE	7.6	Vanuatu Islands	0.05 m
2010 Chile	27 Feb. 06:34:11.5 36.122ºS, 72.898ºW	8.8	Maule, Chile	0.28 m
2011 Japan	11 Mar 05:46:24.1 38.297ºN 142.373ºE	9.0	Tohoku Island, Japan	0.7 m

Table 1. Historical tsunami events that have affected Monterey California.

Grid	Region	Reference Inundation Model (RIM)			Forecast Model		
		Coverage	Cell	Time	Coverage	Cell	Time
		Lat. [^{o}N]	Size	Step	Lat. [^{o}N]	Size	Step
		Lon. [^{o}W]	[“]	[sec]	Lon. [^{o}W]	[“]	[sec]
A	South Carolina	30-40	36	3.75	30-40	120	12.0
		127-117	(1001×1001)		127-117	(301×301)	
B	Monterey Bay	36.3 -37.1	3	0.25	36.3 -37.1	18	2.0
		122.52 –121.53	(1198×981)		122.52 – 121.53	(199×161)	
C	Monterey Harbor	33.58-36.71	1/3	0.25	36.58-36.66	2×1	2.0
		121.958-121.77	(2031×1405)		121.95-121.84	(253×289)	
Minimum offshore depth [m]			1		1		
Water depth for dry land [m]			0.1		0.1		
Friction coefficient (n^2)			0.0009		0.0009		
CPU time for a 4-hour simulation (min)			1489		10.4		
Warning point coordinates			121.88667W, 36.605N				

Table 2. Model setup and input parameters of Monterey forecast model and reference model.

Event	Time (UTC)	Source Zone	Mw	Lat. (°)	Lon. (°)	Source
1946 Unimak	1946-04-01 12:28:56	ACSZ	[4]8.5	53.32N	163.19W	[4]7.5 × b23 + 19.7 × b24 + 3.7 × b25
1964 Alaska	1964-03-28 03:36:14	ACSZ	[2]9.2	61.10N	147.50W	[4]Tang *et al*. (2006)
1994 Kuril	1994-10-04 13:23:28.5	KISZ	[1]8.3	43.60N	147.63E	[4]9.0 × a20
1996 Andreanov	1996-06-10 04:04:03.4	ACSZ	[1]7.9	51.10N	177.410W	[3]2.40 × a15 + 0.80 × b16
2001 Peru	2001-06-23 20:34:23.3	CSSZ	[1]8.4	17.28S	72.71W	[5]5.70 × a15 + 2.90 × b16 + 1.98 × a16
2006 Tonga	2006-05-03 15:27:03.7	NTSZ	[1]8.0	20.39S	173.47W	[3]6.6 × b29
2006 Kuril	2006-11-15 11:15:08.0	KISZ	[1]8.3	46.71N	154.33E	[3]4 × a12 + 0.5 × b12 + 2 × a13 + 1.5 × b13
2007 Kuril	2007-01-13 04:23:48.1	KISZ	[1]8.1	46.17N	154.80E	[3]-3.64 × b13
2007 Peru	2007-08-15 23:41:57.9	CSSZ	[1]8.0	13.73S	77.04W	[5]4.3 × a9 + 4.1 × b9
2009 Samoa	2009-09-29 17:48:10	NTSZ	[2]8.1	15.509ºS	172.034ºW	[4]6.45 × b34 + 6.21 × c35;
2010 Chile	2010-02-27 06:43:14	CSSZ	[2]8.8	35.909ºS	72.733ºW	[3]17.24 × a88 + 11.86 × b88 + 20.78 × z88 + 18.39 × b89 + 8.82 × a90 + 16.75 × b90 + 7.05 × z90
2011 Japan	2011-03-11 05:46:24	KISZ	[2]9.1	38.297ºN	142.372ºE	[3]4.66 × b24 + 12.23 × b25 + 26.31 × a26 + 21.27 × b26 + 22.75 × a27 + 4.98 × b27

[1]Centroid Moment Tensor

[2]United States Geological Survey (USGS)

[3]Tsunami source was obtained in real time and applied to the forecast

[4]Tsunami source was obtained in hindcast study

[5]Tsunami source was obtained in real time based on older propagation database (Gica et al., 2008)

Table 3 Historical events used for model validation for Monterey, California, where ASCZ represents the Aleutian-Alaska-Cascadia subduction zone, KISZ the Kamchatka-Kuril-Japan-Izu-Mariana-Yap subduction zone, CSSZ the Central South America subduction zone, and NTSZ the New Zealand-Kermadec-Tonga subduction zone.

Scenario	Source Zone	Tsunami Source	Alpha (m)
ACSZ 1-10	Aleutian-Alaska-Cascadia	A1-A10, B1-B10	28.4
ACSZ 11-20	Aleutian-Alaska-Cascadia	A11-A20, B11-B20	28.4
ACSZ 21-30	Aleutian-Alaska-Cascadia	A21-A30, B21-B30	28.4
ACSZ 31-40	Aleutian-Alaska-Cascadia	A31-A40, B31-B40	28.4
ACSZ 41-50	Aleutian-Alaska-Cascadia	A41-A50, B41-B50	28.4
ACSZ 46-55	Aleutian-Alaska-Cascadia	A46-A55, B46-B55	28.4
ACSZ 56-65	Aleutian-Alaska-Cascadia	A56-A65, B56-B65	28.4
CSSZ 1-10	Central and South America	A1-A10, B1-B10	28.4
CSSZ 11-20	Central and South America	A11-A20, B11-B20	28.4
CSSZ 21-30	Central and South America	A21-A30, B21-B30	28.4
CSSZ 31-40	Central and South America	A31-A40, B31-B40	28.4
CSSZ 41-50	Central and South America	A41-A50, B41-B50	28.4
CSSZ 51-60	Central and South America	A51-A60, B51-B60	28.4
CSSZ 61-70	Central and South America	A61-A70, B61-B70	28.4
CSSZ 71-80	Central and South America	A71-A80, B71-B80	28.4
CSSZ 81-90	Central and South America	A81-A90, B81-B90	28.4
NTSZ 1-10	New Zealand-Kermadec-Tonga	A1-A10, B1-B10	28.4
NTSZ 11-20	New Zealand-Kermadec-Tonga	A11-20, B11-20	28.4
NTSZ 21-30	New Zealand-Kermadec-Tonga	A21-30, B21-30	28.4
NTSZ 30-39	New Zealand-Kermadec-Tonga	A30-39, B30-39	28.4
NVSZ 1-10	New-Britain-Solomons-Vanuatu	A1-A10, B1-B10	28.4
NVSZ 11-20	New-Britain-Solomons-Vanuatu	A11-A20, B11-B20	28.4
NVSZ 21-30	New-Britain-Solomons-Vanuatu	A21-A30, B21-B30	28.4
NVSZ 28-37	New-Britain-Solomons-Vanuatu	A28-A37, B28-37	28.4
MOSZ 1-10	Manus Ocean Convergence Boundary	A1-A10, B1-B10	28.4
MOSZ 8-17	Manus Ocean Convergence Boundary	A8-A17, B8-B17	28.4
NGSZ 1-10	New Guinea	A1-A10, B1-B10	28.4
NGSZ 6-15	New Guinea	A6-A15, B6-B15	28.4
EPSZ 1-10	East-Philippines	A1-A10, B1-B10	28.4

EPSZ 9-18	East-Philippines	A9-A18, B9-B18	28.4
RNSZ 1-10	Ryukyu-Kyushu-Nankai	A1-A10, B1-B10	28.4
RNSZ 13-22	Ryukyu-Kyushu-Nankai	A13-A22, B13-B22	28.4
KISZ 1-10	Kamchatka-Yap-Mariana-Izu-Bonin	A1-A10, B1-B10	28.4
KISZ 11-20	Kamchatka-Yap-Mariana-Izu-Bonin	A11-A20, B11-B20	28.4
KISZ 21-30	Kamchatka-Yap-Mariana-Izu-Bonin	A21-A30, B21-B30	28.4
KISZ 32-41	Kamchatka-Yap-Mariana-Izu-Bonin	A32-A41, B32-B41	28.4
KISZ 42-51	Kamchatka-Yap-Mariana-Izu-Bonin	A42-A51, B42-B51	28.4
KISZ 52-61	Kamchatka-Yap-Mariana-Izu-Bonin	A52-A61, B52-B61	28.4
KISZ 56-65	Kamchatka-Yap-Mariana-Izu-Bonin	A56-A65, B56-B65	28.4
KISZ 66-75	Kamchatka-Yap-Mariana-Izu-Bonin	A66-A75, B66-B75	28.4
NTSZ b22	New Zealand-Kermadec-Tonga	B22	1.0
EPSZ b15	East-Philippines	B15	0.0001

Table 4 Tsunami source of 51 synthetic scenarios used for stability testing, where ACSZ = Alaska-Aleutian-Canada source zone, CSSZ = Central and South America source zone; NTSZ = New Zealand-Kermadec-Tonga source zone; NVSZ = New Britain-Solomons-Vanuatu source zone; MOSZ = Manus OCB source zone; NGSZ = North New Guinea source zone; EPSZ = East Philippines source zone; RNSZ = Ryukyu-Kyushu-Nankai source zone; KISZ = Kamchatka-Kuril-Japan trench source zone.

Appendix A.

Development of the Monterey, California, tsunami forecast model occurred prior to parameters changes that were made to reflect modification to the MOST model code. As a result, the input file for running both the optimized tsunami forecast model and the high-resolution reference inundation model in MOST have been updated accordingly. Appendix A1 and A2 provide the updated files for Monterey, California.

A.1 Forecast model .in file:

```
0.0001 Minimum amplitude of input offshore wave (m)
1.0    nput minimum depth for offshore (m)
0.1    nput "dry land" depth for inundation (m)
0.0009 Input friction coefficient (n**2)
1      let a and b run up
300.0  blowup limit
1.0    input time step (sec)
43200  input amount of steps
12     Compute "A" arrays every n-th time step, n=
1      Compute "B" arrays every n-th time step, n=
36     Input number of steps between snapshots
1      ...Starting from
1      ...saving grid every n-th node, n=
```

A.2 Reference model .in file:

```
0.0001 Minimum amplitude of input offshore wave (m)
1.0  Input minimum depth for offshore (m)
0.1   Input "dry land" depth for inundation (m)
0.0009 Input friction coefficient (n**2)
1     let a and b run up 300.0 blowup limit
0.25   input time step (sec)
115200 input amount of steps
15     Compute "A" arrays every n-th time step, n=
1 COmpute "B" arrays every n-th time step, n=
120   Input number of steps between snapshots
1 ...Starting from
1 ...saving grid every n-th node, n=
```

Appendix B. Propagation database: Pacific Ocean Unit Sources

These propagation source details reflect the database as of February 2013, and there may have been updates in the earthquake source parameters after this date.

Appendix C. SIFT testing results

Authors: Lindsey Wright, Yong Wei

C1. Purpose

Forecast models are tested with synthetic tsunami events covering a range of tsunami source locations. Testing is also done with selected historical tsunami events when available.

The purpose of forecast model testing is three-fold. The first objective is to assure that the results obtained with NOAA's tsunami forecast system, which has been released to the Tsunami Warning Centers for operational use, are consistent with those obtained by the researcher during the development of the forecast model. The second objective is to test the forecast model for consistency, accuracy, time efficiency, and quality of results over a range of possible tsunami locations and magnitudes. The third objective is to identify bugs and issues in need of resolution by the researcher who developed the Forecast Model or by the forecast software development team before the next version release to NOAA's two Tsunami Warning Centers.

Local hardware and software applications, and tools familiar to the researcher(s), are used to run the Method of Splitting Tsunamis (MOST) model during the forecast model development. The test results presented in this report lend confidence that the model performs as developed and produces the same results when initiated within the forecast application in an operational setting as those produced by the researcher during the forecast model development. The test results assure those who rely on the Santa Monica tsunami forecast model that consistent results are produced irrespective of system.

C2. Testing procedure

The general procedure for forecast model testing is to run a set of synthetic tsunami scenarios and a selected set of historical tsunami events through the forecast system application and compare the results with those obtained by the researcher during the forecast model development and presented in the Tsunami Forecast Model Report. Specific steps taken to test the model include:

1. Identification of testing scenarios, including the standard set of synthetic events, appropriate historical events, and customized synthetic scenarios that may have been used by the researcher(s) in developing the forecast model.
2. Creation of new events to represent customized synthetic scenarios used by the researcher(s) in developing the forecast model, if any.
3. Submission of test model runs with the forecast system, and export of the results from A, B, and C grids, along with time series.
4. Recording applicable metadata, including the specific version of the forecast system used for testing.
5. Examination of forecast model results from the forecast system for instabilities in both time series and plot results.
6. Comparison of forecast model results obtained through the forecast system with those obtained during the forecast model development.
7. Summarization of results with specific mention of quality, consistency, and time efficiency.
8. Reporting of issues identified to modeler and forecast software development team.

9. Retesting the forecast models in the forecast system when reported issues have been addressed or explained.

Synthetic model runs were tested on a DELL PowerEdge R510 computer equipped with two Xeon E5670 processors at 2.93 Ghz, each with 12 MBytes of cache and 32GB memory. The processors are hex core and support hyperthreading, resulting in the computer performing as a 24 processor core machine. Additionally, the testing computer supports 10 Gigabit Ethernet for fast network connections. This computer configuration is similar or the same as the configurations of the computers installed at the Tsunami Warning Centers so the compute times should only vary slightly.

C3. Results

The Monterey forecast model was tested with NOAA's tsunami forecast system version 3.2.

The Monterey forecast model was tested with four synthetic scenarios and one historical tsunami event. Test results from the forecast system and comparisons with the results obtained during the forecast model development are shown numerically in Table 1 and graphically in Figures 1 to 5. The results show that the forecast model is stable and robust, with consistent and high quality results across geographically distributed tsunami sources and mega-event tsunami magnitudes. The model run time (wall clock time) was 22.77 minutes for 12 hours of simulation time, and 7.60 minutes for 4 hours. This run time is well within the 10 minute run time for 4 hours of simulation time and satisfies time efficiency requirements.

Four synthetic events were run on the Monterey forecast model. The modeled scenarios were stable for all cases tested, with no instabilities or ringing. Results show that the largest modeled height was 266 centimeters (cm) and originated in the New Zealand-Kermadec-Tonga (NTSZ 30-39) source. Amplitudes greater than 100 cm were recorded for 3 of the 4 test sources. The smallest signal of 99 cm was recorded at the Kamchatka-Yap-Mariana-Izu-Bonin (KISZ 21-30) source. Direct comparisons of output from the forecast tool with results of both the Tohoku 2011 historical event and available development synthetic events, demonstrated that the wave patterns were nearly identical in shape, pattern, and with very small difference in the amplitude. These differences are mainly attributed to update of the tsunami propagation database over the last years.

Source Zone	Tsunami Source	α [m]	SIFT Max (cm)	Development Max (cm)	SIFT Min (cm)	Development Min (cm)
Mega-tsunami scenarios						
KISZ	A21-A30, B21-B30	28.4	99.3	100.1	-99.9	-100.1
ACSZ	A56-A65, B56-B65	28.4	123.2	122.1	-77.7	-77.78
CSSZ	A81-A190, B81-B90	28.4	104.0	104.0	-94.6	-94.41
NTSZ	A30-39, B30-39	28.4	266.4	266.3	-265.5	-265.2
Historical events						
Tohoku 2011			72.3	72.3	-72.0	72.0

Table C1. Table of maximum and minimum amplitudes (cm) at the Monterey, California warning point for synthetic and historical events tested using SIFT 3.2 and obtained during development.

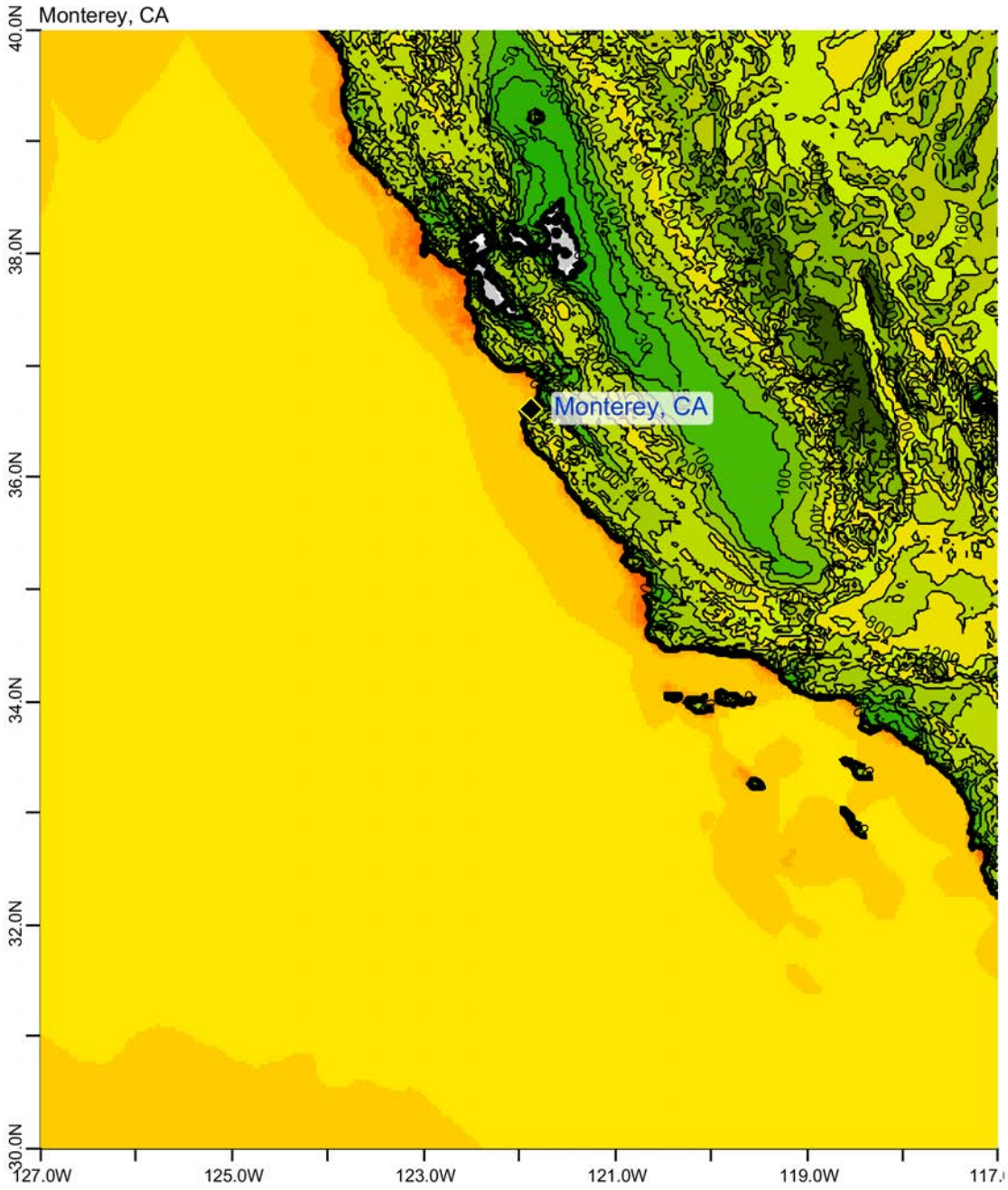

Figure C1. Max computed wave amplitude of A grid, Monterey, California, for synthetic event KISZ 21-30.

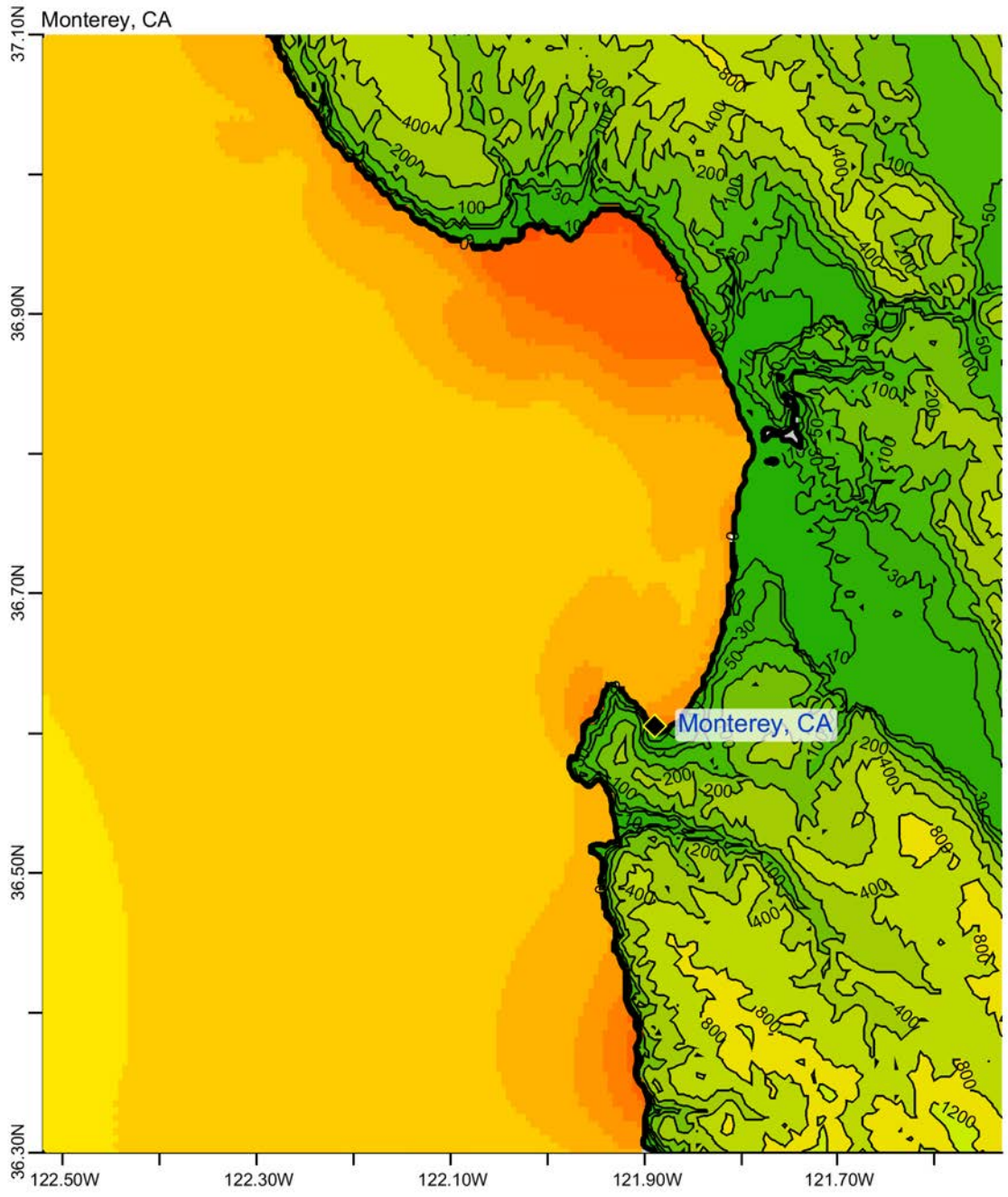

Figure C2. Max computed wave amplitude of B grid, Monterey, California, for synthetic event KISZ 21-30.

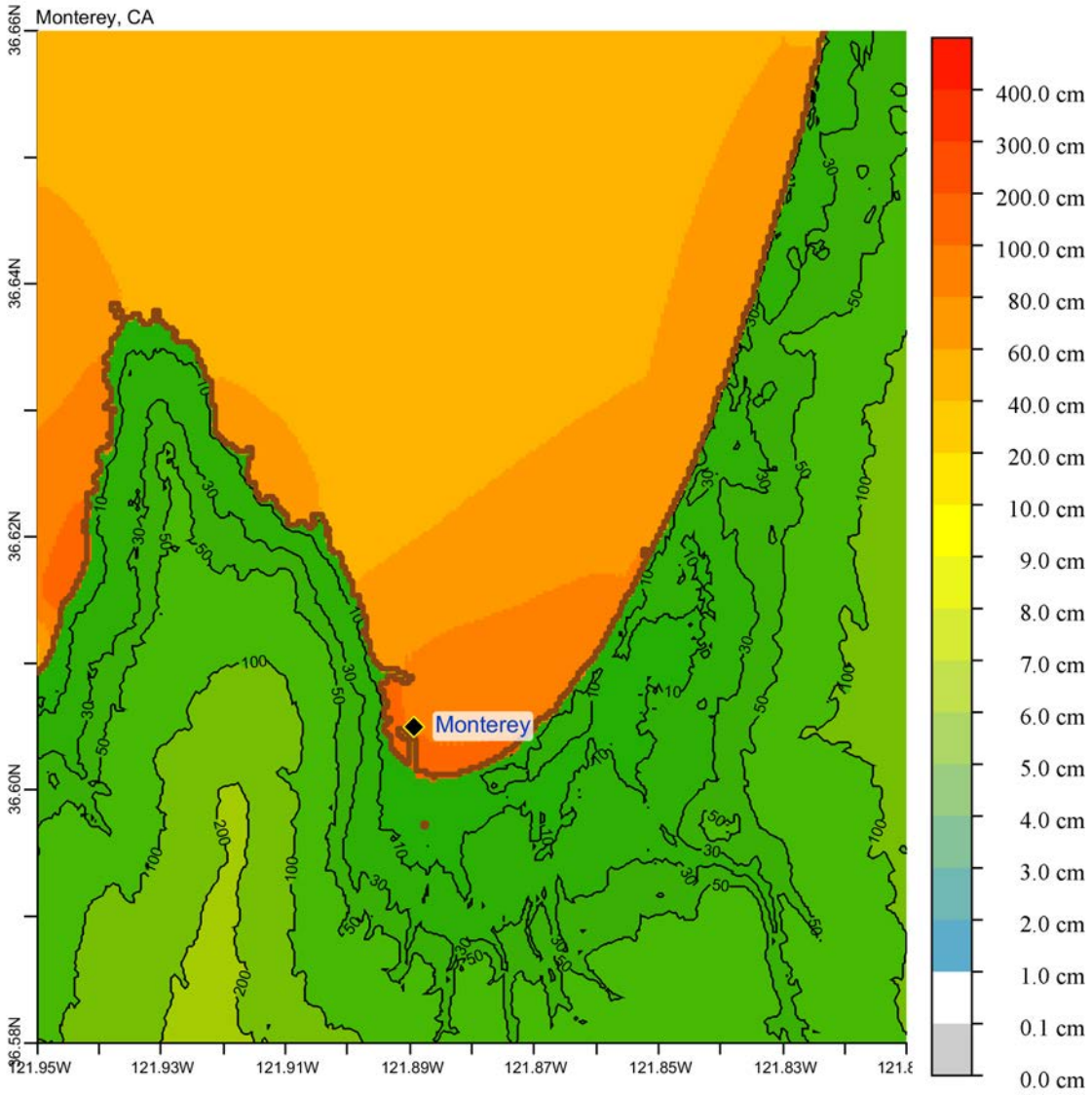

Figure C3. Max computed wave amplitude of C grid, Monterey, California, for synthetic event KISZ 21-30.

(a)

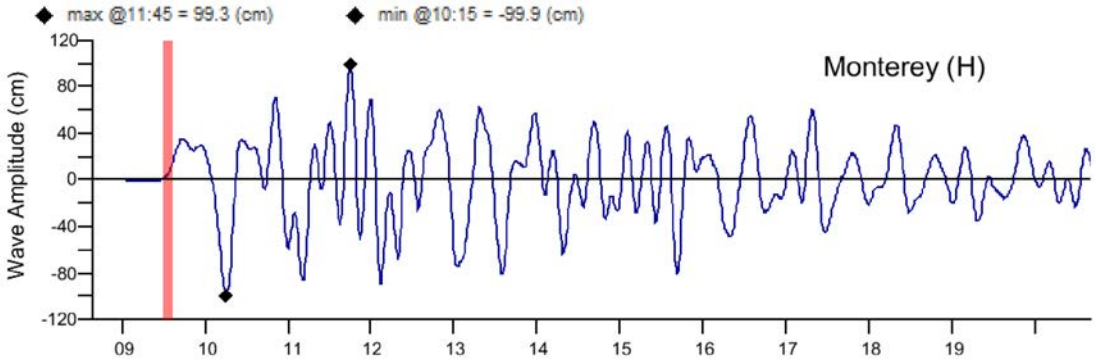

(b)

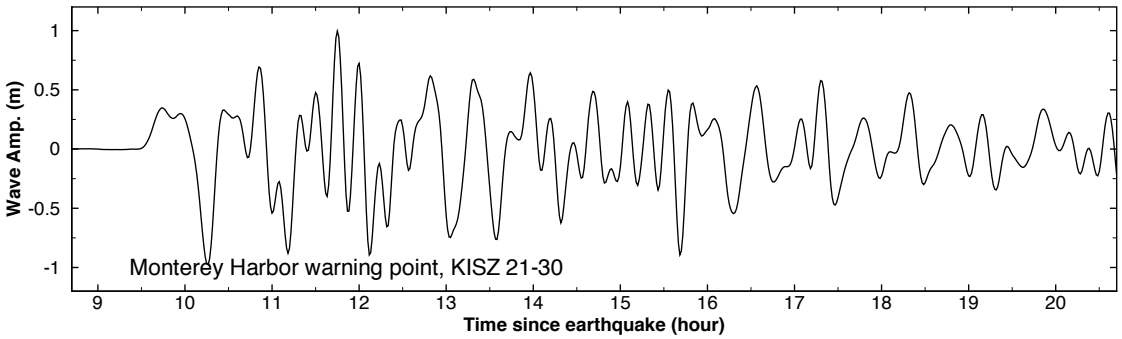

Figure C4. Computed time series at Monterey tide gage, for synthetic event KISZ 21-30: (a) time series computed in SIFT; (b) time series shown in the forecast model report.

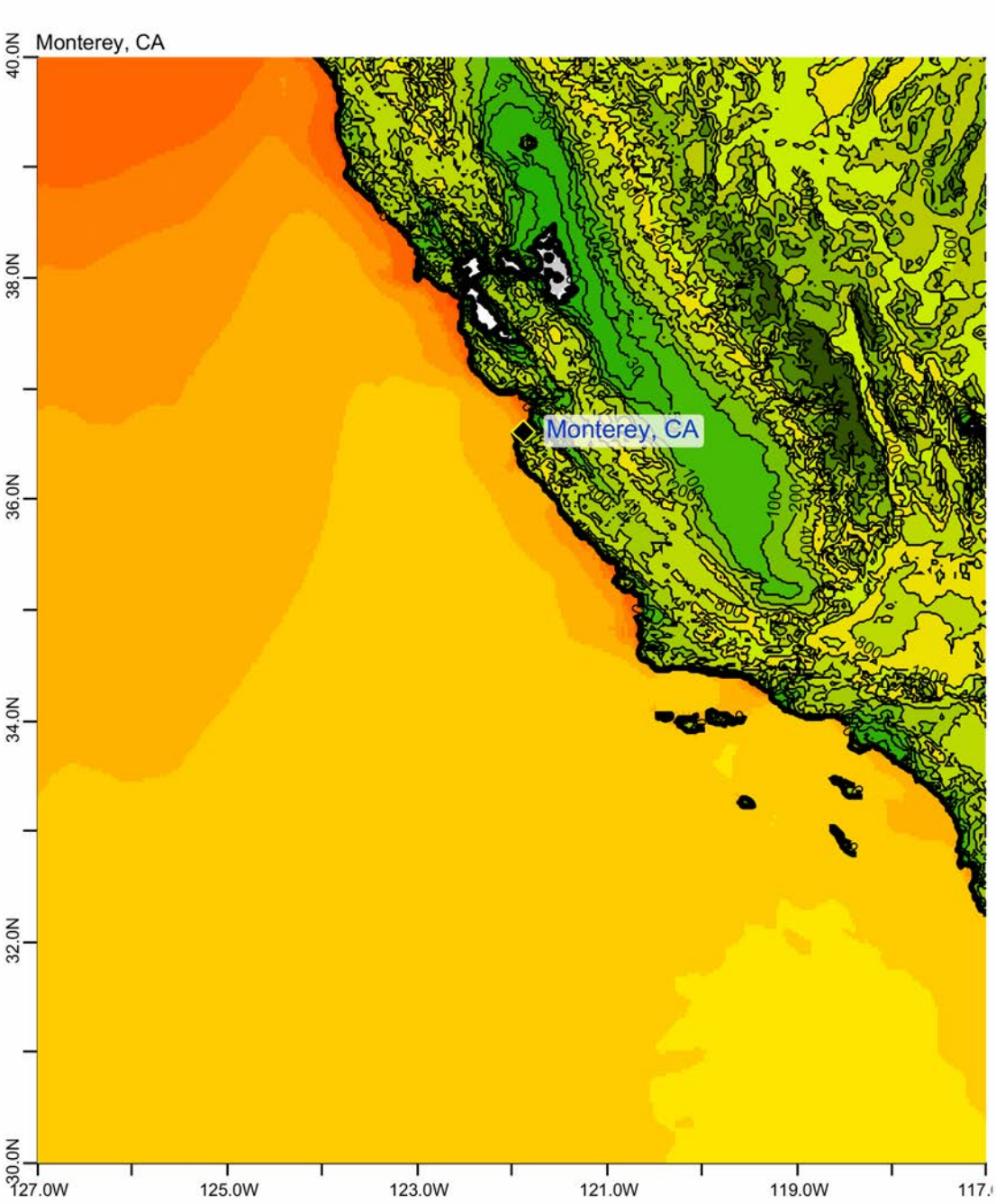

Figure C5. Max computed wave amplitude of A grid, Monterey, California, for synthetic event ACSZ 56-65.

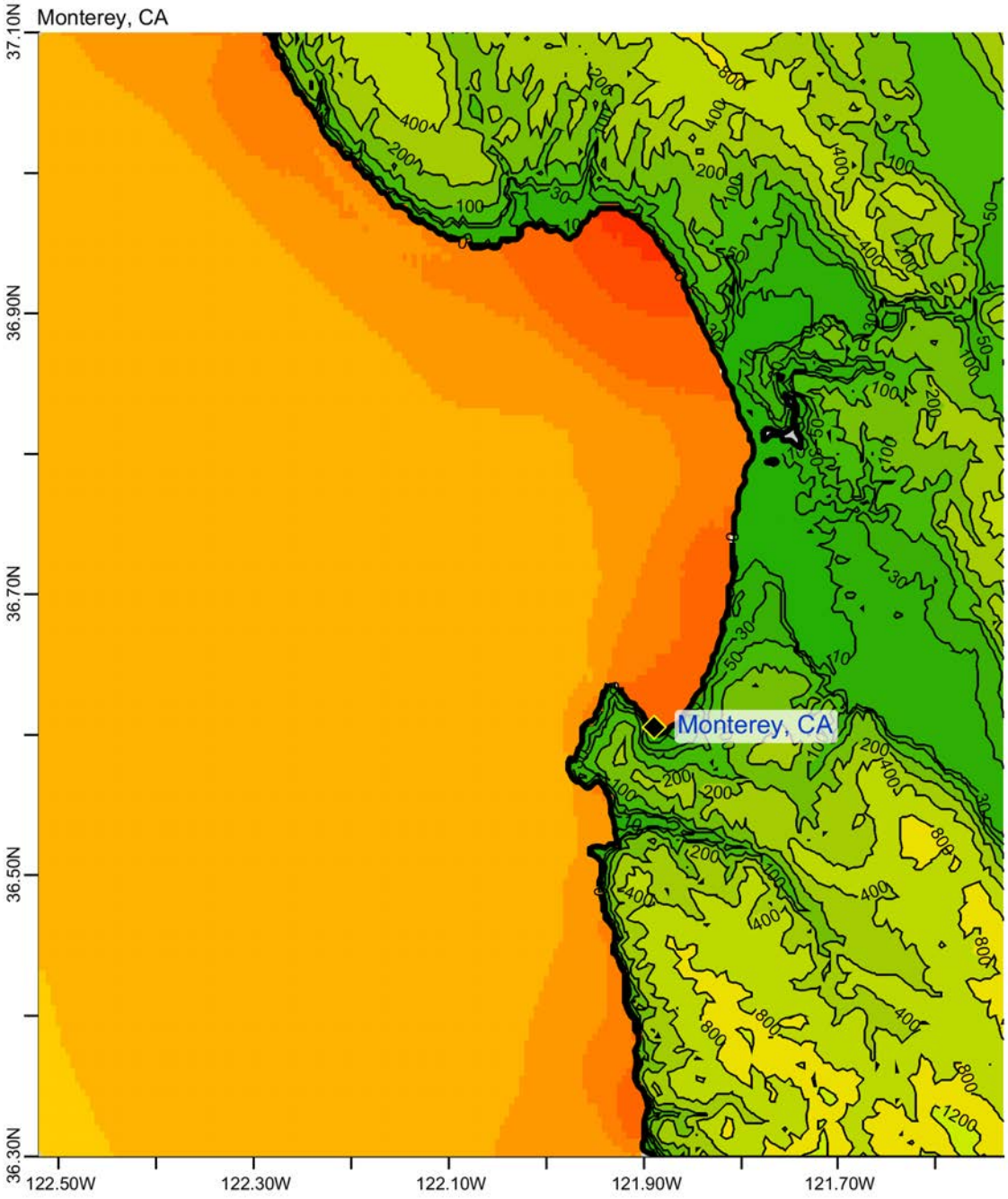

Figure C6. Max computed wave amplitude of B grid, Monterey, California, for synthetic event ACSZ 56-65.

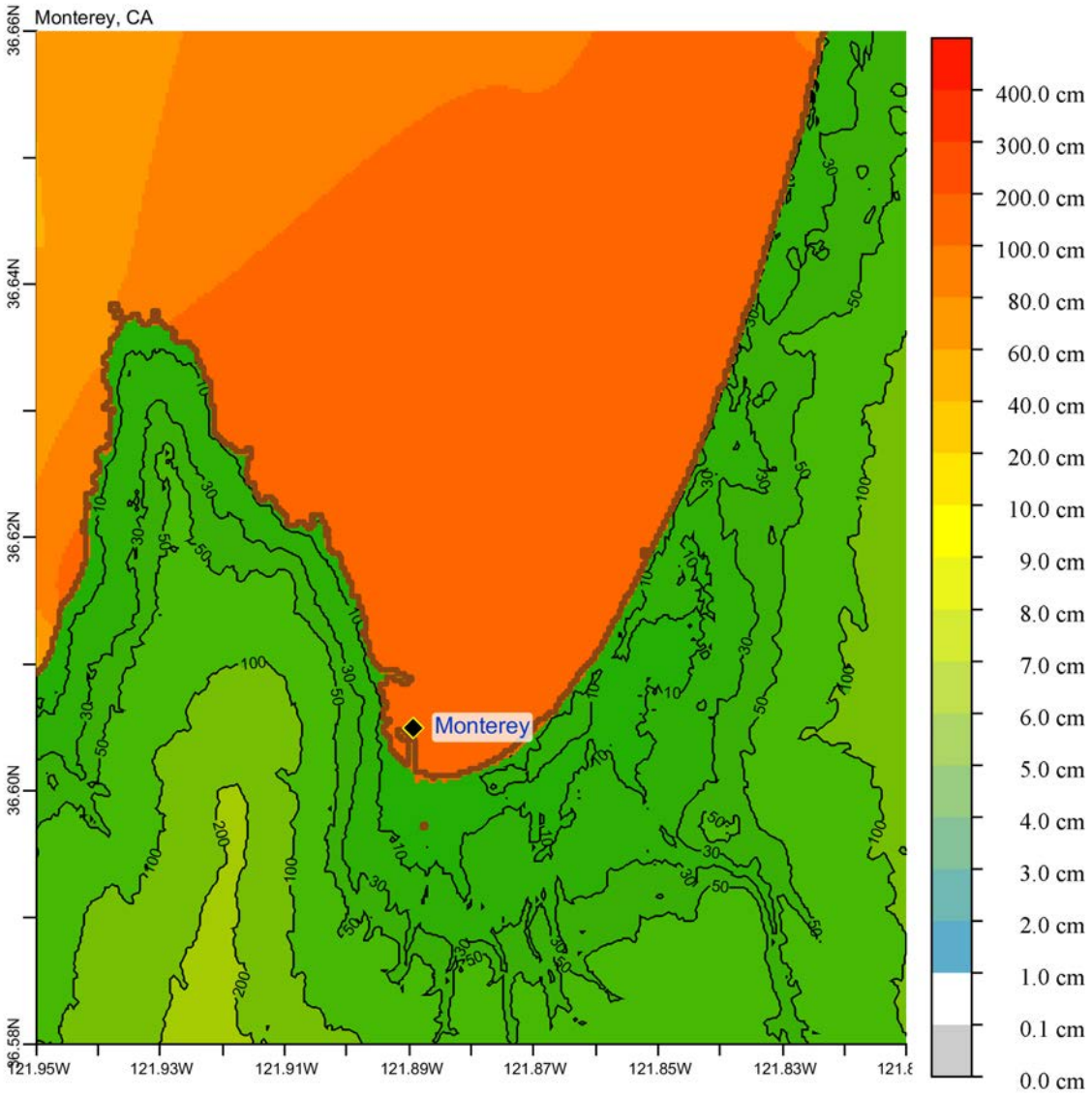

Figure C7. Max computed wave amplitude of C grid, Monterey, California, for synthetic event ACSZ 56-65.

(a)

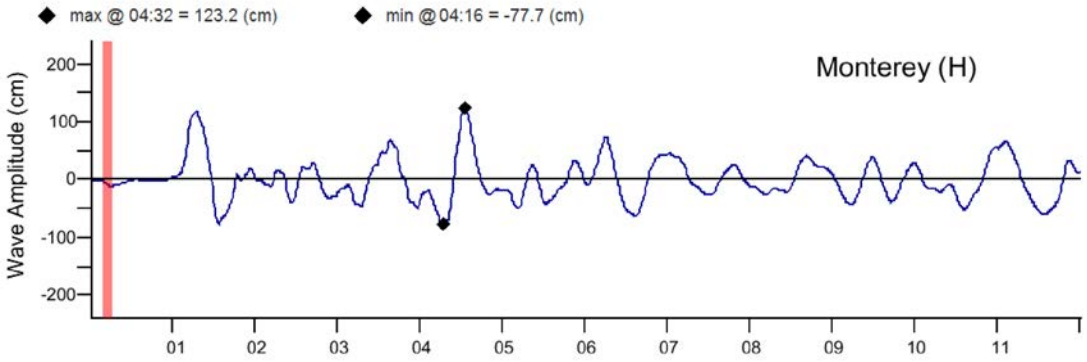

(b)

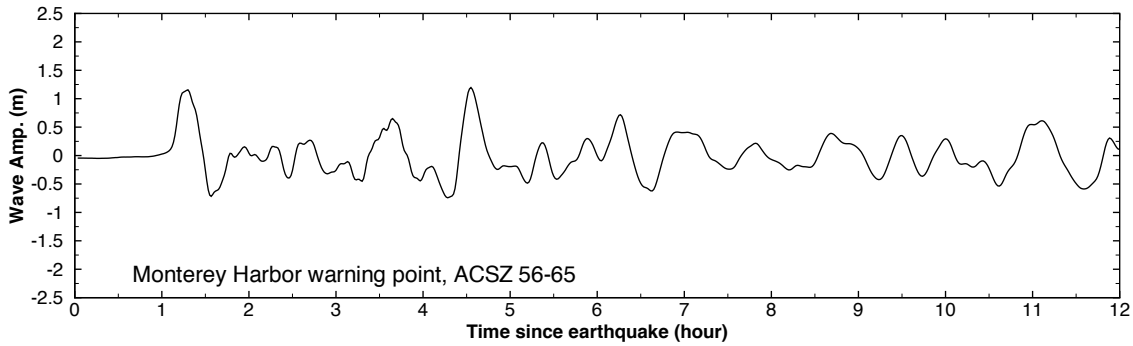

Figure C8. Computed time series at Monterey tide gage, for synthetic event ACSZ 56-65: (a) time series computed in SIFT; (b) time series shown in the forecast model report.

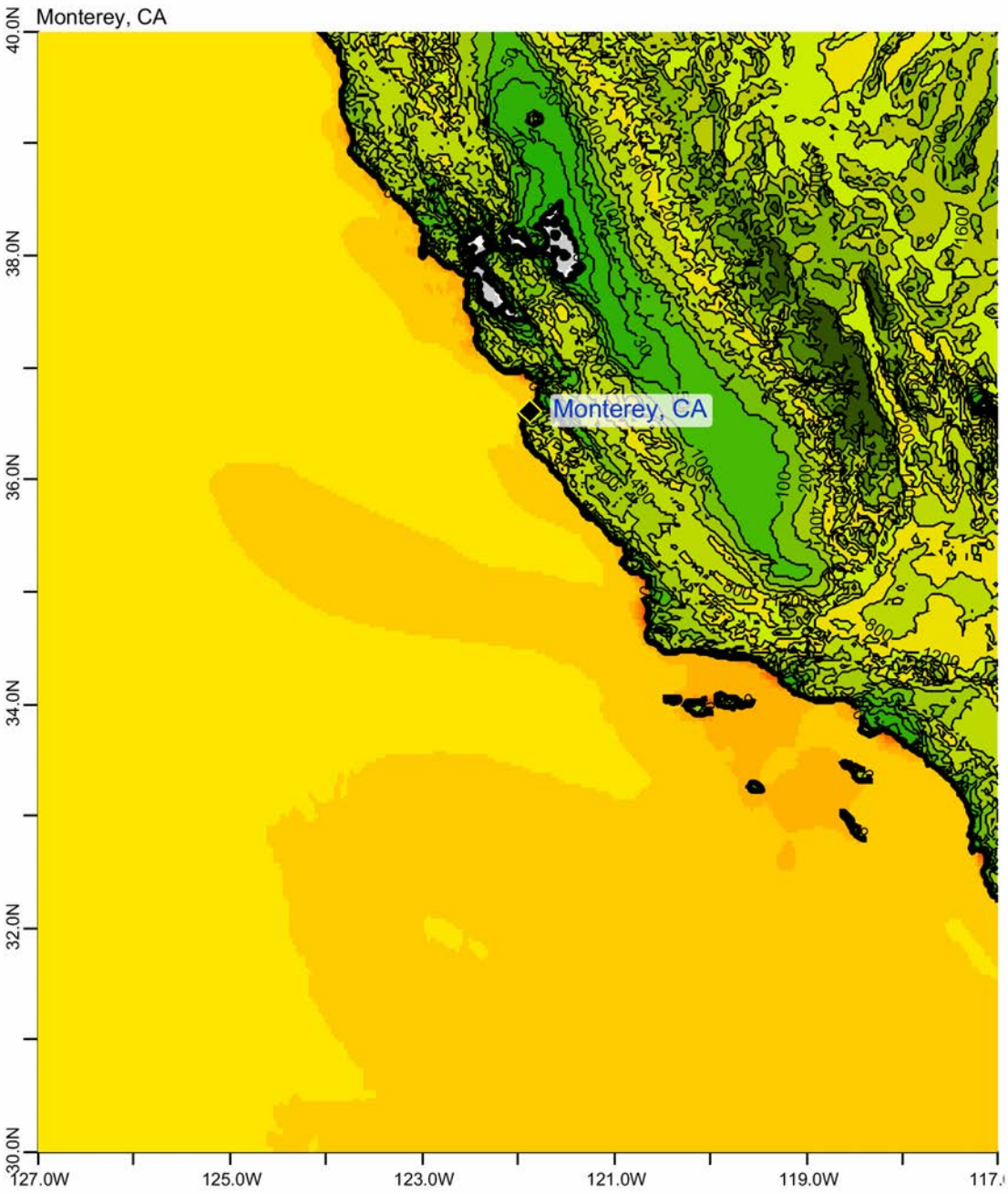

Figure C9. Max computed wave amplitude of A grid, Monterey, California, for synthetic event CSSZ 81-90.

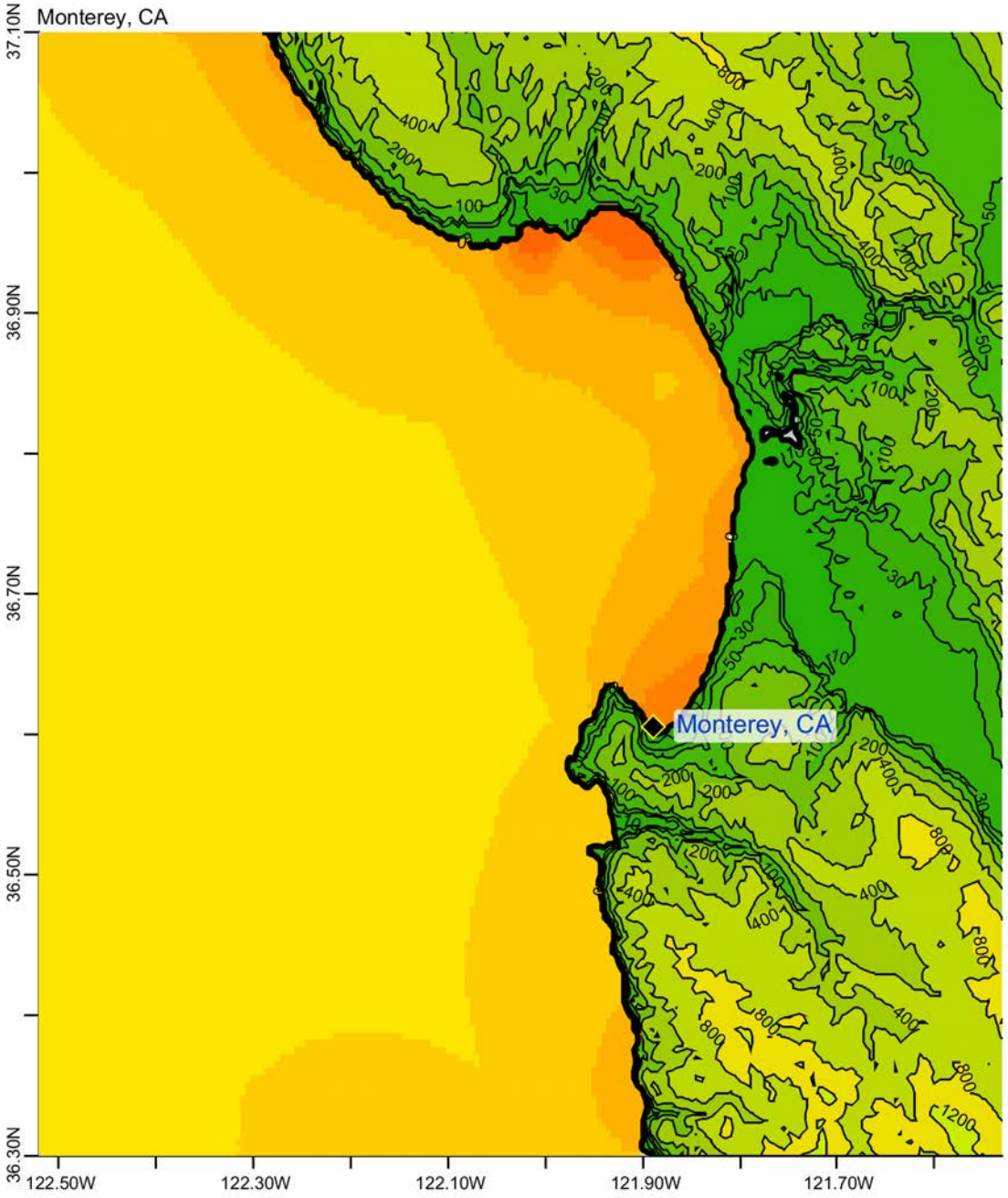

Figure C10. Max computed wave amplitude of B grid, Monterey, California, for synthetic event CSSZ 81-90.

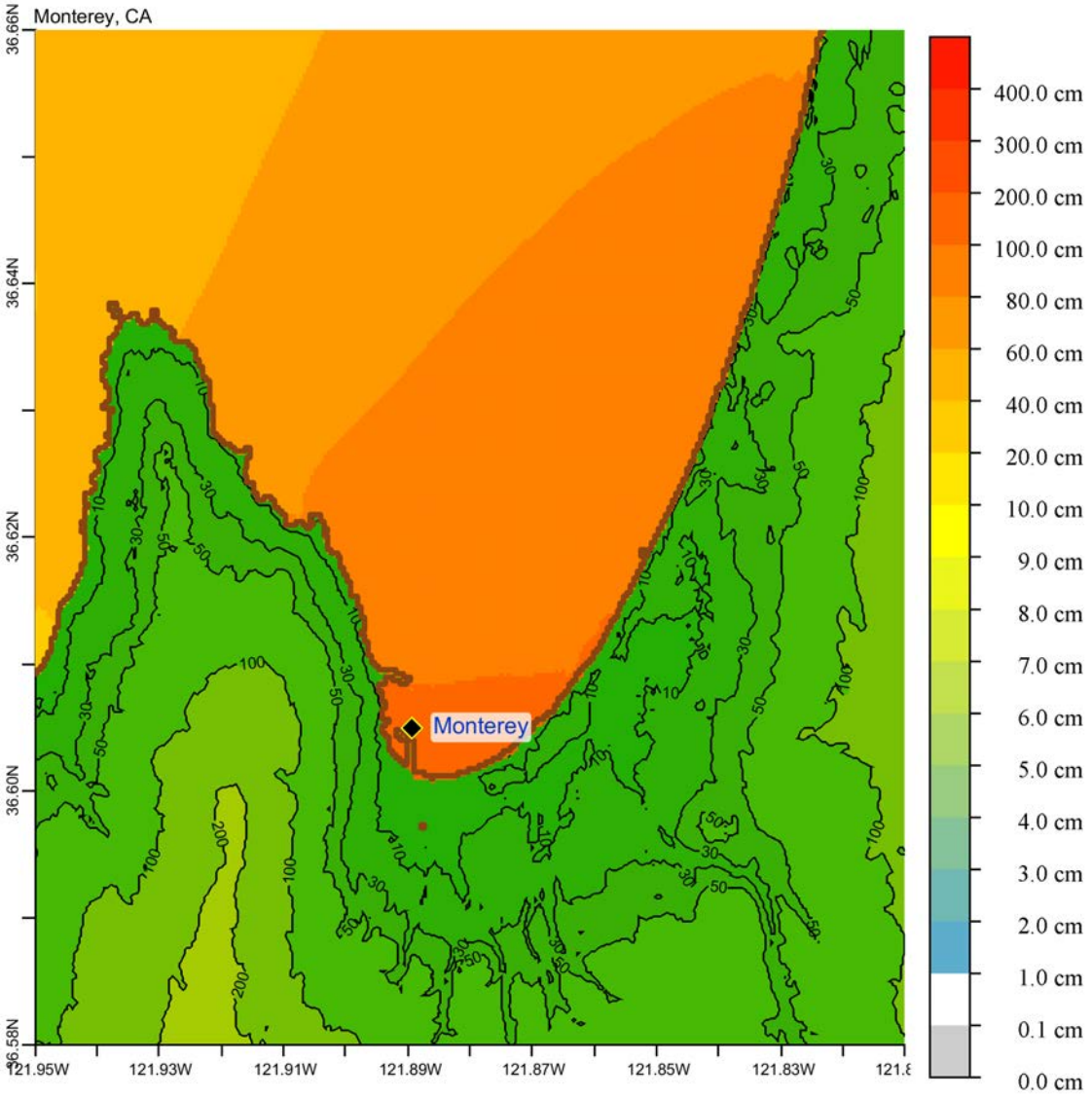

Figure C11. Max computed wave amplitude of C grid, Monterey, California, for synthetic event CSSZ 81-90.

(a)

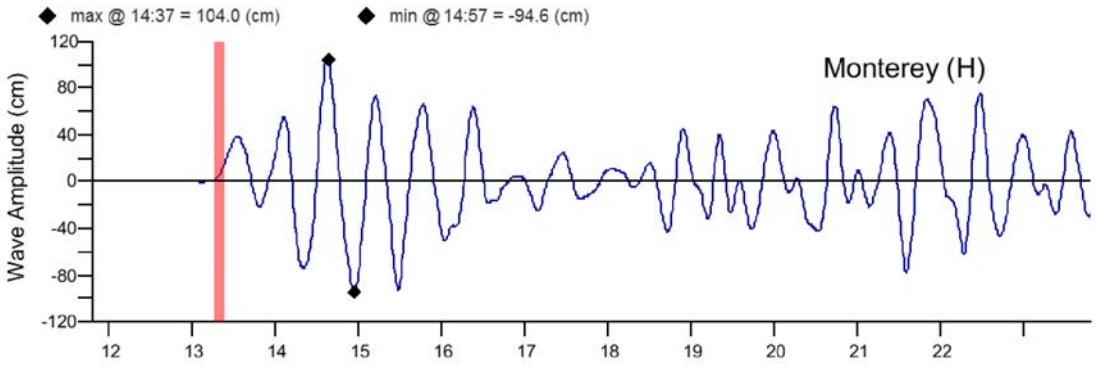

(b)

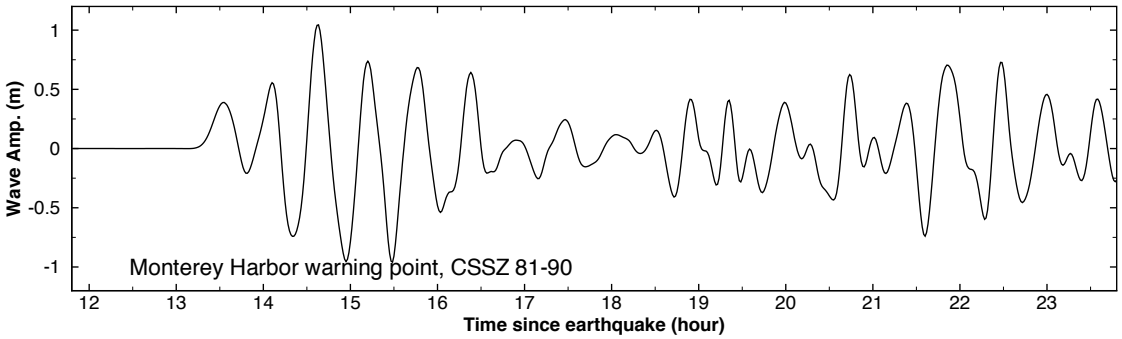

Figure C12. Computed time series at Monterey tide gage, for synthetic event CSSZ 81-90: (a) time series computed in SIFT; (b) time series shown in the forecast model report.

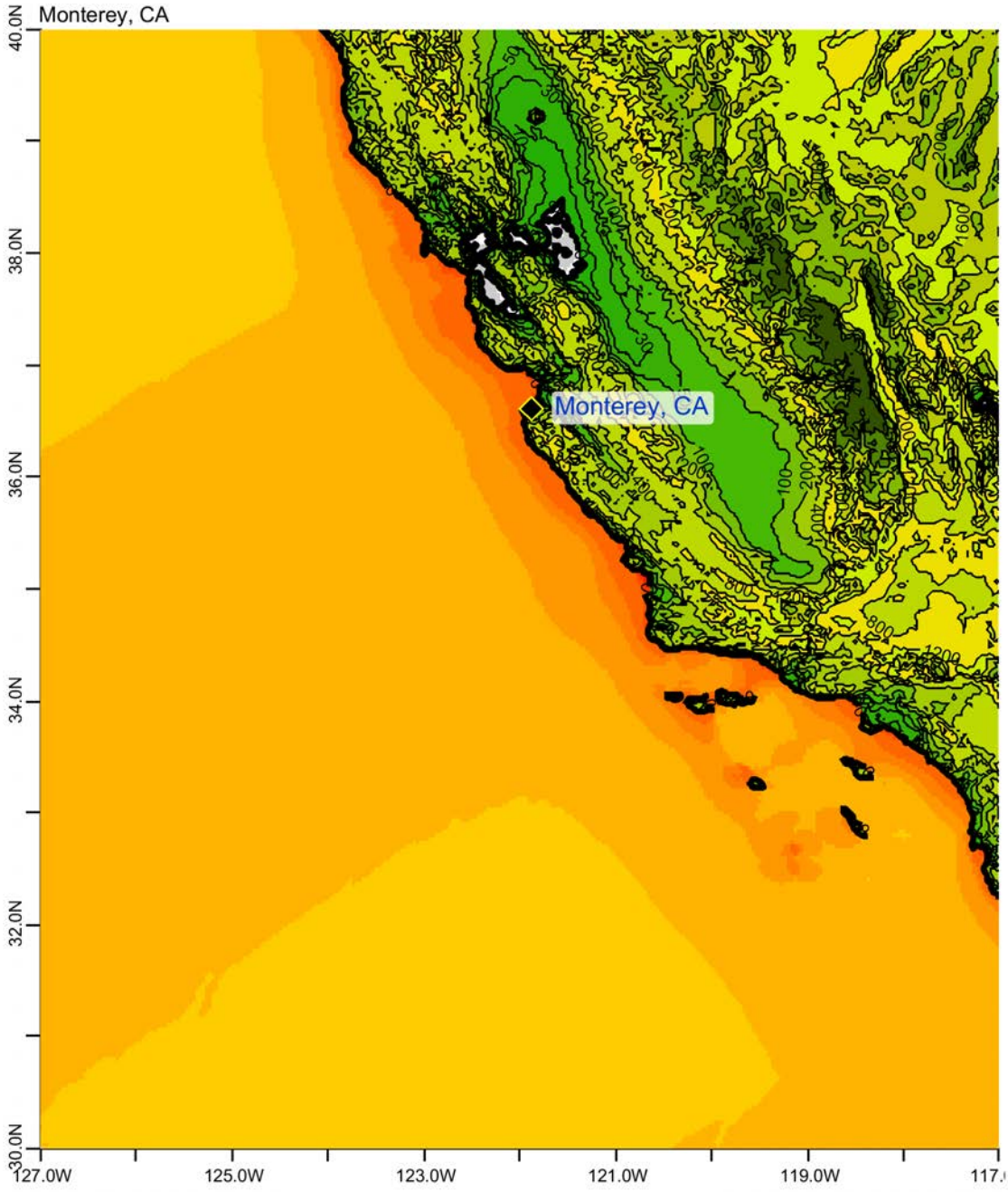

Figure C13. Max computed wave amplitude of A grid, Monterey, California, for synthetic event NTSZ 30-39.

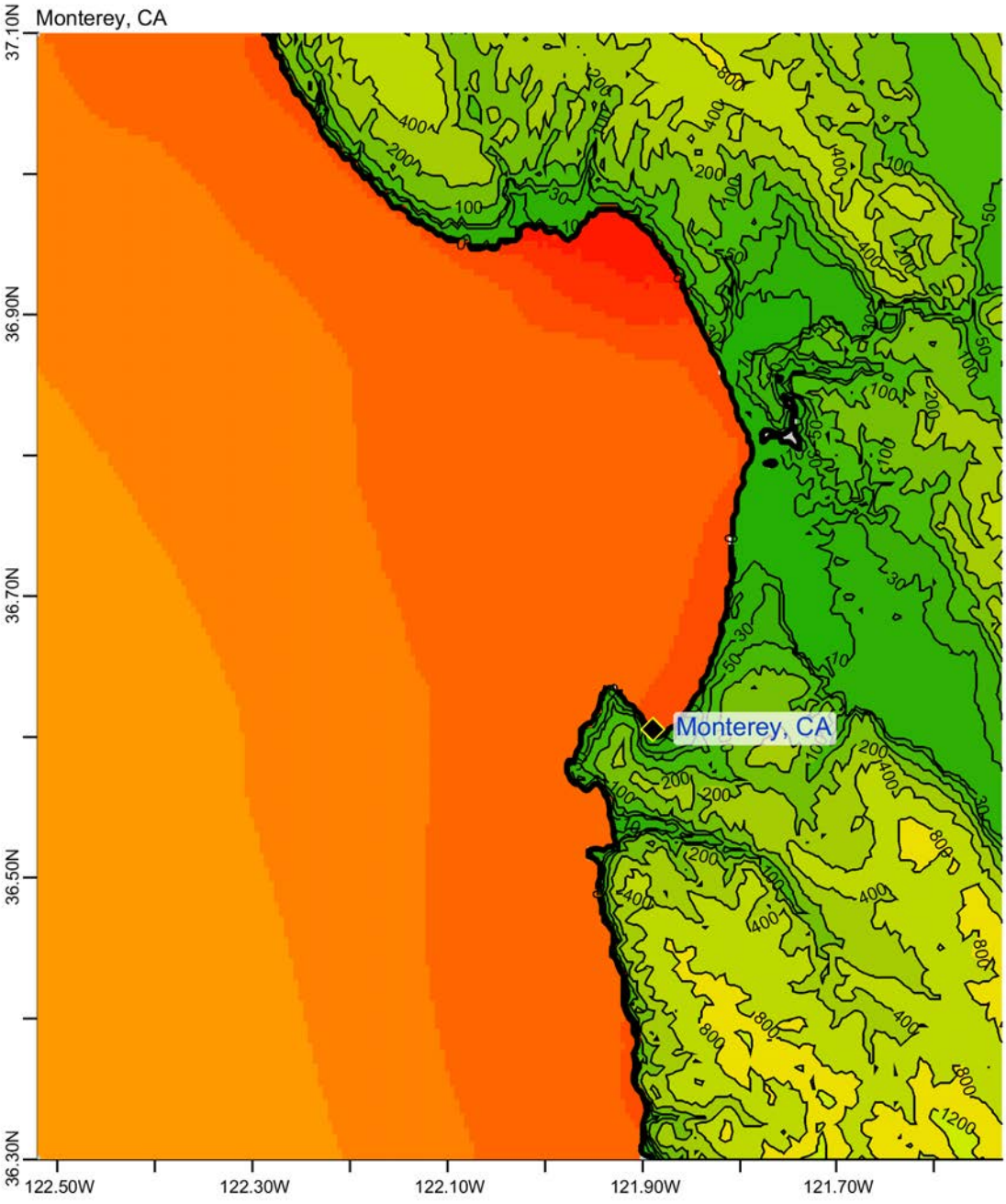

Figure C14. Max computed wave amplitude of B grid, Monterey, California, for synthetic event NTSZ 30-39.

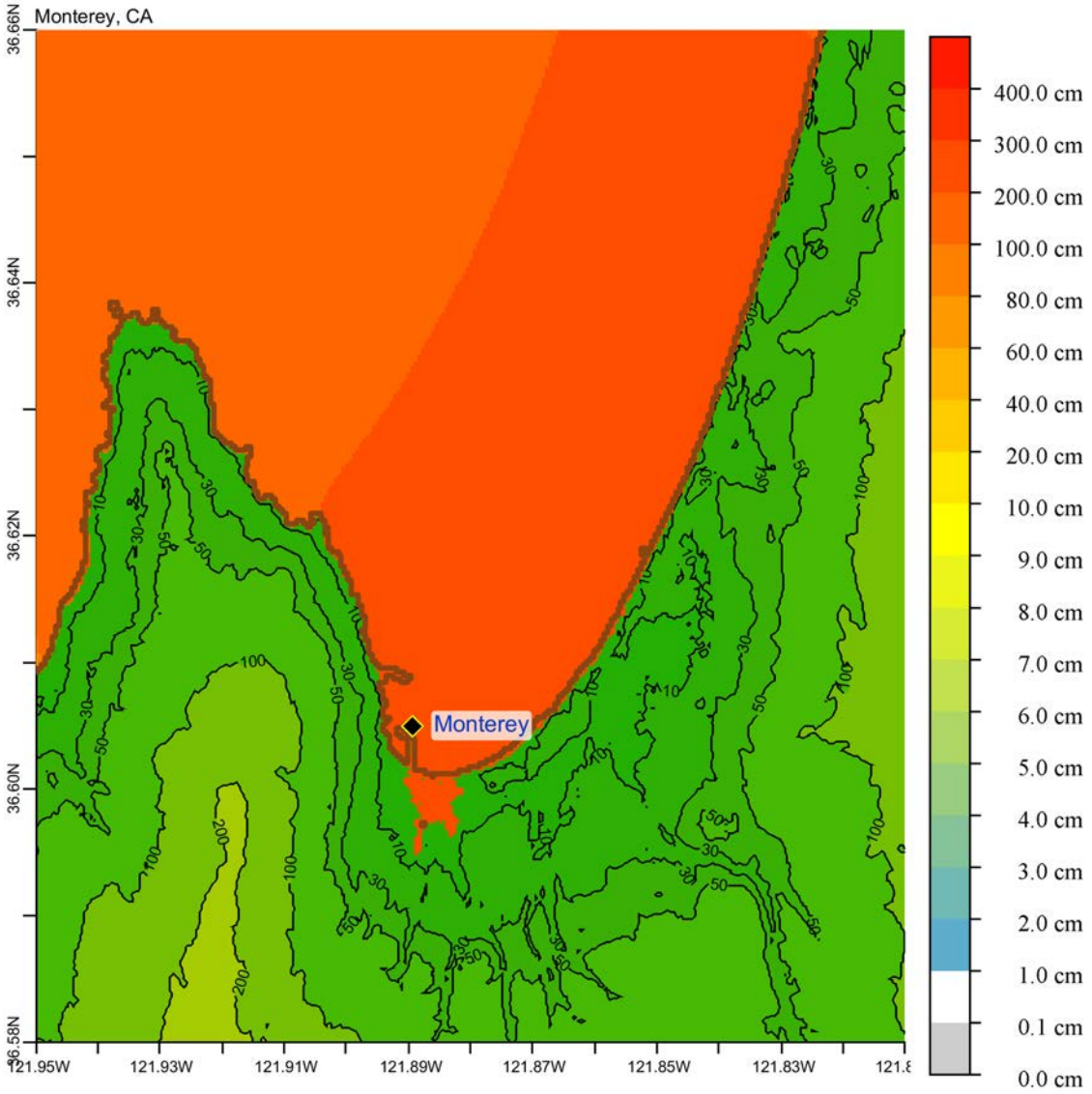

Figure C15. Max computed wave amplitude of C grid, Monterey, California, for synthetic event NTSZ 30-39.

(a)

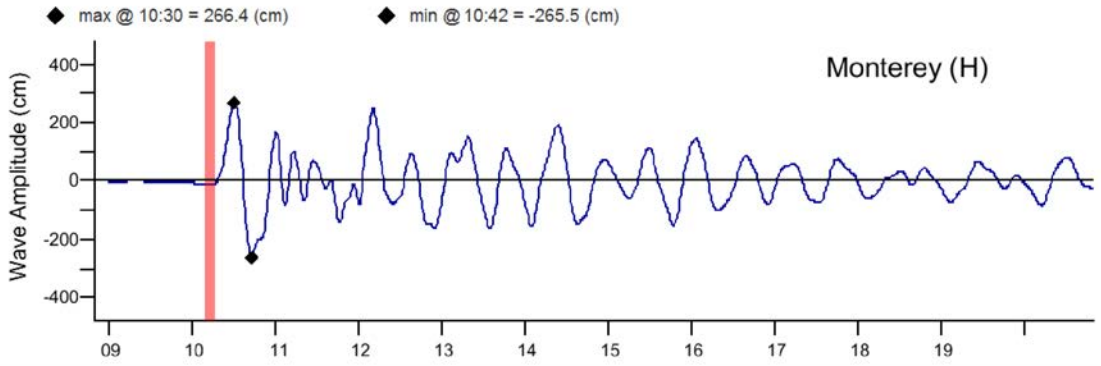

(b)

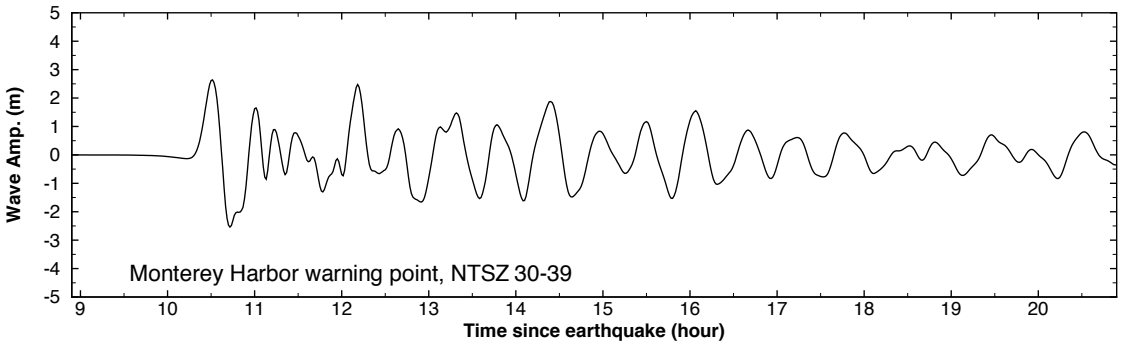

Figure C16. Computed time series at Monterey tide gage, for synthetic event NTSZ 30-39: (a) time series computed in SIFT; (b) time series shown in the forecast model report.

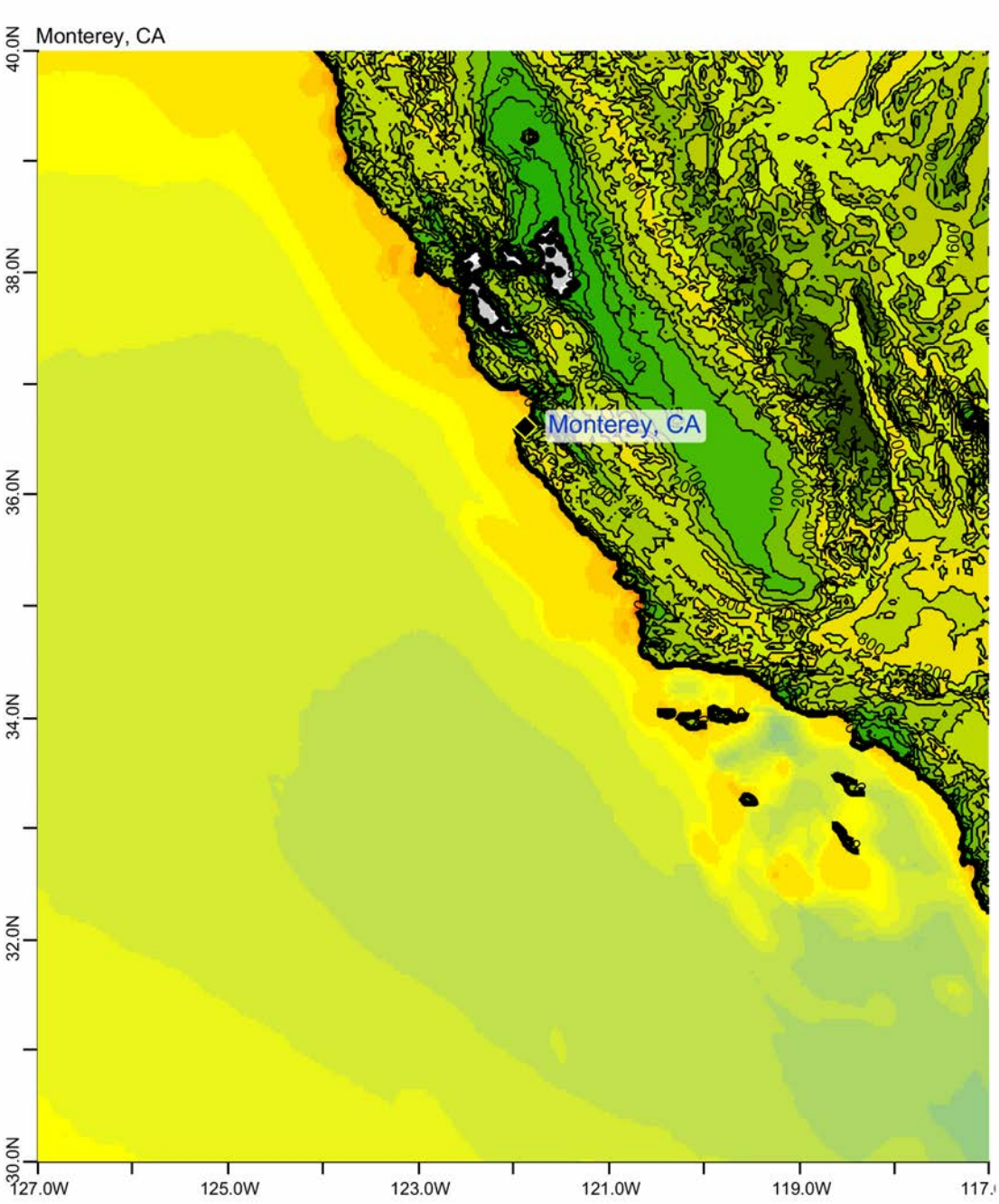

Figure C17. Max computed wave amplitude of C grid, Monterey, California, for the 11 March 2011 Japan event.

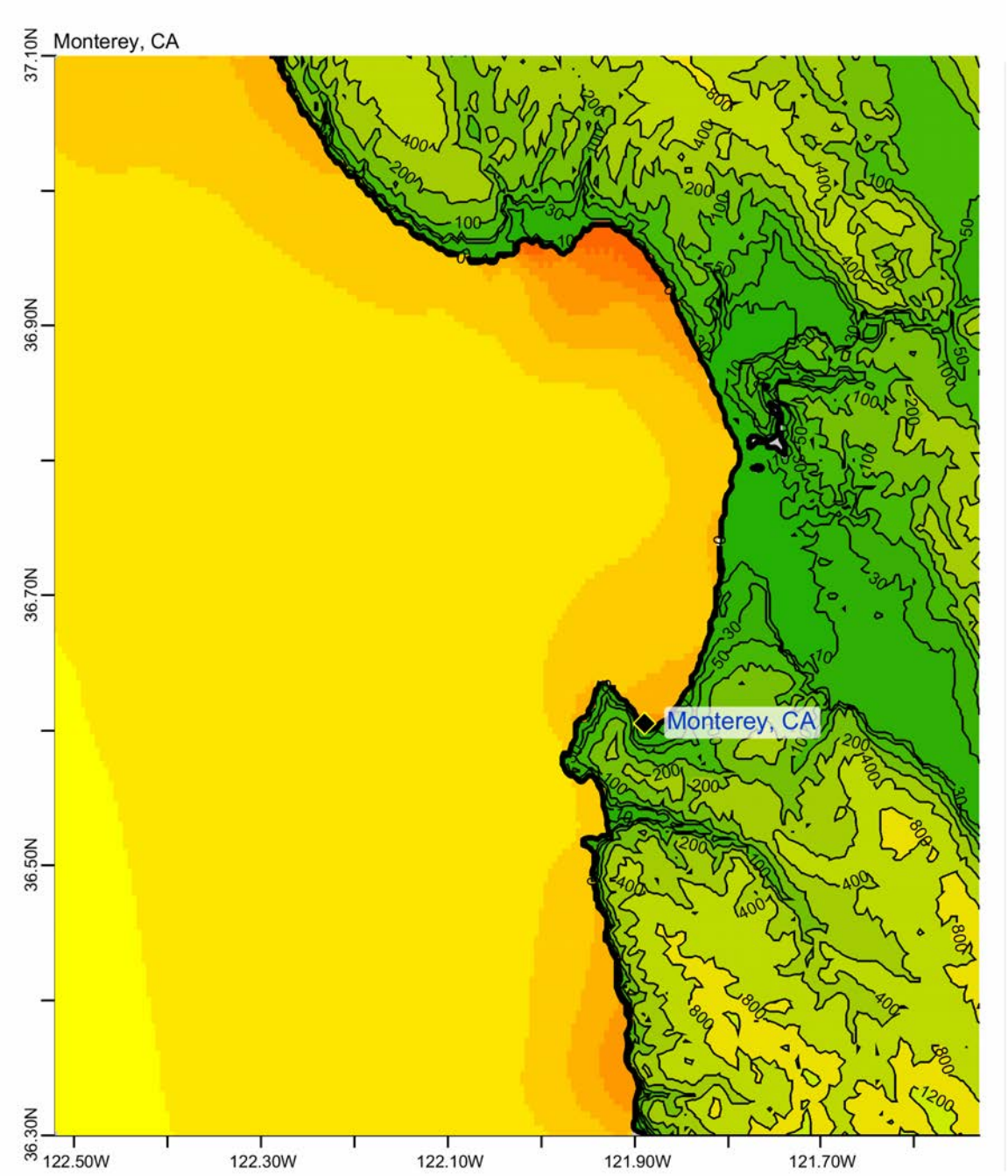

Figure C18. Max computed wave amplitude of B grid, Monterey, California, for the 11 March 2011 Japan event.

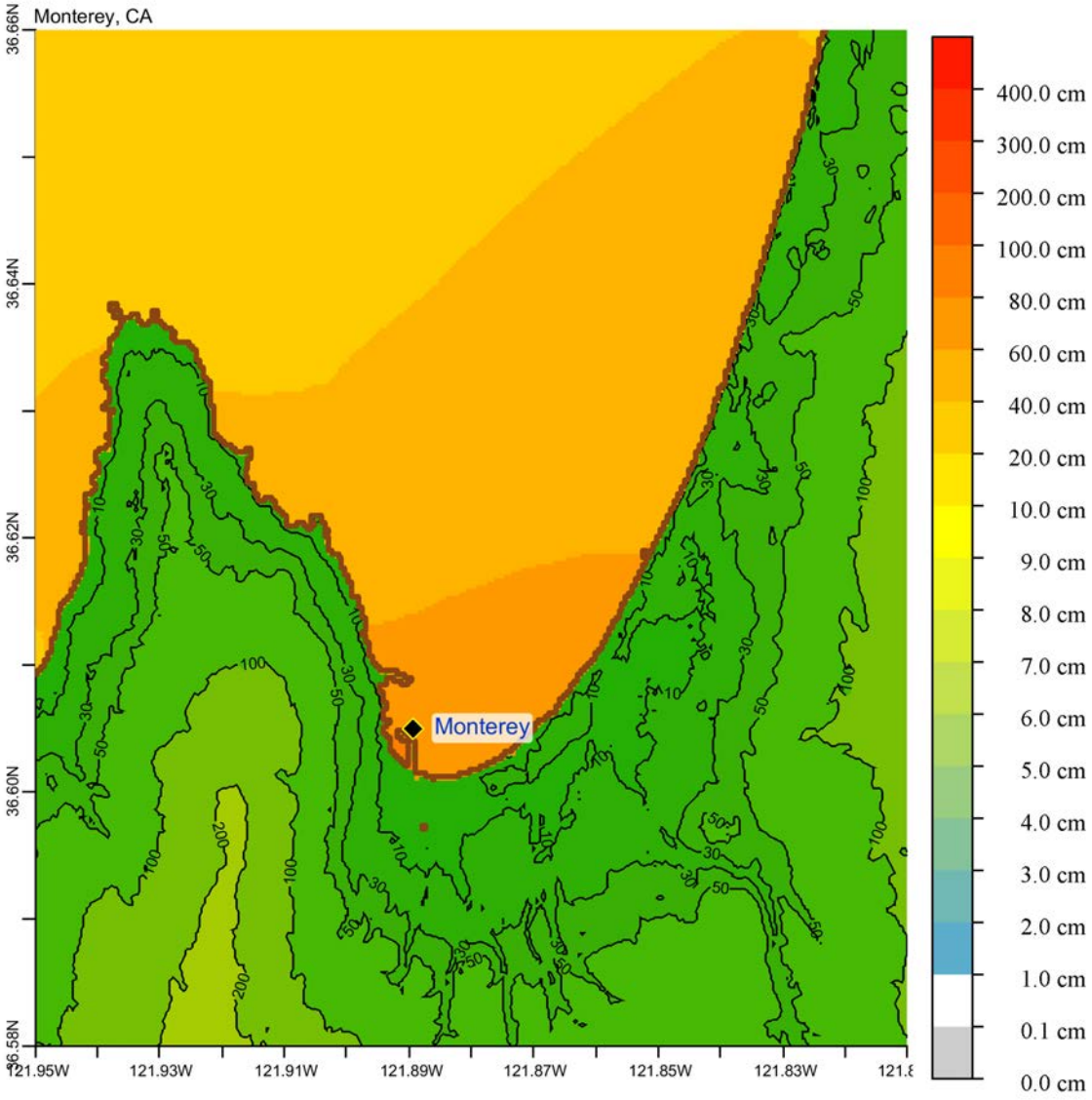

Figure C19. Max computed wave amplitude of C grid, Monterey, California, for the 11 March 2011 Japan event.

(a)

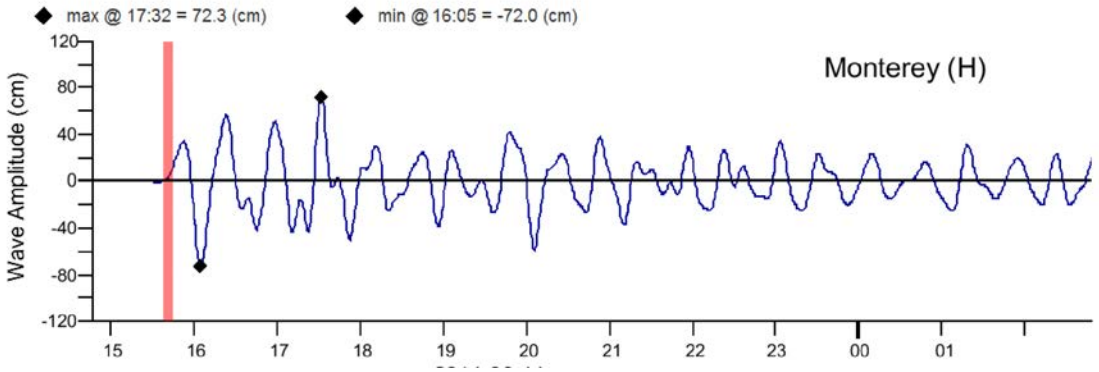

(b)

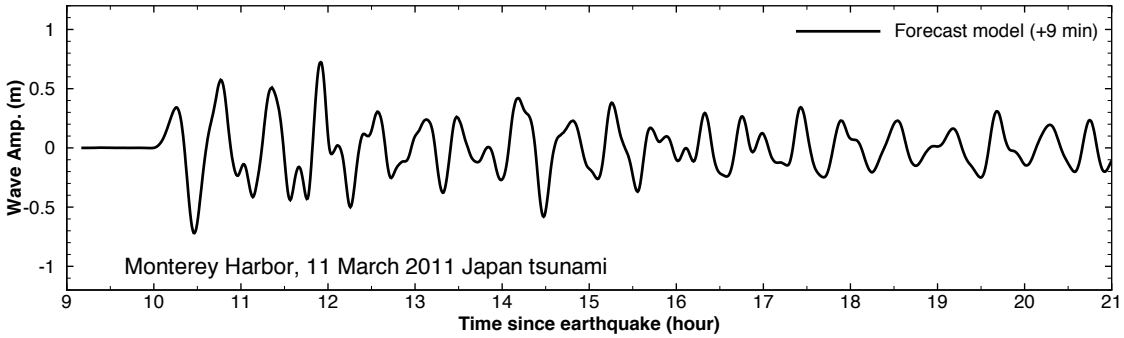

Figure C20. Computed time series at Monterey tide gage, for the 11 March 2011 Japan tsunami: (a) time series computed in SIFT. Time in *x* axis is in UTC; (b) time series shown in the forecast model report. *x* axis shows time since the earthquake, not the UTC time.